Trajectory Optimization for Target Localization Using Small Unmanned Aerial Vehicles

by

Sameera S. Ponda

B.S. Aerospace Engineering with Information Technology,
Massachusetts Institute of Technology (2004)

Submitted to the Department of Aeronautics and Astronautics
in partial fulfillment of the requirements for the degree of

Master of Science in Aeronautics and Astronautics

at the

MASSACHUSETTS INSTITUTE OF TECHNOLOGY

September 2008

Author .....
Department of Aeronautics and Astronautics
August 21, 2008

Certified by .....
Prof. Emilio Frazzoli
Associate Professor of Aeronautics and Astronautics
Thesis Supervisor

Certified by .....
Dr. Richard M. Kolacinski
Principal Member of Technical Staff, Draper Laboratory
Thesis Supervisor

Accepted by .....
Prof. David L. Darmofal
Associate Department Head
Chair, Committee on Graduate Students

Trajectory Optimization for Target Localization Using Small Unmanned Aerial Vehicles

by

Sameera S. Ponda

Submitted to the Department of Aeronautics and Astronautics
on August 21, 2008, in partial fulfillment of the
requirements for the degree of
Master of Science in Aeronautics and Astronautics

Abstract

Small unmanned aerial vehicles (UAVs), equipped with navigation systems and video capability, are currently being deployed for intelligence, reconnaissance and surveillance missions. One particular mission of interest involves computing location estimates for targets detected by onboard sensors. Combining UAV state estimates with information gathered by the imaging sensors leads to bearing measurements of the target that can be used to determine the target's location. This 3-D bearings-only estimation problem is nonlinear and traditional filtering methods produce biased and uncertain estimates, occasionally leading to filter instabilities. Careful selection of the measurement locations greatly enhances filter performance, motivating the development of UAV trajectories that minimize target location estimation error and improve filter convergence. The objective of this work is to develop guidance algorithms that enable the UAV to fly trajectories that increase the amount of information provided by the measurements and improve overall estimation observability, resulting in proper target tracking and an accurate target location estimate.

The performance of the target estimation is dependent upon the positions from which measurements are taken relative to the target and to previous measurements. Past research has provided methods to quantify the information content of a set of measurements using the Fisher Information Matrix (FIM). Forming objective functions based on the FIM and using numerical optimization methods produce UAV trajectories that locally maximize the information content for a given number of measurements. In this project, trajectory optimization leads to the development of UAV flight paths that provide the highest amount of information about the target, while considering sensor restrictions, vehicle dynamics and operation constraints. The UAV trajectory optimization is performed for stationary targets, dynamic targets and multiple targets, for many different scenarios of vehicle motion constraints. The resulting trajectories show spiral paths taken by the UAV, which focus on increasing the angular separation between measurements and reducing the relative range to the target, thus maximizing the information provided by each measurement and improving the performance of the estimation.

The main drawback of information based trajectory design is the dependence of the Fisher Information Matrix on the true target location. This issue is addressed in this project by executing simultaneous target location estimation and UAV trajectory optimization. Two estimation algorithms, the Extended Kalman Filter and the Particle Filter are considered, and the trajectory optimization is performed using the mean value of the target estimation in lieu of the true target location. The estimation and optimization algorithms run in sequence and are updated in real-time. The results show spiral UAV trajectories that increase filter convergence and overall estimation accuracy, illustrating the importance of information-based trajectory design for target localization using small UAVs.

Thesis Supervisor: Prof. Emilio Frazzoli
Title: Associate Professor of Aeronautics and Astronautics

Thesis Supervisor: Dr. Richard M. Kolacinski
Title: Principal Member of Technical Staff, Draper Laboratory

Acknowledgments

First of all I would like to thank my advisors Rich Kolacinski and Emilio Frazzoli. This thesis would really not have been possible without your endless support, advice and inspiration. Thank you so much for the frequent meetings and discussions, for always inspiring and guiding me, for giving me new ideas, and for showing me new ways to think. You have really helped me grow as an engineer and I am very grateful to have had the privilege of working with you both.

To Brent Appleby, George Schmidt, and Linda Fuhrman, thank you for providing me with the opportunity of being a Draper Fellow. It has been a truly great experience and I really appreciate all your advice and support, with the thesis, career development, and life in general.

To my MIT professors, Jon How, Nick Roy and John Deyst, I very much appreciate your guidance and support throughout this thesis. Thank you for always taking the time to advise me and point me in new directions. To Barbara Lechner and Marie Stuppard thanks for always being there to help me out and for all your encouragement and support.

To all my Draper colleagues, especially Paul DeBitetto, Chris Dever, Louis Breger, Greg Andrews, Adam Rzepniewski, Laurent Duchesne, Marc McConley, Chris Gibson, Dale Landis, Tom Thorvaldsen, Scott Berry, and Bryan Wasileski, thank you for your support and inspiration and your willingness to always help out. I appreciate the knowledge and perspective you have helped me build over the last few years and I've learned so much from all of you. Thank you for making the Draper Fellowship such a fabulous experience.

To the other Draper Fellows, especially Andrea Henshall, Matt Karmondy, Paul Tisa, Ben Werner, Paul Rosendall and Josh Joseph, thanks for always being there to discuss ideas, to provide help with classes, to support me with research, and to get those frequent cups of coffee with me. And to all my Ares lab mates, especially Marco and John, thank you for all your wisdom, help and support. It's been a real pleasure to work with you all.

To my parents, thank you for always supporting me and being there for me, to listen and to give advice. I'm really grateful for the plentiful opportunities you have given me throughout my life. You have always been a source of inspiration and encouragement and I love you both very much.

I would also like to thank all my dear friends for making these past two years unforgettable, especially Will, Cara, Rayna, Sam, Robin, Eric, and Mike. And last but not least, to my roommates Laura and Bryan, who amused themselves by taking bets on when this thesis would be finished. Thanks for all your support and friendship, for giving me ideas and sources, for listening to my presentations, and for always being there for me. I couldn't have done it without you guys.

This thesis was prepared at the Charles Stark Draper Laboratory, Inc., under Independent Research and Development Project Numbers 22026-001 and 22951-001.

Publication of this thesis does not constitute approval by Draper Laboratory of the findings or conclusions contained therein. It is published for the exchange and stimulation of ideas.

Contents

THIS PAGE INTENTIONALLY LEFT BLANK

List of Figures

THIS PAGE INTENTIONALLY LEFT BLANK

List of Tables

THIS PAGE INTENTIONALLY LEFT BLANK

Chapter 1

Introduction

1.1 Motivation

Since knowing your adversary is an essential strategic and tactical requirement, most missions in modern warfare are centered on collecting and processing as much information about the opponent and the environment as possible. Examples of such missions include point, area, and route reconnaissance tasks, persistent surveillance, threat identification, target tracking and post-battle reconnaissance for damage assessment [51]. Even though these missions vary in scope and requirements, they all focus on collecting and exploiting information about the environment, with the purpose of minimizing the uncertainty regarding the enemy's location, behavior, intentions, and courses of action. The first step in successfully analyzing the adversary is executing proper Intelligence, Surveillance and Reconnaissance (ISR) procedures to collect and process information [3] [4] [2].

ISR has traditionally been accomplished using several different tools and techniques, ranging from satellites and high-altitude aircraft equipped with high-resolution sensors, to land-based reconnaissance teams carrying cameras and radar devices [1]. Recent advances in technology are encouraging the use of small unmanned aerial systems (UAS) for ISR procedures. UAS have repeatedly proven their usefulness by assisting soldiers in several different types of missions. Equipped with onboard electro-optical (EO) and/or infrared (IR) cameras, as well as navigation and com-

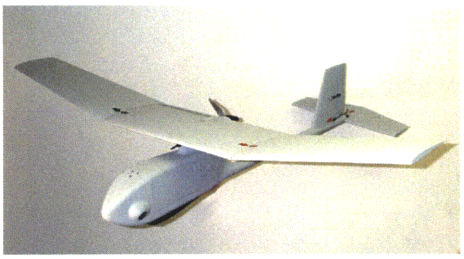

(a) Raven (AeroVironment, Inc)

(b) Wasp Block III (AeroVironment, Inc)

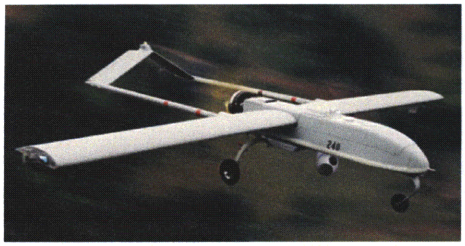

(c) RQ-7B Shadow 200 (AAI Corporation)

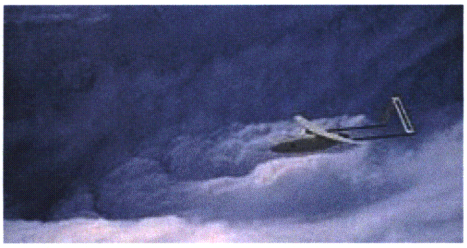

(d) Aerosonde (AAI Corporation)

Figure 1-1: Examples of small unmanned aerial systems

munications hardware, current small UAS are capable of surveying the environment, providing the operator with real-time visual information rapidly, inexpensively and with low risk to human life. Figure 1-1 shows a few examples of small UAS platforms, such as Raven and Shadow, which are currently used by the U.S. Army for many military missions overseas.

A particulary interesting ISR mission for small UAS is to localize and track targets detected by onboard sensors. Using imagery data of a target from different vehicle locations as well as knowledge of the vehicle positions and orientations at the time of the measurements, an estimate of the geodetic coordinates of the target can be computed. This capability would be very useful in environments for which no *a priori* information is available. For example, information obtained by the UAS could be relayed to troops or to military systems which use absolute targeting methods, and therefore, require geodetic coordinate information in order to engage the target. In addition to ISR missions, this localization capability would be invaluable for several other applications such as traffic monitoring, forest fire localization, scientific surveys in dangerous conditions, border and harbor patrol, search and rescue, and wildlife

tracking, among others.

The main challenges involved with target localization include: maintaining the target in the field of view, and developing a vehicle trajectory such that the target location estimation error is minimized. For a human operator, maintaining the target in the field of view is an extremely challenging task. This is because of limited vehicle maneuverability, a noisy environment (mainly due to wind and gusts) and an overall lack of proprioceptive feedback provided to the operator from the vehicle. As for the latter task of flying the vehicle in such a way that the target location estimation error is minimized, it is difficult for a human operator to have an intuitive understanding of how best to accomplish this. For the stationary target case circular trajectories which maintain an orthogonal line-of-sight to the target are widely accepted in the literature as optimal trajectories. However, if the target is moving, the operator may not know what the best vehicle path is. Autonomous flight path generation and trajectory design, therefore, are essential to successful target localization. The purpose of this work is to provide methods for creating trajectories that enable small UAS to autonomously perform vision-based target localization in the most accurate manner.

1.2 Problem Description

This section describes the problem of target localization using UAS equipped with image-based sensors. By taking imagery data of a ground target from several different vehicle locations, an estimate of the target location can be computed through triangulation (see Figure 1-2). For the purpose of this thesis, image processing for target recognition is assumed and the process of obtaining a "measurement" consists of finding the pixel location in the image that corresponds to the centroid of the target. Then, using the vehicle position, attitude, the pointing angle of the camera with respect to the vehicle, and the pixel location of the target, the measurement provides a relative position vector from the vehicle to the target. The magnitude of this vector, however, is unknown and the resulting measurement is a bearing to the target (one

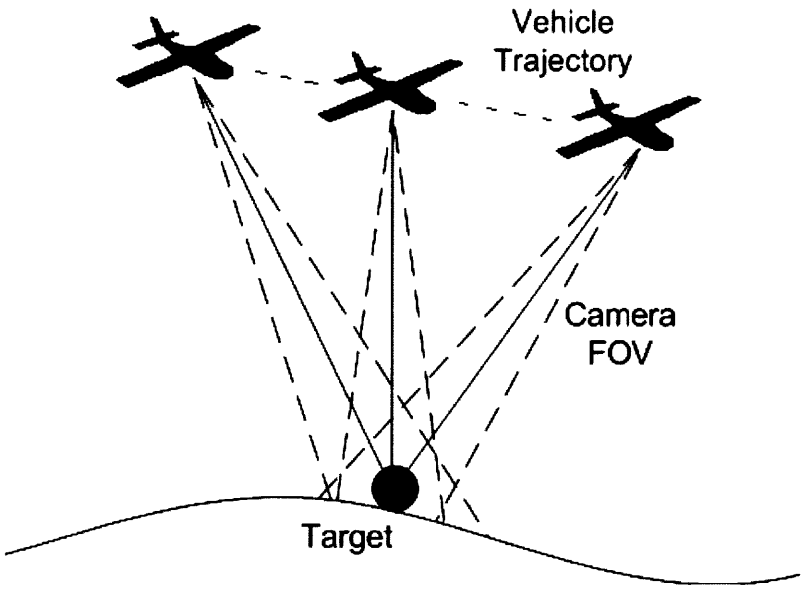

Figure 1-2: Illustration of target localization using a UAV with vision

angle in the 2-D case and two angles in the 3-D case). Given several measurement vectors, the absolute target position can be computed by finding the point in space that minimizes the sum of the squares of the distances between that point and the nearest points lying on the measurement vectors.

The task of target acquisition presents several challenges. Most modern small UAS are equipped with GPS capabilities and inertial sensors, but are designed to be inexpensive and therefore include low quality sensors and poor navigation filtering algorithms, leading to inaccurate vehicle state estimation. Given these large navigation errors it is difficult to achieve a high level of precision in the target location estimate since the errors in the vehicle state propagate into the targeting algorithms. The resulting target estimation error is a combination of errors in the vehicle position, vehicle orientation, and sensor noise. Under simplifying assumptions involving the noise correlations, the target estimation error equation can be described, in a gross sense, as

$$\sigma^2_{TOTAL} = \sigma^2_{x,NAV} + \sigma^2_{\theta,NAV}R^2 + \sigma^2_{x,SEN} + \sigma^2_{\theta,SEN}R^2 + \sigma^2_{\Delta T}V^2 + \sigma^2_{\Delta T}R^2\omega^2 \quad (1.1)$$

Here R is the relative range to the target, V is the relative velocity between the

vehicle and the target, and ω is the angular velocity of the vehicle. The first two terms are the contribution due to errors in the vehicle state estimation, the next two terms are due to the sensor errors, and the last two terms are from integration errors in the target state estimation. The state errors in vehicle position propagate directly into the target estimation, whereas the targeting error contribution due to errors in vehicle orientation is a function of the relative range to the target. Therefore, errors in vehicle attitude lead to increasingly large target localization errors as the relative distance between the vehicle and the target increases. The purpose of this work is to find methods to reduce this target location estimation error given noisy and inaccurate vehicle navigation. The vehicle navigation system is provided and certain amounts of vehicle state errors are unavoidable, but the trajectory of the UAV can be controlled to reduce the uncertainty or entropy about the target estimation and mitigate the effect of the noisy vehicle state estimates.

This problem can be addressed within the framework of Information Theory, which explains the connections between the entropy or uncertainty about the estimation process and the information provided by the measurements. Here entropy is a measure of the uncertainty of a random variable. It can also be thought of as the self-information contained in that random variable. Entropy in the discrete case is defined by

$$H(X) = -\sum_{x \in X} p(x) \log p(x) \tag{1.2}$$

where X is the random variable and $p(x)$ is its probability distribution. This definition of entropy provides a measure of how rich in information a data stream is, and is normally used to determine the minimum amount of bits required for communicating a certain amount of information. In an estimation process, the entropy of the estimation is a measure of how much information the measurements provide about the estimation process. Different sets of measurements produce different amounts of entropy in the estimation. As more measurements are taken, the entropy becomes lower and, correspondingly, the uncertainty in the estimation is reduced. However, not all measurements lead to an equal reduction in uncertainty. Some measurements pro-

vide more information about the process to be estimated than others, increasing the accuracy of the estimation. For the target localization problem, the UAV trajectory affects the amount of information received about the target, since the information content of the measurements is a function of both the UAV and the target states. The goal of this thesis is to provide information-theoretic methods for designing vehicle trajectories that provide the highest amount of information about the target and thus reduce the uncertainty in the target location estimate.

In order to design UAV trajectories that increase the performance of the target localization algorithm it is necessary to understand the relationship between the vehicle state errors and the target location estimate, as well as the underlying geometry of the problem. For example, due to the lever arm effect of the vehicle orientation errors it is desirable to reduce the relative range to the target. It is also desirable to make the measurement vectors as orthogonal as possible to minimize the intersection of the error bounds associated with each measurement. Section 1.2.3 provides more detail on the relationships between the vehicle state errors and the target estimation errors. These relationships can then be exploited to determine the optimal locations for taking measurements, leading to the development of vehicle trajectories that reduce the target localization error. Other elements that affect flight path generation, such as vehicle constraints, sensor constraints, computational limitations and mission requirements must also be considered. Target dynamics, environmental constraints, and disturbances must be taken into account as well, and the varying nature of these suggests that the solution should be updated in real time. The following sections provide more detail about the problem considered in this thesis, define the scope, and state the major assumptions made.

1.2.1 Platform Vehicle

The platform vehicle for this project is restricted to a small fixed-wing airplane. The concept of a UAS introduced above involves the entire unmanned system, including the vehicle, the ground station and other components. For this thesis the component of interest is the platform vehicle itself and this unmanned aerial vehicle will heretofore

be referred to as a UAV. The small UAVs considered in this thesis are equipped with rudimentary navigation systems involving low-grade inertial sensors and GPS receivers. They also have onboard imaging sensors (both IR and EO), controllable actuators (elevators and rudders), and basic onboard processing and communication capabilities. An example of such a vehicle is the Raven, made by AeroVironment, Inc (see Figure 1-1). Since most small UAVs are designed to be inexpensive and rugged the quality and accuracy of the sensors and onboard navigation systems leaves much to be desired. Typical navigation errors for these systems involve standard deviations of about 13 feet for position accuracy using GPS, 10 degrees for attitude using gyros (roll and pitch), and 5 degrees for heading using a magnetometer or electronic compass. Furthermore, in urban settings, magnetometer readings can be severely affected by the surrounding magnetic fields and the resulting heading errors are much larger.

In addition to poor navigation systems, small UAVs are also limited in their physical capabilities. Most have low control authority with either rudders or ailerons as actuators but not usually both, making coordinated turns difficult. The lightweight small UAVs are mostly battery operated and therefore have limited power and endurance. The environmental conditions for most small UAV operations include winds and gusts on the order of the vehicle's nominal speeds and maneuverability, which makes controlling the vehicle very difficult. The Raven for example has a nominal cruise speed of 30 mph, a climb rate of 900 ft/min, and a turn rate of 15 degrees/sec [60]. Controlling small UAVs in normal environmental conditions is therefore a very challenging task and the achievable accuracy in following a prescribed trajectory is fairly poor without real-time replanning capabilities.

The vehicle specifications of the Raven are listed in Table 1.1. The imaging sensors onboard the Raven include 2 electro-optical (EO) cameras or an infrared (IR) camera option. The electro-optical cameras are mounted such that one is forward looking and the other is side-looking, and the operator can select which camera is active and can receive the video output from one camera at the ground station in near real-time. Other UAV platforms include cameras mounted on gimbals which can be controlled to point the camera in the desired direction. An example of such a system is used in

Table 1.1: Raven Aircraft Characteristics [60]

Wingspan	55 in
Length	36 in
Structure	modular, Kevlar^{TM} composite
Weight	4.2 lb
Payload Nose Weight	6.5 oz
Operating Altitude	150 to 1,000 ft AGL
Nominal Low Altitude	100 ft
Cruise Speed	30 mph (13.5 m/s)
Range	10 km (LOS)
Climb Rate	900 ft/min at 2,000 ft AGL
Turn Rate	360 degrees in 24 sec
Aircraft Batteries	$LiSO_2$ (single-use), Li-Ion (rechargeable)
Flight Duration	60+ min rechargeable, 90+ min single-use

[61]. For both gimballed and fixed camera systems there are restrictions associated with obtaining imagery. For example, for the Raven the video clarity begins to degrade after 500 feet above ground level [60]. Due to radar horizon considerations, the UAV is restricted to maintain an altitude of at least 100 feet in order to properly communicate with the ground station, limiting how close the vehicle can get to the target. Effects that obscure the measurement process (poor lighting, fog or reduced visibility, recognition of targets at night, reflections etc) and frame drop-outs are problematic for most image based target localization algorithms. However, treatment of these conditions is assumed to be taken care of by the image processing algorithms and is therefore beyond the scope of this thesis.

In order to compute trajectories in real time it is necessary to have sufficient computational resources available for executing the algorithm. Most small UAVs currently have limited onboard computational capabilities. Algorithms can be executed on a ground station system and the answers relayed to the UAV, but the UAV must have sufficient communication bandwidth for this approach to be feasible. In general it is desirable to make the optimization algorithms as efficient and quick as possible so that they can be utilized in a real-time framework with limited communications bandwidth and computational resources.

1.2.2 Target Types and Behaviors

The targets of most interest within the current scope of the project include small stationary ground targets and small slow-moving ground targets. Small UAVs operate at an altitude between 100 to 1000 ft above ground level. The lower limit is due to radar horizon restrictions which make communication between the UAV and the ground station difficult below 100 ft. Even though the upper limit of operation is 1000 ft the image quality degrades above 500 ft, so the useful imagery data obtained by small UAVs involves mostly small stationary and slowly moving ground targets. These targets include cars, trucks, tanks, small buildings, portable missile launchers, and enemy combatants, among others. For this thesis the targets are characterized according to their motion and behavior and the main target types considered include stationary targets and targets whose behavior can be modeled as stochastic (slowly moving targets for which prior motion models are not available).

The stationary targets are the simplest to consider and will be used to analyze the baseline capabilities and performance of the optimization algorithms. The slowly moving stochastic targets can move in any random direction but have constraints on their achievable range and acceleration within a given time-frame. These targets include targets exhibiting random walk behavior, vehicles moving at a constant velocity, and vehicles following circular trajectories. Since, in practice, it is uncertain whether a motion or behavioral model of the target will be available, it is desirable to treat the behavior of all moving targets as stochastic. If further information is available, such as road maps or target classifications, it could be incorporated to improve estimation accuracy and convergence, however, for the purpose of this work no prior information is assumed.

1.2.3 System Dynamics and Measurement Model

The UAV is assumed to have six degrees of freedom (6DOF), 3 translational and 3 rotational. The target is assumed to remain on the ground, although its position must be estimated in three-dimensional space. In order to obtain a measurement it is

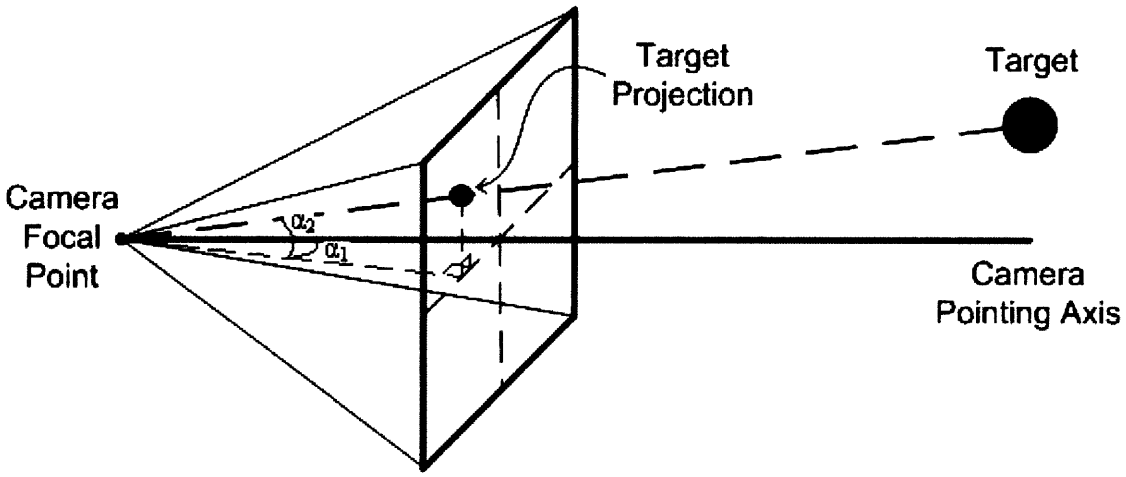

Figure 1-3: Measurement process

necessary at each measurement time to have: the UAV position and orientation, the camera pointing angle with respect to the UAV, and an image of the target in the video capture. The camera pointing angle with respect to the UAV is typically well known and can be either fixed or controllable for a camera mounted on gimbals. The vehicle position and orientation are taken from the UAV navigation system and usually have large errors that propagate into the target location estimation. As mentioned before the target location estimation error is affected by vehicle position errors, vehicle orientation errors and sensor noise. The vehicle position errors translate directly into the target estimation. The vehicle orientation errors scale with the relative range to the target and produce large estimation errors for measurements taken from far away. The image of the target taken at the appropriate measurement time can be processed to extract the pixel location of the centroid of the target. This pixel location can be transformed into two bearing angles (α_1 and α_2) from the camera pointing axis to a vector that passes through the target and through the camera focal point (see Figure 1-3). Using a series of simple rotations (from the camera frame to the UAV frame, and from the UAV frame to the earth relative frame), the two angles α_1 and α_2 can be transformed into overall azimuth and elevation angles (β and ϕ) between the target and the UAV. The resulting "measurement" can be modeled as a line from the UAV to the target and the azimuth and elevation angles used to define the bearing to the

target. Figure 1-4 shows the overall bearing angles to the vehicle with the target at the origin. The measurements are then given by,

$$\beta = \tan^{-1}\left(\frac{r_x}{r_y}\right) \tag{1.3}$$

$$\phi = \tan^{-1}\left(\frac{r_z}{\sqrt{r_x^2 + r_y^2}}\right) \tag{1.4}$$

The following equations can be used to describe the normalized components of the relative vector ($\mathbf{r}$) between the target and the vehicle using the bearing angles,

$$\begin{aligned} \frac{r_x}{|\mathbf{r}|} &= \sin\beta\cos\phi \\ \frac{r_y}{|\mathbf{r}|} &= \cos\beta\cos\phi \\ \frac{r_z}{|\mathbf{r}|} &= \sin\phi \end{aligned} \tag{1.5}$$

It is important to note that image-based measurements only provide bearing information to the target and not range. The magnitude of the relative vector, $|\mathbf{r}|$, therefore cannot be determined using only one measurement. Two or more measurements are needed to obtain an estimate of the target location.

Another major consideration for the design of the vehicle trajectory is ensuring that the target remains within the field of view (FOV) of the camera. A measurement is only valid if the target falls within the camera FOV. For a small UAV, the FOV constraints are usually fairly tight. Typical cameras used onboard small UAVs have vertical and horizontal FOVs of approximately 10 degrees and 20 degrees respectively. Using a gimballed camera system, such as in [61], the FOV constraints are more lenient since the camera can be pointed to face the target and therefore can usually maintain the target in the field of view. For the purpose of this thesis a gimballed camera system is assumed.

Additional constraints include limits on the allowable range to the target. As specified in [60], the visual quality of the measurements deteriorates above 500 ft AGL and, due to radar horizon considerations, the UAV cannot descend below 100

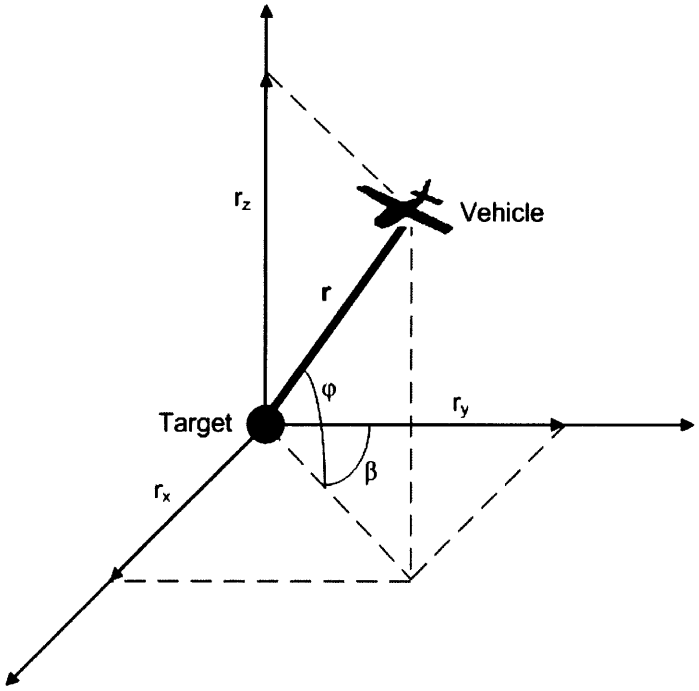

Figure 1-4: Azimuth (β) and elevation (ϕ) between vehicle and target

ft AGL. Given the resolution and FOV specifications of the camera, the range to the target must be low enough to ensure that there are enough pixels to properly identify the target. Additional complications arise from the skewing of the image due to the angle of the camera. These distortions change as the pitch and bank angle of the UAV change, complicating the measurement process. As mentioned before, for the purpose of this work it is assumed that software for image processing and target recognition is available and proper measurements are obtained.

1.2.4 Error Propagation

As mentioned in the previous sections, errors in the vehicle state estimation and the measurement process propagate into the target location estimate. This error propagation is highly dependent on the geometry of the vehicle trajectory. The purpose of this work is to exploit this dependence in order to produce trajectories that minimize the target localization error. In order to do this it is first necessary to understand how the errors propagate through to the estimation. Figure 1-5 illustrates how errors in vehicle position and orientation affect the target localization process.

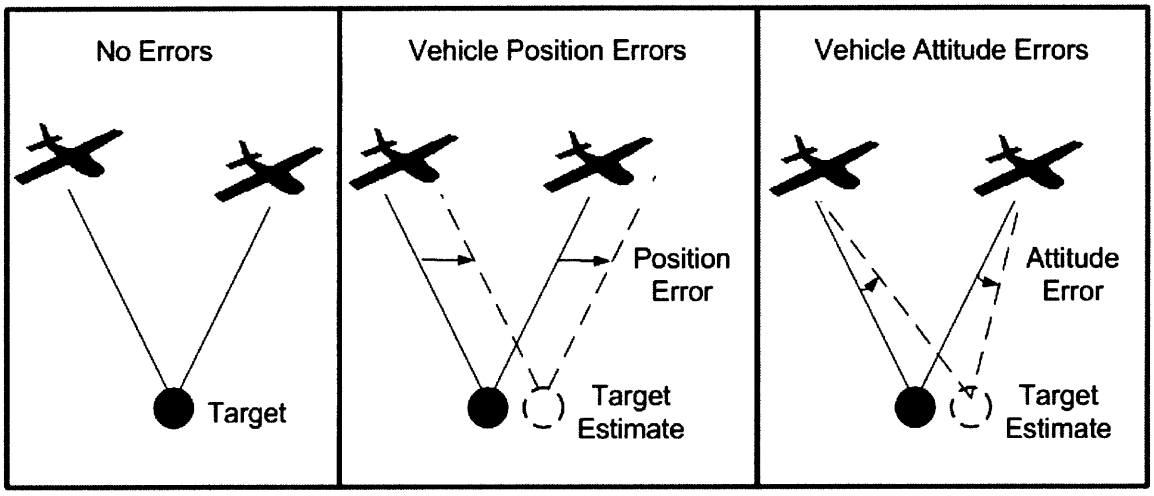

Figure 1-5: Effect of vehicle navigation errors on target location estimate

The vehicle position errors translate directly into the target location estimate, but the separation angle or orthogonality between the measurements controls how much the estimation is affected by vehicle position errors. For the vehicle orientation errors, separation angle between measurements and relative range to the target affect how much of the error is propagated through to the target localization. Figure 1-6 shows the effect of orthogonality and range on the resulting combined localization error. Orthogonal measurements produce a lower combined error than non-orthogonal measurements for both position and attitude errors. For vehicle position errors, a closer range to the target does not affect the combined error, but for vehicle attitude errors a reduced range greatly improves the target localization (see Figure 1-6).

In order to further study how the localization error is affected by the vehicle trajectory, an algorithm can be used to estimate the location of a stationary target using visual measurements taken from different vehicle positions. The algorithm is implemented in the MATLAB environment and uses an Extended Kalman Filter (EKF) to process the measurements. The vehicle navigation errors are assumed to be zero mean, white, and Gaussian, with standard deviations of 5 deg for attitude and heading. Figure 1-8 shows the resulting mean and variance of the localization error for four different vehicle trajectories; a full circle above the target, a quarter circle above the target, a fly-by to one side of the target, and a half fly-by (trajectories

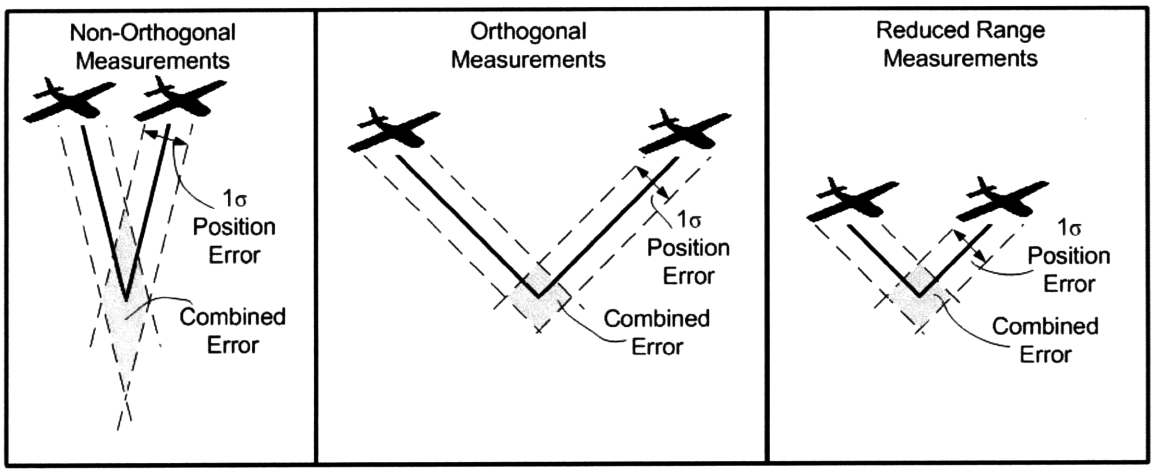

(a) Vehicle position errors

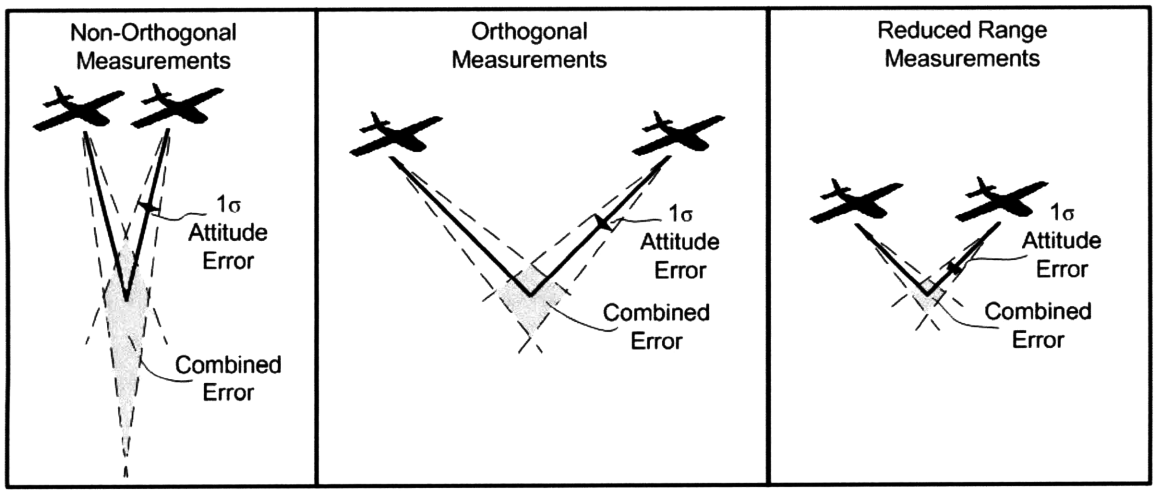

(b) Vehicle attitude errors

Figure 1-6: Effect of measurement orthogonality and range on target localization

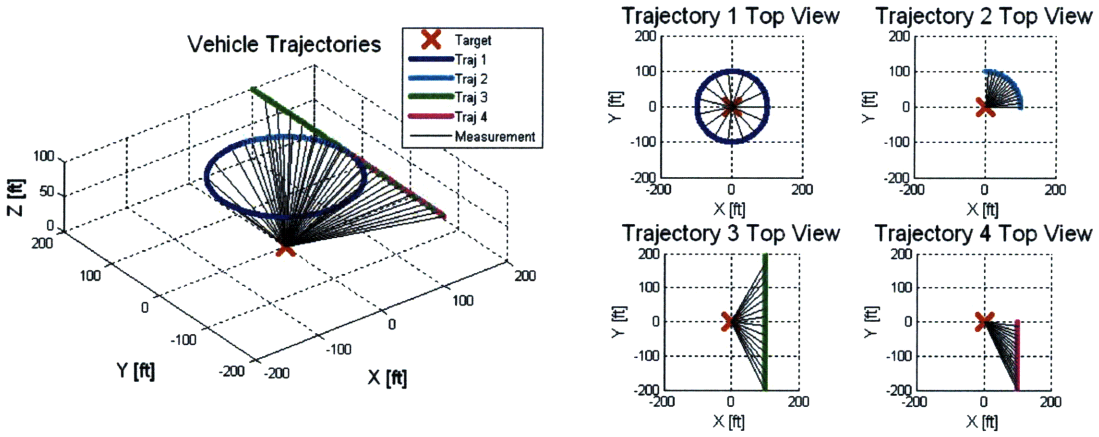

Figure 1-7: Vehicle trajectories for 3-D target localization

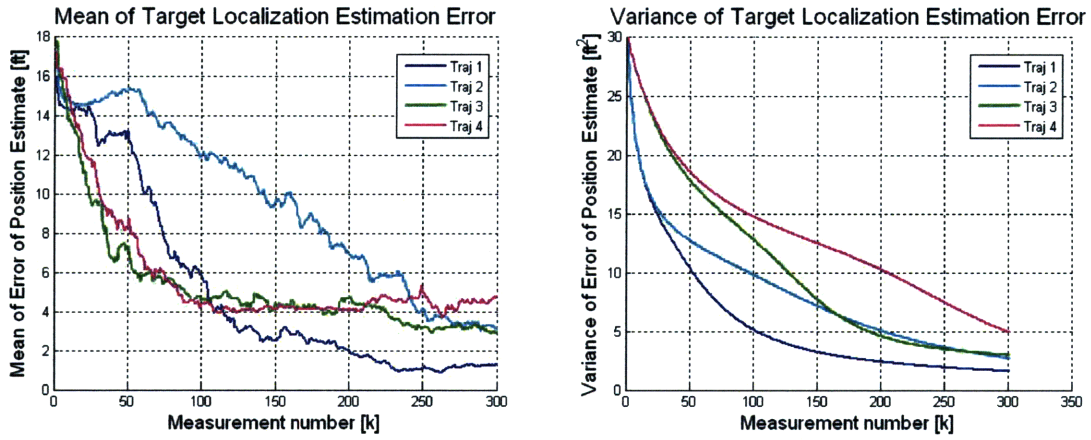

(a) Mean of Error

(b) Variance of Error

Figure 1-8: 3-D target localization results for trajectories in Figure 1-7

shown in Figure 1-7).

The plots in Figure 1-8 suggest that the geometry of the problem is significant since completing a full circle around the target results in a much lower mean and variance for the target localization error than the other trajectories. In particular, spreading the measurements over a full circle increases the separation angle or orthogonality between the measurements, thus improving the overall geometry for the estimation. This is similar to the geometric dilution of precision (GDOP) problem often seen in GPS, where the GDOP criterion is used to find the configuration of satellites that provides the best geometry and results in the lowest position estimation error.

Additional tests conducted to study the effects of range to the target show that lowering the range to the target reduces the target localization error. This is because the effects of the vehicle attitude errors on the target position estimate increase as the relative distance between the vehicle and the target increases.

While comparisons of ad-hoc trajectories show the underlying importance of selecting a good flight path, they do not provide a proper framework for designing such a path. It is necessary to develop a methodical way to analyze the geometry and understand how the errors in vehicle position, attitude and heading propagated into the target location estimate. The approach taken in this thesis is to use the Fisher Information Matrix to provide a framework for quantifying how much "information" is provided by a set of measurements. Maximizing this information content by positioning the vehicle leads to the development of flight trajectories that minimize the target localization error.

1.3 Literature Review

The problem of trajectory design for vision-based target localization has several related areas of research. The task of target localization and tracking has been studied extensively in many different contexts. There are numerous texts such as [9] and [64] dedicated entirely to target localization and tracking applications. For bearings-only target localization several important considerations for filter development and observability requirements have been explored in the context of passive sonar applications. More current research involves the extension of many of the passive sonar concepts to vision-based target localization using UAVs.

In addition to localization of targets, the dual problem of self localization using external references has also been extensively explored. Navigation using bearings-only measurements dates back to the days of celestial navigation where sailors triangulated their position based on angular measurements taken with respect to the stars. Modern day star trackers are still used for correcting dead-reckoning errors and bounding navigation drift in space applications. UAV navigation using feature tracking also

attempts to assist vehicle state estimates by using bearing measurements to fixed features in the environment. Research in simultaneous localization and mapping (SLAM), which deals with vehicle navigation as well as external target localization, has also been advancing rapidly. The following sections provide more detail for a few areas that are particulary relevant to the problem of trajectory design for vision-based target localization.

1.3.1 Bearings-only Target Tracking

The problem of bearings-only target estimation and tracking has a rich history in the context of passive sonar applications for underwater vehicles which dates back to the 1960's. Early research focuses mainly on analytical derivations for the observability criteria of the estimation process, and comparisons of the convergence properties and performance of the different types of filters used for passive target localization. Since bearings-only target estimation involves a non-linear measurement process, several filtering and observability complications arise. Lindgren and Gong [48] analyze the observability associated with a least-squares estimation approach and show that, for a constant velocity target and a constant velocity vehicle moving in a 2-D plane, the target estimation is unobservable until the vehicle executes a maneuver (change in heading). Nardone and Aidala [55] extend this work to show that a unique tracking solution cannot be obtained for a constant velocity target from a constant velocity vehicle; a vehicle maneuver is necessary for the observability matrix to be non-singular. However, the type of maneuver is important, and there exist maneuvers for which the target state will still remain unobservable. In other words, vehicle maneuvers are necessary but not sufficient conditions for estimation observability. Later work by Hammel [25] and also by Levine [47] extend these results to three-dimensional target and vehicle motion, Fogel and Gavish [18] derive the observability conditions for bearings-only target estimation for the case of N^{th} order target dynamics, and Becker [11] shows the necessary conditions for observability using a simple linear approach.

Several filter designs for bearings-only target estimation have been proposed. Lindgren and Gong use a least-squares approach [48], and maximum likelihood esti-

mation is used by De Vlieger [16] and by Tao [67]. Kalman Filtering techniques are used by Aidala [6] and by Nardone, Lindgren and Gong [54]. Since the bearings-only estimation problem involves nonlinear measurements, an Extended Kalman Filter (EKF) approach needs to be used instead of the normal Kalman Filter. The traditional EKF however is sensitive to initialization techniques and measurement errors which can cause premature covariance collapse and other filter instabilities [6]. The vehicle trajectory affects the observability and convergence of the target estimation, suggesting that a good trajectory design can reduce filter instability and estimation errors. A pseudolinear filter formulation is explored by Aidala and Nardone [7], which attempts to linearize the dynamics and measurement models. However by linearizing the dynamics the noise becomes non-Gaussian which, when propagated through the filter, causes estimation bias. For the bearings-only tracking problem, the bias is introduced only in the position estimate, and is highly dependent on the geometry of the vehicle maneuvers, once again suggesting that the estimation performance can be improved by proper design of the vehicle trajectory. Comparisons of the properties and performance between several different filtering algorithms are explored by Nardone, Lindgren and Gong [54]. A particularly interesting filter is the modified polar coordinates filter, proposed by Aidala and Hammel [5], which has become widely used in the passive target localization literature. The filter uses an EKF algorithm with a state vector choice, based on polar coordinates, that attempts to separate the observable and unobservable components of the estimated state by using a different coordinate system. The resulting filter is stable and asymptotically unbiased. Although this filtering approach became popular because of its convergence properties, it is important to stress that the choice of coordinate system does not affect the physics and geometry involved in the problem, it is merely a tool to improve the mathematic formulation and numerical properties of the estimation algorithm. In fact, the covariance formulation for the modified polar coordinate filter shows the dependence of the target estimation on the vehicle maneuvers, once again suggesting that the estimation can be improved by designing a good trajectory.

Although these previous works provide insight into the bearings-only tracking

problem, most of them assume constant velocity target motion, which is a rather limiting assumption. Later work by De Vlieger uses a piecewise linear model of the target motion and a Maximum Likelihood Estimator (MLE) approach for target tracking [16]. He uses numerical methods to condition the Jacobian of the measurement model to increase the observability of the estimation. Goshen-Meskin and Bar-Itzhack derive the observability requirements for piecewise constant linear systems [23]. Tao shows that for an MLE approach it is important to consider the correlation of the noise, and that ignoring it degrades the performance of the estimation [67]. Le Cadre also uses a piecewise linear model of the target and explores estimation from a multi-sensor platform [71]. He shows that the Fisher Information Matrix (FIM) can be used as a measure of the performance of the estimation and that some trajectories lead to more information than others. He explores positioning and trajectories of multi-array sensors for passive sonar target localization [71]. He also showes that the Fisher Information Matrix is additive for multiple sensors, and that focusing on the target velocity component can improve target localization performance [44]. Nardone also explores vehicle trajectory generation, presenting a closed-form solution to the estimation problem for a constant velocity target and a vehicle with piecewise constant velocity segments [56].

To deal with maneuvering sources, several modifications to the classical estimation algorithms have been explored. Some attempt to smooth the trajectory, adjusting maneuvers within the constraints of a known target behavior model. Others consist of designing multiple filters for different known maneuvers and using statistical properties of the innovation to switch between the algorithms. Another approach has been to support multiple Kalman filters simultaneously and develop an estimate by combining all the filters [1]. Later research by Bar-Shalom et al. [9] has focused on using interacting multiple models (IMM) and hidden Markov models (HMM) are used by Le Cadre [45] to support stochastic behavior of the target. Particle filtering or Sequential Monte Carlo techniques have also been explored by Ristic, Arulampalam, and Gordon [64]. Particle filters have the advantage of being able to deal with nonlinear systems

[1]For a review of different filtering methods for maneuvering targets see [45]

and non-Gaussian noise models making them particularly well suited to bearings-only tracking. They can also accommodate unknown and stochastic target models making them more versatile than classical filters. However, they require increased computational resources and, for proper and fast convergence, need a fairly accurate description of the measurement likelihood function and a good initial distribution on the estimated target location.

Later work using particle filtering focuses on tracking and estimation of multiple targets. Multiple target motion analysis suffers from the difficulty of associating measurements with the specific target tracks, making it a simultaneous data association and target estimation problem. Many algorithms based on the EKF, such as the Multiple Hypothesis Tracker (MHT), the Probabilistic MHT (PMHT), and the Joint Probabilistic Data Association Filter (JPDAF), have attempted to track multiple targets, however the hypothesis associations must be exhaustively enumerated leading to an NP-hard problem. Particle filters provide an easier framework for multiple target tracking. Hue, Le Cadre, and Perez solve the multiple target tracking problem for 2-D constant velocity targets using a particle filter combined with a Gibbs sampler [32] [31] [35] [34]. They show that using adaptive resampling techniques the multi-target estimation is greatly improved. They also show that particle filters can adequately support multiple measurement models for proper data fusion [34]. Le Cadre, Gauvrit, and Trarieux [43] and Hue, Le Cadre, and Perez [33] attempt to approximate the Cramér-Rao Lower Bound (CRLB) for the multiple target motion analysis case to quantify the performance of the multi-target estimation. Given the strong dependence of estimation performance on the vehicle's maneuvers, subsequent research of interest for this thesis focuses mainly on developing methods for optimizing the vehicle trajectory to achieve the best target estimation performance. The details of this research are described in section 1.3.2.

1.3.2 Vehicle Trajectory Optimization

In order to design optimal vehicle trajectories it is necessary to specify a performance criteria or objective function that can be optimized to provide the desired system

behavior. For the target localization problem this objective function must capture the geometry of the localization process. A common approach is to use objective functions derived from the Fisher Information Matrix (FIM). The FIM quantifies the amount of information provided by a set of measurements about the target state or parameter to be estimated. The inverse of the FIM provides a lower bound on the mean-square error achievable by any estimator of the target state. This bound is referred to in literature as the Cramér-Rao Lower Bound (CRLB), and is a lower bound on the covariance of the estimation for any unbiased estimator. It is important to note that the CRLB does not depend on the specific estimator used but is derived from the geometry and the properties of the system. It presents a tight lower bound on covariance for any unbiased estimator and, if an estimator achieves this lower bound, it is referred to as an *efficient* estimator.

It is desirable to obtain estimation results with the lowest possible covariance and thus the CRLB can be used to design an objective function to be minimized. Lowering the CRLB will naturally result in a lower covariance if the estimator is efficient, however it is important to note that a non-efficient estimator is not guaranteed to have a lower covariance even if the CRLB is lower. In practice though, lowering the CRLB results in lower covariance for most well-designed estimators. An equivalent objective function can be derived by maximizing the Fisher Information Matrix, which is a symmetric, positive definite matrix. This can be achieved by maximizing any norm of the matrix, and choosing a physically significant norm has been the subject of much research [72]. Some norms provide more information than others, however computational ease is also a factor in most optimization scenarios. For example, the determinant of the FIM provides more geometric information for the bearings-only problem than the trace of the FIM, but the trace is easier to compute and can be updated recursively whilst the determinant is much more involved and must be recomputed at every measurement time.

Past research on vehicle trajectory optimization by Le Cadre et al. includes [40], [41], and [42], where the determinant of the FIM is used as a cost function and the target and vehicle trajectories are assumed to be piecewise linear. Maximizing the

determinant of the FIM is equivalent to minimizing the volume of the confidence ellipsoid around the estimate of the target. It is a function of the multiplication of the eigenvalues and therefore could favor solutions with highly eccentric uncertainty ellipsoids (as long as one eigenvalue is small the multiplication will be small regardless of the other values). An interesting point in [40] is that the determinant of the FIM does not satisfy the Additive Monotonicity Property[2], therefore optimizing a control value $u[k+1]$ and adding it to an already existing sequence of optimal controls $U = \{u[0], ..., u[k]\}$ does not necessarily provide the optimal answer for the whole sequence of controls. Le Cadre et al. derive approximations for the determinant of the FIM to use as objective functions in the optimization [40] [41] [42]. However, Oshman and Davidson [57] use the determinant of the FIM directly and show that the trajectories obtained result in better target estimation than methods based on lower bounds or approximations of the determinant.

For the bearings-only tracking problem another complication arises from the non-linear measurement model. The Jacobian of the measurement, H, is time-varying due to the nonlinearity of the measurement model and this in turn causes the FIM to be time-varying as well. It also complicates the observability analysis, however, for a constant velocity target, the estimation will be observable if the vehicle maneuvers involve non-zero bearing rates between the trajectory legs [55] [25]. Fawcett [17] computes the CRLB for the estimation of a 2-D constant velocity target. He also derives an analytic approximation for the FIM in the modified polar coordinate framework. The objective function for the optimization is the standard deviation value for the range only, since this is the state of most interest and least information (or largest uncertainty) in the bearings-only tracking framework. He compares the Maximum Likelihood Estimator (MLE) covariance results and shows that they match the CRLB fairly well. Another approach taken by Helferty and Mudgettin is to minimize the trace of a weighted sum of the CRLB [27] [28]. This method favors equal uncertainty in all observation axes. It is interesting to note that objective functions based on the CRLB instead of the FIM may "blow up" due to the singularity in the estimation

[2]For a description and explanation of the Additive Monotonicity Property see [40]

process if the estimation is unobservable. They compute the CRLB by first deriving a continuous time version of the FIM, resulting in vehicle paths that are independent of the number and frequency of observations, giving slightly different trajectories than the discrete-time case [27] [28]. To the author's knowledge, there are no approaches that use the trace of the FIM since most of the angular information between the measurements is lost. The trace of the CRLB, however, represents the sum of the eigenvalues of the covariance matrix and is equivalent to the sum of the squares of each axis of the confidence ellipsoid. This approach makes sure that there are no axes with large uncertainties, leading to smaller range errors than trajectories based on the determinant of the FIM. Another approach is to use the error covariance of the target state estimate instead of the CRLB. In practice however, one does not have access to the true target state, therefore computation of the CRLB and of the target state error covariance matrix is equivalent. Logothetis, Isaksson, and Evans use scalar functions based on the error covariance of the final target state and compare the trace, determinant and maximum eigenvalue, as potential objective functions [50]. Frew uses the determinant of the error covariance matrix provided at every time step as the objective function of choice [20].

All of the above research involves computing trajectories by solving the optimization numerically. Other approaches taken by Liu [49] and by Passerieux and Van Cappel [59] involve using a classical optimal control framework to solve the optimization analytically. Liu gives the analytic expression for a lower bound on the determinant of the FIM and computes the Hamilton-Jacobi-Bellman equation to maximize this lower bound [49]. The target is assumed to be stationary and the dynamics are 2-D. Since the results are analytic expressions, these results are not immediately scalable to more complicated scenarios (moving targets and 3-D dynamics). Passerieux and Van Cappel use a cost function based on the log of the determinant of the FIM computed at the final time only [59]. Since the objective is to find a path that maximizes the information for the whole set of measurements only the final time FIM is considered, which greatly simplifies the Hamiltonian. The objective function used is referred to as the global accuracy criterion, $Q = -\log|J(T)|$, and it minimizes the volume of

the uncertainty ellipsoid at the final time T. Classical control techniques based on the Hamiltonian and Euler's equations are used to solve the case of a constant velocity target in 2-D. Analytic expressions for the costates are computed and the Euler equations are integrated analytically as well. Results show that the vehicle wants to maneuver towards the target and in such a way that bearing rate is maximized, supporting the intuition about the problem and results from past research with numerical optimization approaches. Again these results are not easily scalable to more complex target motions or 3-D dynamics.

Later research focuses on optimal vehicle maneuvers for estimation of stochastic targets, eliminating the assumptions of stationary or constant velocity targets and allowing for random target motion. Tremois and Le Cadre attempt to deal with maneuvering targets by using hidden Markov models [70] [45]. They use a dynamic programming algorithm to find the sequence of states that maximizes the conditional probability given a set of measurements. The optimization of the vehicle trajectory consists of controlling a partially observable Markov decision process (POMDP) using a cost functional based on the Fisher Information Matrix. The results show that when the vehicle is far from the target it is best to move orthogonally to the line of sight to the target, thus increasing the overall observability of the estimation. When the vehicle is near the target however, it is better to get closer to it to minimize the effect of range on the angular errors. These results agree with the intuition provided by the geometry of the problem and with previous results by Liu [49] and by Passerieux and Van Cappel [59]. The results show the limiting behavior of the information-based optimization but not the strategy for the intermediate cases. Another approach taken by Singh, Ba-Ngu, Doucet, and Evans is to model the target as a Jump Markov Linear Model (JMLM) and use the score-gradient estimator as the objective function [65]. Hernandez assumes stochastic target behavior and computes the FIM and the PCRLB recursively for the 2-D case. He also shows an efficient search method for improved numerical optimization [29].

1.3.3 Vision-Based Target Localization

Although most of the previous research in bearings-only tracking and vehicle trajectory optimization has been done within a passive sonar context, recent attention has been given to the problem of vision-based target localization, which shares the same mathematical framework as the passive sonar problem. Small UAVs equipped with video cameras are gaining popularity and their use in target tracking is the topic of many current research endeavors. Ivey and Johnson consider the problem of developing a vision-based target tracking filter for use on board a UAV [36]. They attempt to estimate the target location as well as its size and orientation using both an Extended Kalman Filter (EKF) and a Square-Root Unscented Kalman Filter (SRUKF). Barber, Redding, Mclain, Beard, and Taylor explore the problem of localizing stationary targets using small fixed-wing UAVs [10]. They use a Recursive Least Squares (RLS) filtering approach and account for navigation biases and wind to improve the estimation. They also explore the problem of flight path optimization by finding an optimal altitude and radius for a circular trajectory above the stationary target. Due to its symmetry a circular trajectory leads to a lower target localization error making it widely accepted as the optimal trajectory. Rafi, Khan, Shafiq, and Shah also analyze circular trajectories of fixed altitude for tracking stationary and constant velocity targets, and optimize the radius of the circle for the lowest target localization error [62]. They explore vehicle constraints such as airplane turn radius and velocity requirements as well as camera field-of-view constraints. The use of gimballed cameras is considered to increase the overall FOV and to ensure that the target is always within sight. Quigley, Goodrich, Griffiths, Eldredge, and Beard also explore the use of gimballed cameras on board a small UAV, stating that the gimbals improve the quantity and quality of the imaging [61]. They use a gimbal mechanism with an azimuth limit of 135 degrees and show in hardware that the gimbals are robust and can withstand crashes. They also address the problem of trajectory planning, using Hopf bifurcation techniques that result in spiral trajectories which converge to a constant radius circle (altitude is assumed constant). These results for the stationary target case rely

on limit cycle behavior, and although an ad-hoc approach at trajectory planning is taken, the results capture the geometric intuition of the bearings-only target tracking problem. Frew explores the problem of trajectory planning using a 2-D ground robot equipped with a vision-based sensor [20]. He uses the determinant of the error covariance matrix of the target state as the objective function for the optimization and generates trajectories that are valid for a ground robot with a limited field of view. Similar work by Kuang and Liu uses omnidirectional 2-D robots with stereo vision to track a target [39]. A least squares filter is implemented and maneuver optimization that minimizes the error estimation in a least squares sense is considered.

The problem of coordinated flight for multiple UAVs has also been studied. Frew, Dixon, Argrow and Brown design trajectories for a network of UAVs for radio source localization using an information-theoretic approach [19]. They explore receding horizon techniques as well as a cost function based on the recursive form of the FIM. Bethke, Valenti, and How consider the use of multiple quad-rotor UAVs for cooperative target tracking using a RLS approach [12]. Watanabe, Johnson and Calise consider a formation of two airplanes circling a stationary target [73]. The trajectories are created using an optimization cost function based on the variance of the target position estimate and an assumption of constant altitude. Whitacre and Campbell explore the problem of designing orbits for two UAVs circling a target [74]. An approximation of the information matrix for the target tracking problem is used as the cost function and the results show coordinated periodic orbits assuming constant altitude. Wise and Rysdyk show coordinated flight for two UAVs for tracking a moving target in windy conditions [75]. The guidance laws used are based on Helmsman behavior, Lyapunov vector fields and controlled collective motion and the different approaches are compared. Ousingsawat and Campbell design trajectories for multiple vehicles to track stationary, moving and multiple targets [58]. They use an objective function based on the determinant of the FIM and receding horizon control techniques to develop the vehicle trajectories. Arambel, Silver, Krant, Antone, and Strat also consider the problem of tracking multiple ground targets, but using a multi-hypothesis approach [8]. A novel application of the target tracking problem is considered by

Calise, Johnson, Sattigeri, Watanabe and Madyasthain, where vision-based localization is used for detecting and tracking other aircraft and enabling formation flight of a fleet [13]. The target tracking filter used is an EKF based on a modified polar coordinate framework (described in [5]).

In addition to vehicle guidance, control and navigation, extensive research has been done in the areas of automatic target recognition (ATR) and machine vision[3]. Specific challenges of vision-based target tracking include dealing with image differences and distortions due to the changes in the projection angle of the camera to the target as the target and the vehicle move [26]. Furthermore, changes in the lighting, reflections and the target itself may further complicate the automatic target recognition process. Research in image processing and algorithm development for vision-based target tracking methods has focused mainly on obtaining and processing a set of "measurements" from the image, that is, recognizing the target in successive frames. For the purpose of this thesis, a measurement is assumed to be given if the target is close enough and within the field of view of the camera, and therefore the specifics of the automatic target recognition process are beyond the scope of this thesis.

1.3.4 Sensor Placement Techniques

Another important area of research for this thesis involves exploring techniques for optimally placing sensors in order to estimate parameters of interest. The mathematical framework for sensor placement problems is very similar to that of trajectory optimization, however, the motion constraints of the system are not included. In general, sensor placement techniques involve positioning stationary sensors in an optimal configuration so as to minimize the estimation error of the parameter of interest, whereas most trajectory optimization problems involve active positioning of a moving sensor with given motion constraints. Therefore the sensor placement scenario could be considered a limiting case of the general trajectory generation problem involving

[3]For a complete description of machine vision and related challenges see [30]. For a survey on recent vision-based target tracking and autonomous vehicle navigation developments see [37]

an unconstrained vehicle dynamics assumption. Uciński provides an excellent review of the state-of-the-art of optimal measurement methods for distributed parameter system identification [72]. Several sensor placement methods involve optimizing over cost functions based on the FIM in order to maximize the information content provided by a set of measurements. There are a few issues with using a FIM based approach. One of the main issues is that the calculation of the FIM involves the parameter to be estimated, which, by virtue of the problem statement, is an unknown quantity. If the estimation and sensor placement problems are combined, the dependence of sensor optimization on the parameters to be estimated creates a highly nonlinear problem which is difficult to solve using classical techniques. Another issue is deciding on a scalar cost function based on the FIM. There are many different types of optimality criteria and in several cases it is unclear which the best one to choose is. Uciński gives several examples of past research in sensor placement and describes the advantages and disadvantages of different optimality criteria [72].

More current research focuses on the problem of data fusion. Grocholsky, Makarenko, and Durrant-Whyte explore the use of multiple sensor platforms for bearings-only tracking [24]. They use the log of the determinant of a predicted version of the FIM as the cost function and develop sensor trajectories that optimize the amount of information provided. Sinha, Kirubarajan, and Bar-Shalom study the problem of coordinating the placement of UAVs equipped with Ground Moving Target Indicators (GMTI) for tracking ground targets [66]. They compute a recursive version of the FIM and use gradient methods to numerically optimize the placement of the UAVs. Martínez and Bullo focus on sensor placement techniques for target tracking using range based measurements [53]. They compute the determinant of the FIM and provide an analytic derivation of the cost function. An interesting result is that assuming uncorrelated noise between the sensors leads to configurations which place multiple sensors at one location [72]. Mandic and Frazzoli study the placement of ground sensors for the localization of a sniper using acoustic (range-based) measurements [52]. An expression for the determinant of the FIM is provided and gradient methods are used to numerically optimize the placement of the sensors. To deal with the unknown

nature of the target an *a priori* stochastic distribution for the target is considered and an expected value of the cost over the target distribution is used in the optimization. Frew explores the problem of optimal sensor placement using range and bearing sensors equipped with communications capabilities, producing results that differ from the classical approach of decentralized sensors [21]. Kaplan and Cevher study sensor management for fusing bearings-only sensors with different constraints and capabilities [38]. They use an information-theoretic approach to optimize the location of the sensors for target localization. Most of the current research in sensor placement and data fusion focuses on information-theoretic methods because of the ease of computation and the intuition provided by an information based approach. But perhaps the most valuable property of the Fisher Information Matrix is that it is additive, providing a framework for easily integrating multiple sensors, fusing different types of sensors, optimizing the trajectory of one sensor, or combining all of these to produce optimal trajectories for multiple coordinated sensors.

1.4 Thesis Objectives

This thesis focuses on developing trajectories for small UAVs to perform target localization using vision-based sensors. The main goal of this thesis is to provide methods for designing UAV trajectories that increase the information provided to the estimation, and to show that by using these optimal trajectories the estimation performance can be greatly enhanced. One of the objectives of this thesis involves exploring different filtering algorithms and showing in detail the relationship between the Fisher Information Matrix, the observability matrix, and the covariance matrices of some of these filtering methods, motivating the use of information-theoretic trajectory optimization to enhance estimation performance and increase observability. Most current literature states that the Fisher Information Matrix and Cramér-Rao Lower Bound are used to provide theoretical limits on the estimation performance and are therefore independent of the particular estimation algorithm used. In fact, the derivations and connections provided in Chapter 2 show that the FIM truly represents the physical

and geometrical properties of the system and that the estimation performance of most traditional filtering methods is closely tied to the FIM.

A contribution of this work involves developing estimation algorithms for the 3-D bearings-only target localization problem. In particular, an Extended Kalman Filter and a Particle Filter are designed for use in 3-D target localization for many different target motion scenarios. The resulting performance of the filtering algorithms shows that these methods can be used to track stationary and moving targets, even when the target motion is unknown. Another contribution involves deriving the FIM for the 3-D bearings-only target localization problem and comparing several different objective functions, showing that the A-optimality criterion, the trace of the inverse of the FIM, is the best suited objective function for the 3-D bearings-only target localization problem. The determinant of the FIM is widely used in the literature as the objective function of choice for information-based optimization problems, however, for the 3-D bearings-only target localization problem, the sensitivity of the determinant of the FIM to the relative range to the target is much larger than its sensitivity to the angular separation between measurements, and optimization using the determinant tends to ignore important information regarding the angular separation between measurements. The A-optimality criterion, however, more accurately represents the physical and geometric consideration for reducing the error in the 3-D bearings-only target localization problem. Furthermore, this choice of objective function is shown to be equivalent to the geometric dilution of precision (GDOP) criteria used in GPS navigation to select the optimal configuration of satellites, providing a geometric interpretation for FIM based optimization.

Another contribution of this work involves developing optimal information-based trajectories for several different cases of target motion and vehicle dynamics for the 3-D bearings-only target localization problem, and showing the basic trends associated with these trajectories, thereby providing a physical intuition about the problem. A rigorous mathematical framework is provided for performing information-theoretic optimization in many different scenarios and a few of the cases in the literature are shown to be particular instances of these scenarios. For example, unconstrained vehicle tra-

jectory optimization (or the sensor placement case shown in Section 3.2.1 produces circular trajectories above the target, a result which is widely accepted throughout the literature [10] [62]. Considering vehicle velocity and turn rate constraints produces spiral trajectories that minimize the relative range to the target while making subsequent measurement vectors as orthogonal as possible. Both the circle and the spiral trajectories demonstrate the tradeoff between reducing the relative range to the target and increasing the angular separation between the measurements, thus providing the best geometric configuration for the measurements and supporting the intuitions developed in Section 1.2.4. Several different scenarios for vehicle constraints are considered and the results show that the optimal trajectories attempt to spiral in as close to the target as possible, within the vehicle's turn rate constraints, and subsequently circle the target to come in for another spiral pass. The information increase is shown to be sharper and the information rate higher when the relative range to the target is the lowest. Several cases of slow and fast moving targets are considered and the trajectories are shown to follow spirals, adjusting their shape to account for the target's motion. The multiple target scenario is also considered, once again showing the spiral trajectory, and also showing that the optimal information-theoretic move is to spiral towards farther targets instead of circling around near targets again, since the information rate is higher for farther targets.

Another contribution involves addressing the problem of the dependence of the FIM on the actual target location by invoking the Certainty Equivalence Principle and executing simultaneous estimation and optimization, using the estimated target location for the FIM computations in the optimization. This approach is demonstrated to have increased estimation convergence and better observability. The optimal UAV trajectories are shown to follow the spiral shape once again, and the estimation achieves the desired accuracy and convergence using only half the measurements needed in the case of the predefined circular UAV trajectory. The combined estimation and optimization algorithms are shown to run in real time and within the computational resources of a small UAV. Another approach for dealing with the uncertainty in the target location involves using a probabilistic distribution of the target

location in the optimization by taking the expected value of the FIM over the target distribution. This approach is combined with a particle filter algorithm, where the particles with their respective weights are used to represent the stochastic target distribution in the optimization. Although this method shows enhanced robustness, the computational requirements are not within the limitations of small UAV processors and therefore can not be used in real time. However, this approach could be used to initialize the UAV trajectory for situations with unusual initial target distributions. The main objective of this thesis is to show that the Fisher Information Matrix provides a good framework for the trajectory optimization problem. In addition to representing the system dynamics physically and geometrically, the FIM is additive and can be updated recursively, which provides a simple and computationally efficient way of integrating several measurements. This additive property can be used to combine measurements from several different types of sensors over many time-steps, making the FIM ideally suited for estimation problems involving heterogenous teams with several different sensing systems collaborating to provide a target location estimate.

1.5 Thesis Layout

This section describes the layout of the thesis. Chapter 1 provides an introduction and motivates the problem of target localization using small UAVs. It then describes the system dynamics and the main challenges associated with this problem and includes a review of the current literature, discussing relevant previous work. It ends with a description of the thesis objectives and contributions. Chapter 2 describes the estimation process and the criteria used to quantify the performance of a given estimator. It also presents a few common estimation algorithms and shows their relationship to the Fisher Information Matrix. It ends with examples of two estimation algorithms, the Extended Kalman Filter and the Particle Filter, applied to the problem of target localization with bearings-only measurements using a UAV with a predefined trajectory. Chapter 3 describes the task of vehicle trajectory optimization with

the goal of improving the target localization by increasing the information provided by the measurements and improving the observability of the estimation. It focuses on deriving and comparing different cost functionals based on the Fisher Information Matrix and shows optimal vehicle trajectories which maximize the amount of information obtained for different cases of target behavior and vehicle constraints. The optimization in Chapter 3 assumes that the target location is known, an obviously invalid assumption which is the problem faced in most joint estimation and trajectory planning problems. Chapter 4 explores the issue of uncertain target location by invoking the Certainty Equivalence Principle [63] and tying together the target location estimation from Chapter 2 and the vehicle trajectory optimization from Chapter 3. The estimation and optimization algorithms are run sequentially and updated in real-time. The combined algorithm is shown to converge and the estimation results are significantly better than those obtained in Chapter 2 using the predefined vehicle trajectories. Another approach explored in Chapter 4 to accommodate stochastic target behavior involves performing the optimization using the expected value of the FIM over a probabilistic distribution on the target instead of the deterministic FIM based on the true target value. This approach is combined with a particle filter, using the particles and their weights to represent the stochastic target distribution. The results in Chapter 4 show that improved estimation performance is obtained by planning trajectories in real-time to maximize the information, rather than using a predefined circular trajectory above the target which is currently the most common approach. Chapter 5 concludes with a summary and discussion of the results and a description of future work.

THIS PAGE INTENTIONALLY LEFT BLANK

Chapter 2

Target Location Estimation

The problem of target localization and tracking using bearings-only measurements is a difficult task. The filtering algorithms involve a nonlinear measurement process, which, when linearized, can lead to time-varying parameters, biases and in some cases premature filter collapse as explained by Aidala in [6]. The most common estimation algorithms used for bearings-only target localization are: Least Squares (batch and recursive forms), Maximum Likelihood Estimator, Extended Kalman Filter, and Particle Filters or Bayesian Methods. This chapter describes the overall estimation process and performance expectations. It also shows details for a few of the most common estimation algorithms and ends with applications of these techniques to the problem of target localization using bearings-only measurements.

2.1 Estimation Performance

The most common measures of performance for an estimator are the mean and covariance of the estimation error. The objective of an estimator is to ensure that the mean of the estimation error is as small as possible. The covariance of the estimation error represents the uncertainty associated with the accuracy of the estimation results. The covariance should ideally also be as low as possible but can only be lowered up to a certain limit defined by the Cramér-Rao Lower Bound (CRLB). The CRLB is based on the physical properties of the system and the geometry associated with

the estimation problem. It provides a tight lower bound on the achievable covariance of the estimator. The performance of any unbiased estimator can be quantified by comparing its covariance to the Cramér-Rao Lower Bound. Any unbiased estimator that achieves this lower bound is called *efficient*. The CRLB is really a measure of the achievable mean square error of the estimation process, but for an unbiased estimator the mean square error is equivalent to the covariance of the estimation. It is important to note that the CRLB is not a function of the estimation method but of dynamics of the system and the geometry of the estimation problem. Therefore it provides a limit on the best possible answer (lowest uncertainty) that can be obtained for a particular system using a specific set of measurements. Its inverse is referred to as the Fisher Information Matrix (FIM) and provides a measure of the amount of information contained in a given set of measurements about the states to be estimated. The following section introduces the formal definitions of the FIM and the CRLB.

2.1.1 Cramér-Rao Lower Bound and the Fisher Information Matrix

This section shows the derivation of the Fisher Information Matrix and the Cramér-Rao Lower Bound. The concept of Fisher Information can be addressed within the framework of Information Theory, which explains the connections between the entropy or uncertainty about an estimation process and the information provided by measurements. Here, the entropy of a random variable is a measure of its uncertainty, or the self-information contained in that random variable. It quantifies the average number of bits needed to represent a data sequence. Entropy in the discrete case is defined by

$$H(X) = -\sum_{x \in X} p(x) \log_2 p(x) \tag{2.1}$$

where X is the random variable and $p(x)$ is its probability distribution. This definition of entropy provides a measure of how rich in information a data stream is, and can be

used to determine the minimum amount of bits required for communicating a certain amount of information. The concept can be extended to the problem of parameter estimation, where the entropy of the estimation is a measure of how much information the measurements provide about the estimation process. Not all measurements provide equal amounts of information and some measurement sets contain more overall information than others, leading to a reduced entropy and uncertainty in the estimation process. Another concept closely related to entropy is Fisher Information. The Fisher Information Matrix is used to quantify the information contained in a set of measurements about an estimation process. The FIM can then be used to determine the location of measurements such that this information content is maximized, thus lowering the uncertainty in the estimation.

To derive the Fisher Information Matrix we start with the information inequality, as described in [46], which is given by

$$\mathbf{P} = \mathbb{E}_{\mathbf{x}}\left\{[\delta_{\mathbf{x}}(\mathbf{z}) - \mathbf{x}][\delta_{\mathbf{x}}(\mathbf{z}) - \mathbf{x}]^T\right\} \geq \mathbf{J}(\mathbf{x})^{-1} \tag{2.2}$$

Here $\mathbf{x}$ is the vector of parameters to be estimated, $\delta_{\mathbf{x}}(\mathbf{z})$ is any estimator of the parameters $\mathbf{x}$ given the data $\mathbf{z}$, and $\mathbf{P}$ represents the covariance matrix of the estimation error. The Cramér-Rao Lower Bound is the lower bound on the estimation error covariance and is given by $\mathbf{J}(\mathbf{x})^{-1}$ where $\mathbf{J}(\mathbf{x})$ is the Fisher Information Matrix for $\mathbf{x}$.

For the scalar case, the Fisher Information is defined by the following expression,

$$J(x) = \mathbb{E}_{\mathbf{x}}\left\{\left[\frac{\partial}{\partial x}\log p(x, \mathbf{z})\right]^2\right\} \tag{2.3}$$

where $p(x, \mathbf{z})$ is the joint probability density of the parameter x and the measurements $\mathbf{z}$. If the following regularity condition is met,

$$\int_D \frac{\partial^2}{\partial x^2} p(x, \mathbf{z}) dx = 0 \tag{2.4}$$

where D is the domain of the probability density $p(x, \mathbf{z})$, then the FIM can also be

written as

$$J(x) = \mathbb{E}_{\mathbf{x}}\left\{-\frac{\partial^2}{\partial x^2}\log p(x,\mathbf{z})\right\} \tag{2.5}$$

It is interesting to note that the score function, $\frac{\partial}{\partial x}\log p(x,\mathbf{z})$, can be rewritten as

$$\frac{\partial}{\partial x}\log p(x,\mathbf{z}) = \frac{\frac{\partial}{\partial x}p(x,\mathbf{z})}{p(x,\mathbf{z})} \tag{2.6}$$

which is the normalized relative rate at which the density $p(x,\mathbf{z})$ changes at a specific value of x. One interpretation of Fisher information is that the greater $J(x)$ is at $x = x_0$, the higher the relative rate of density change is and the easier it is to separate x_0 from the surrounding values of x. Therefore x can be estimated more accurately when the information is higher (this is true for large samples under certain assumptions, see [46]).

As described in [46], the Fisher Information Matrix for the multi-parameter case is given by

$$\begin{aligned}\mathbf{J}(\mathbf{x}) &= \mathbb{E}\big\{[\nabla_{\mathbf{x}}\log p(\mathbf{x},\mathbf{z})][\nabla_{\mathbf{x}}\log p(\mathbf{x},\mathbf{z})]^T\big\} \\ &= \mathbb{E}\big\{-\nabla_{\mathbf{x}}[\nabla_{\mathbf{x}}\log p(\mathbf{x},\mathbf{z})]^T\big\}\end{aligned} \tag{2.7}$$

where $\mathbf{x} = [x_1 \dots x_n]^T$ is the vector of the n parameters to be estimated, $\nabla_{\mathbf{x}} = [\frac{\partial}{\partial x_1} \dots \frac{\partial}{\partial x_n}]^T$ is the gradient operator with respect to $\mathbf{x}$, and $\mathbf{J}(\mathbf{x})$ is $n \times n$. Using the following fact,

$$p(\mathbf{x},\mathbf{z}) = p(\mathbf{z}|\mathbf{x})p(\mathbf{x}) \tag{2.8}$$

the FIM can be rewritten as

$$\mathbf{J}(\mathbf{x}) = \mathbf{J_D}(\mathbf{x}) + \mathbf{J_P}(\mathbf{x}) \tag{2.9}$$

where

$$\mathbf{J_D}(\mathbf{x}) = \mathbb{E}\{-\nabla_{\mathbf{x}}[\nabla_{\mathbf{x}} \log p(\mathbf{z}|\mathbf{x})]^T\} \tag{2.10}$$

$$\mathbf{J_P}(\mathbf{x}) = \mathbb{E}\{-\nabla_{\mathbf{x}}[\nabla_{\mathbf{x}} \log p(\mathbf{x})]^T\} \tag{2.11}$$

Here $\mathbf{J_P}(\mathbf{x})$ represents the *a priori* information about the parameters and $\mathbf{J_D}(\mathbf{x})$ is the information obtained from the measurements. Note that the definition of the Fisher Information Matrix assumes constant or slowly-varying parameters.

Computing the Fisher Information Matrix at each time-step is a tedious process since it involves accounting for all the measurements taken up to that time. It is desirable to use a recursive version of the FIM instead that can be updated every time a new measurement is obtained. Tichavsky et al. [69] present a recursive method for computing the FIM at time k, which is illustrated below for the target tracking problem. The details of the derivation are presented in Appendix A and in [69] and [64].

For the target tracking problem the bound of interest is given by

$$\mathbf{P}_{k|k} = \mathbb{E}\{[\hat{\mathbf{x}}_{k|k} - \mathbf{x}_k][\hat{\mathbf{x}}_{k|k} - \mathbf{x}_k]^T\} \geq \mathbf{J}_k^{-1} \tag{2.12}$$

where $\mathbf{x}_k$ is the true state of the target at time k, $\hat{\mathbf{x}}_{k|k}$ is the estimate of the target at time k given the measurements obtained up to that time, and $\mathbf{P}_{k|k}$ is the covariance of the error for the estimate at time k given all the measurements up to time k. The recursive form of $\mathbf{J}_k$ is given by

$$\mathbf{J}_{k+1} = \mathbf{D}_k^{22} - \mathbf{D}_k^{21}(\mathbf{J}_k + \mathbf{D}_k^{11})^{-1}\mathbf{D}_k^{12} \tag{2.13}$$

where

$$\begin{aligned}
\mathbf{D}_k^{11} &= -\mathbb{E}\left\{\nabla_{\mathbf{x}_k}\left[\nabla_{\mathbf{x}_k}\log p(\mathbf{x}_{k+1}|\mathbf{x}_k)\right]^T\right\} \\
\mathbf{D}_k^{21} &= -\mathbb{E}\left\{\nabla_{\mathbf{x}_k}\left[\nabla_{\mathbf{x}_{k+1}}\log p(\mathbf{x}_{k+1}|\mathbf{x}_k)\right]^T\right\} \\
\mathbf{D}_k^{12} &= -\mathbb{E}\left\{\nabla_{\mathbf{x}_{k+1}}\left[\nabla_{\mathbf{x}_k}\log p(\mathbf{x}_{k+1}|\mathbf{x}_k)\right]^T\right\} = [\mathbf{D}_k^{21}]^T \\
\mathbf{D}_k^{22} &= -\mathbb{E}\left\{\nabla_{\mathbf{x}_{k+1}}\left[\nabla_{\mathbf{x}_{k+1}}\log p(\mathbf{x}_{k+1}|\mathbf{x}_k)\right]^T\right\} \\
&\quad -\mathbb{E}\left\{\nabla_{\mathbf{x}_{k+1}}\left[\nabla_{\mathbf{x}_{k+1}}\log p(\mathbf{z}_{k+1}|\mathbf{x}_{k+1})\right]^T\right\} \qquad (2.14)
\end{aligned}$$

Note that the dimensions of all the matrices involved in the recursion are $n \times n$, unlike the non-recursive computation of the FIM which involves inversion and multiplication of increasingly large matrices as the number of measurements grows.

The application of the recursive FIM for a nonlinear system with Gaussian noise is illustrated in the following derivation. The system model is assumed to be of the following form,

$$\mathbf{x}_{k+1} = \mathbf{f}(\mathbf{x}_k) + \mathbf{w}_k \qquad (2.15)$$

$$\mathbf{z}_k = \mathbf{h}(\mathbf{x}_k) + \mathbf{v}_k \qquad (2.16)$$

where $\mathbf{f}(\mathbf{x}_k)$ and $\mathbf{h}(\mathbf{x}_k)$ are the nonlinear process and measurement models respectively, and the noise variables $\mathbf{w}_k$ and $\mathbf{v}_k$ are uncorrelated, Gaussian, zero-mean white noises with covariances given by $\mathbf{Q}_k$ and $\mathbf{R}_k$ (i.e. $\mathbf{w}_k \sim \mathcal{N}(0, \mathbf{Q}_k)$ and $\mathbf{v}_k \sim \mathcal{N}(0, \mathbf{R}_k)$). The logarithms of the transitional probabilities become

$$-\log p(\mathbf{x}_{k+1}|\mathbf{x}_k) = c_1 + \frac{1}{2}[\mathbf{x}_{k+1} - \mathbf{f}(\mathbf{x}_k)]^T\mathbf{Q}_k^{-1}[\mathbf{x}_{k+1} - \mathbf{f}(\mathbf{x}_k)] \qquad (2.17)$$

$$-\log p(\mathbf{z}_k|\mathbf{x}_k) = c_2 + \frac{1}{2}[\mathbf{z}_k - \mathbf{h}(\mathbf{x}_k)]^T\mathbf{R}_k^{-1}[\mathbf{z}_k - \mathbf{h}(\mathbf{x}_k)] \qquad (2.18)$$

where c_1 and c_2 are constants independent of $\mathbf{x}$.

Using $\mathbf{F}_k = \nabla_{\mathbf{x}_k}\mathbf{f}(\mathbf{x}_k)$ and $\mathbf{H}_k = \nabla_{\mathbf{x}_k}\mathbf{h}(\mathbf{x}_k)$, which are the Jacobians for the system

dynamic model and the measurement model with respect to the estimation state, the equations in (2.14) become

$$\begin{aligned}
\mathbf{D}_k^{11} &= \mathbf{F}_k^T \mathbf{Q}_k^{-1} \mathbf{F}_k \\
\mathbf{D}_k^{12} &= -\mathbf{F}_k^T \mathbf{Q}_k^{-1} \\
\mathbf{D}_k^{21} &= -\mathbf{Q}_k^{-1} \mathbf{F}_k \\
\mathbf{D}_k^{22} &= \mathbf{Q}_k^{-1} + \mathbf{H}_{k+1}^T \mathbf{R}_{k+1}^{-1} \mathbf{H}_{k+1}
\end{aligned} \tag{2.19}$$

The recursive form of the FIM, given in equation (2.13), becomes

$$\mathbf{J}_{k+1} = \mathbf{Q}_k^{-1} + \mathbf{H}_{k+1}^T \mathbf{R}_{k+1}^{-1} \mathbf{H}_{k+1} - \mathbf{Q}_k^{-1} \mathbf{F}_k (\mathbf{J}_k + \mathbf{F}_k^T \mathbf{Q}_k^{-1} \mathbf{F}_k)^{-1} \mathbf{F}_k^T \mathbf{Q}_k^{-1} \tag{2.20}$$

Applying the Matrix Inversion Lemma[1] the FIM reduces to

$$\mathbf{J}_{k+1} = (\mathbf{Q}_k + \mathbf{F}_k \mathbf{J}_k^{-1} \mathbf{F}_k^T)^{-1} + \mathbf{H}_{k+1}^T \mathbf{R}_{k+1}^{-1} \mathbf{H}_{k+1} \tag{2.21}$$

which is very similar in form to the Kalman Filter (see [69] and [68]). In fact, for non-random target dynamics $\mathbf{Q}_k = 0$, and replacing $\mathbf{F}_k$ with the state transition matrix $\Phi_{k+1,k}$, the equation above becomes

$$\mathbf{J}_{k+1} = [\Phi_{k+1,k}^T]^{-1} \mathbf{J}_k \Phi_{k+1,k}^{-1} + \mathbf{H}_{k+1}^T \mathbf{R}_{k+1}^{-1} \mathbf{H}_{k+1} \tag{2.22}$$

which is the covariance propagation equation for the Information Filter form of the Kalman Filter [68].

To initialize the recursion, the matrix $\mathbf{J}_0$ is computed using

$$\mathbf{J}_0 = \mathbb{E}\left\{ \left[\nabla_{\mathbf{x}_0} \log p(\mathbf{x}_0) \right] \left[\nabla_{\mathbf{x}_0} \log p(\mathbf{x}_0) \right]^T \right\} \tag{2.23}$$

where $p(\mathbf{x}_0)$ is the initial density and the expectation is taken with respect to $\mathbf{x}_0$. If the initial distribution is Gaussian with mean $\bar{\mathbf{x}}_0$ and covariance $\mathbf{P}_0$ such that

[1]Matrix Inversion Lemma: $A - AB^T(BAB^T + C)^{-1}BA = (A^{-1} + B^T C^{-1} B)^{-1}$

$p(\mathbf{x}_0) = \mathcal{N}(\bar{\mathbf{x}}_0, \mathbf{P}_0)$ then the initial information matrix is given by

$$\begin{aligned}
\mathbf{J}_0 &= \mathbb{E}\left\{ \left[\nabla_{\mathbf{x}_0} \log p(\mathbf{x}_0)\right] \left[\nabla_{\mathbf{x}_0} \log p(\mathbf{x}_0)\right]^T \right\} && (2.24)\\
&= \mathbb{E}\left\{ \left[-\mathbf{P}_0^{-1}(\mathbf{x}_0 - \bar{\mathbf{x}}_0)\right] \left[-\mathbf{P}_0^{-1}(\mathbf{x}_0 - \bar{\mathbf{x}}_0)\right]^T \right\} && (2.25)\\
&= \mathbf{P}_0^{-1}\mathbb{E}\left\{(\mathbf{x}_0 - \bar{\mathbf{x}}_0)(\mathbf{x}_0 - \bar{\mathbf{x}}_0)^T\right\}\mathbf{P}_0^{-1} && (2.26)\\
&= \mathbf{P}_0^{-1}\mathbf{P}_0\mathbf{P}_0^{-1} = \mathbf{P}_0^{-1} && (2.27)
\end{aligned}$$

An interesting fact is that a consistent estimator (in a mean-squared sense) must have an increasing amount of information. Therefore as more measurements are taken and $k \to \infty$, the FIM approaches infinity and the CRLB (and covariance of the estimation error) approach zero [46]. This suggests that the FIM and the CRLB are directly related to the performance of the estimator and therefore are good candidates for an objective function for the optimization of vehicle trajectories to improve estimation performance.

2.1.2 Estimation Observability

Another concept closely related to the performance of estimators is observability. A system is said to be observable if the current state of the system can be computed in finite time using only the measurements obtained up to that time. For a linear time-invariant system, the observability matrix can be computed to determine if the system is observable. The observability matrix for observable systems is positive definite. If the matrix is positive semi-definite, or singular (has a determinant equal to zero), then the estimation process is unobservable. A similar condition involving the *observability grammian* is used for linear time-varying systems. The observability grammian is given by

$$W_o(t) = \int_0^t \Phi^T(\tau, t)\mathbf{H}^T(\tau)\mathbf{H}(\tau)\Phi(\tau, t)d\tau \qquad (2.28)$$

and this matrix can be evaluated for a specific value of time t. Similar to the observability matrix, if $W_o(t)$ is positive definite the system is observable, otherwise it is unobservable [14]. An equivalent observability condition for the stochastic estimation problem is given by

$$W'_o(t) = \int_0^t \Phi^T(\tau, t)\mathbf{H}^T(\tau)\mathbf{R}(\tau)^{-1}\mathbf{H}(\tau)\Phi(\tau, t)d\tau \tag{2.29}$$

where $\mathbf{R}(t)$ is the covariance of the sensor noise at time t [22]. As before, for a specific time t, if $W'_o(t)$ is positive definite the system is observable, otherwise it is unobservable.

Strictly speaking, observability is a binary concept; an estimation process is either observable or it is not. However, the condition number of the observability matrix can be used as an indication of how accurate and stable the estimation is. Several past research endeavors used this concept of *relative observability* to optimize vehicle maneuvers attempting to increase the relative observability of the estimation (see Section 1.3.2). Throughout the rest of this thesis the term observability will refer to this concept of relative observability. The condition number of the observability matrix, however, does not provide a proper framework for optimization since it is very sensitive to cases where the process is nearly unobservable but not sensitive enough when the measurements provide good observability. The observability grammian is very similar to the Fisher Information Matrix and can be used to determine how much uncertainty is present or how much information is available through the measurements. This can be seen by looking at the discrete version of equation (2.29),

$$W'_{o_k} = \sum_{\imath=0}^{k} \Phi_{k,\imath}^T \mathbf{H}_\imath^T \mathbf{R}_\imath^{-1} \mathbf{H}_\imath \Phi_{k,\imath} \tag{2.30}$$

which, through simple calculations, can be shown to have the same form as equation (2.22) for the Fisher Information Matrix, showing the close connection between increasing information and increasing observability to improve the performance of the estimation process. Both the FIM and the observability matrix capture the fact that

all measurements are not equal and that some sets of measurements provide higher information than others. By finding sets of measurements that provide the highest information the relative observability can be increased and the estimation performance enhanced.

2.2 Estimation Algorithm Review

This section introduces a few of the most commonly used estimation algorithms and shows how they relate to the Fisher Information Matrix and the Cramér-Rao Lower Bound. The algorithms considered include the Least Squares estimation algorithm (LS), the Extended Kalman Filter (EKF), and the Particle Filter (PF). The Least Squares algorithm and the traditional Kalman Filter (KF) are considered optimal when dealing with a linear time-invariant (LTI) system, although the LS algorithm is more restrictive than the KF and is used mainly for parameter estimation, whereas the KF is optimal for any LTI system. When the system is nonlinear, the EKF or the linearized KF can be used instead of the traditional KF. Filter design for nonlinear systems usually entails a linearization assumption which can introduce biases, time-varying effects and other suboptimal behavior into the algorithms. Particle filters are much better at dealing with nonlinear systems with non-Gaussian noise models than classical estimation algorithms such as the LS and the EKF, however, they are suboptimal algorithms which only approach the true system behavior as the number of particles goes to infinity. The following sections describe the LS, EKF and PF algorithms in detail. For the LS and EKF the connection to the Fisher Information Matrix is shown, motivating the use of the FIM in trajectory design to enhance estimation performance.

2.2.1 Least Squares Estimation

The Least Squares Estimation algorithm works by attempting to minimize the sum of the squares of the estimation errors for all the parameters to be estimated. There are several versions of the Least Squares algorithm, some of which include the traditional

Batch Least Squares, Recursive Least Squares, and Extended Least Squares. The Batch Least Square algorithm is the most common form of the LS algorithm and is widely used for parameter estimation throughout the literature. The main disadvantage of a batch processing algorithm is that it recomputes the best estimate given *all* the past data at every time-step. This usually involves working with large matrices, storing large amounts of data, and other computational difficulties. Another major problem for batch processing algorithms is that they cannot deal well with time-varying systems. The Recursive Least Squares algorithm presents an improvement over the Batch Least Squares algorithm by recursively updating the estimation and only processing the current measurement at each time-step. For time-varying parameter estimation the Extended Least Squares algorithm can be used, which involves exponential forgetting, attempting to discount older data to deal with slowly time-varying parameters. The most well-known version of the LS algorithm, however, is the Batch Least Squares algorithm. It is presented below and the relationship between the estimation performance and the FIM is shown.

We assume a system whose dynamics are given by

$$\mathbf{x}_{k+1} = \Phi_{k+1,k}\mathbf{x}_k \tag{2.31}$$

$$\mathbf{z}_k = \mathbf{h}(\mathbf{x}_k) + \mathbf{v}_k \tag{2.32}$$

where $\Phi_{k+1,k}$ is the state transition matrix of the system from time k to $k+1$ and $\mathbf{v}_k$ is the measurement noise which is assumed to be Gaussian and white with zero mean and covariance $\mathbf{R}_k$ (i.e. $\mathbf{v}_k \sim \mathcal{N}(0, \mathbf{R}_k)$).

Since the Least Squares algorithm requires a linear measurement, the Jacobian of the measurement model with respect to the estimation state must be computed. Linearizing the measurement model gives

$$\mathbf{z}_k = \mathbf{H}_k\mathbf{x}_k + \mathbf{v}_k \tag{2.33}$$

where

$$\mathbf{H}_k = \nabla_{\mathbf{x}_k} \mathbf{h}(\mathbf{x}_k) \tag{2.34}$$

Collecting all the measurements for batch processing gives the vector of measurements $\mathbf{Z}_k = \begin{bmatrix} \mathbf{z}_1 \dots \mathbf{z}_k \end{bmatrix}^T$, which can be written as

$$\mathbf{Z}_k = \mathbf{A}_{k,0}\mathbf{x}_0 + \mathbf{V}_k \tag{2.35}$$

$$\mathbf{A}_{k,0} = \begin{bmatrix} \mathbf{H}_1\Phi_{1,0} \\ \vdots \\ \mathbf{H}_k\Phi_{k,0} \end{bmatrix} \tag{2.36}$$

$$\mathbf{V}_k = \begin{bmatrix} \mathbf{v}_1 \\ \vdots \\ \mathbf{v}_k \end{bmatrix} \tag{2.37}$$

Using least squares estimation to minimize the sum of the squares of the estimation error, the estimate of the initial state given k measurements, $\hat{\mathbf{x}}_{0|k}$, is obtained through the following,

$$\begin{aligned} \mathbf{A}_{k,0}^T[\mathbf{Z}_k - \mathbf{A}_{k,0}\hat{\mathbf{x}}_{0|k}] &= 0 \\ \mathbf{A}_{k,0}^T\mathbf{A}_{k,0}\hat{\mathbf{x}}_{0|k} &= \mathbf{A}_{k,0}^T\mathbf{Z}_k \\ \hat{\mathbf{x}}_{0|k} &= \left[\mathbf{A}_{k,0}^T\mathbf{A}_{k,0}\right]^{-1}\mathbf{A}_{k,0}^T\mathbf{Z}_k \end{aligned} \tag{2.38}$$

the solution of which implies that for any $\tilde{\mathbf{x}}_{0|k}$,

$$||\mathbf{Z}_k - \mathbf{A}_{k,0}\hat{\mathbf{x}}_{0|k}||_2 \leq ||\mathbf{Z}_k - \mathbf{A}_{k,0}\tilde{\mathbf{x}}_{0|k}||_2 \tag{2.39}$$

The performance of the estimation can be analyzed by computing the covariance. For the least squares estimation algorithm the covariance matrix is given by

$$\mathbf{P}_{0|k} = \mathbb{E}\left\{[\mathbf{x}_0 - \hat{\mathbf{x}}_{0|k}][\mathbf{x}_0 - \hat{\mathbf{x}}_{0|k}]^T\right\} \tag{2.40}$$

which, using equations (2.35) and (2.38), can be rewritten as

$$\begin{aligned}\mathbf{P}_{0|k} &= \mathbb{E}\{[-[\mathbf{A}_{k,0}^T\mathbf{A}_{k,0}]^{-1}\mathbf{A}_{k,0}^T\mathbf{V}_k][-[\mathbf{A}_{k,0}^T\mathbf{A}_{k,0}]^{-1}\mathbf{A}_{k,0}^T\mathbf{V}_k]^T\} \\ &= [\mathbf{A}_{k,0}^T\mathbf{A}_{k,0}]^{-1}\mathbf{A}_{k,0}^T\mathbb{E}\{\mathbf{V}_k\mathbf{V}_k^T\}\,\mathbf{A}_{k,0}[[\mathbf{A}_{k,0}^T\mathbf{A}_{k,0}]^{-1}]^T \end{aligned} \tag{2.41}$$

Simplifying this expression and using $\mathbb{E}\{\mathbf{V}_k\mathbf{V}_k^T\} = \mathbf{R}_k$ gives

$$\mathbf{P}_{0|k} = [\mathbf{A}_{k,0}^T\mathbf{R}_k^{-1}\mathbf{A}_{k,0}]^{-1} \tag{2.42}$$

which can also be written recursively as

$$\begin{aligned}\mathbf{P}_{0|k} &= [\mathbf{A}_{k,0}^T\mathbf{R}_k^{-1}\mathbf{A}_{k,0}]^{-1} \\ &= [\mathbf{A}_{k-1,0}^T\mathbf{R}_k^{-1}\mathbf{A}_{k-1,0} + \Phi_{k,0}^T\mathbf{H}_k^T\mathbf{R}_k^{-1}\mathbf{H}_k\Phi_{k,0}]^{-1} \\ &= [\mathbf{P}_{0|k-1}^{-1} + \Phi_{k,0}^T\mathbf{H}_k^T\mathbf{R}_k^{-1}\mathbf{H}_k\Phi_{k,0}]^{-1} \end{aligned} \tag{2.43}$$

The information matrix $\mathbf{J}_{0|k}$, which, as mentioned before, is the inverse of the covariance matrix $\mathbf{P}_{0|k}$, can be written recursively using equation (2.43) as

$$\begin{aligned}\mathbf{J}_{0|k} &= \mathbf{A}_{k,0}^T\mathbf{R}_k^{-1}\mathbf{A}_{k,0} \\ &= \mathbf{A}_{k-1,0}^T\mathbf{R}_k^{-1}\mathbf{A}_{k-1,0} + \Phi_{k,0}^T\mathbf{H}_k^T\mathbf{R}_k^{-1}\mathbf{H}_k\Phi_{k,0} \\ &= \mathbf{J}_{0|k-1} + \Phi_{k,0}^T\mathbf{H}_k^T\mathbf{R}_k^{-1}\mathbf{H}_k\Phi_{k,0} \\ &= \sum_{i=1}^{k}\Phi_{i,0}^T\mathbf{H}_i^T\mathbf{R}_i^{-1}\mathbf{H}_i\Phi_{i,0} \end{aligned} \tag{2.44}$$

The covariance and information matrices derived above are for the estimation error of the *initial* state given all the measurements collected up to time k. In order to get the covariance and information matrices for the estimation error of the *final* state (at time k) the following expression is needed,

$$\mathbf{P}_{k|k} = \Phi_{k,0}\mathbf{P}_{0|k}\Phi_{k,0}^T \tag{2.45}$$

which gives

$$\mathbf{P}_{k|k}^{-1} = \mathbf{J}_{k|k} = [\Phi_{k,0}^T]^{-1}\mathbf{J}_{0|k}\Phi_{k,0}^{-1} \tag{2.46}$$

Combining this expression with equation (2.44) gives the recursive form of the inverse of the error covariance or the Fisher Information Matrix,

$$\begin{aligned}
\mathbf{J}_{k|k} &= [\Phi_{k,0}^T]^{-1}\left[\sum_{i=1}^{k}\Phi_{i,0}^T\mathbf{H}_i^T\mathbf{R}_i^{-1}\mathbf{H}_i\Phi_{i,0}\right]\Phi_{k,0}^{-1} \\
&= [\Phi_{k,k-1}^T]^{-1}[\Phi_{k-1,0}^T]^{-1}\left[\sum_{i=1}^{k-1}\Phi_{i,0}^T\mathbf{H}_i^T\mathbf{R}_i^{-1}\mathbf{H}_i\Phi_{i,0}\right]\Phi_{k-1,0}^{-1}\Phi_{k,k-1}^{-1} + \mathbf{H}_k^T\mathbf{R}_k^{-1}\mathbf{H}_k \\
&= [\Phi_{k,k-1}^T]^{-1}\mathbf{J}_{k-1|k-1}\Phi_{k,k-1}^{-1} + \mathbf{H}_k^T\mathbf{R}_k^{-1}\mathbf{H}_k
\end{aligned} \tag{2.47}$$

This equation is identical to the Fisher Information Matrix equation, (2.22), shown in the previous section, thus implying that the FIM is a good metric for assessing the performance of the least squares estimation algorithm.

The estimation of the final state $\hat{\mathbf{x}}_{k|k}$ is obtained from the estimation of the initial state $\hat{\mathbf{x}}_{0|k}$ by using

$$\hat{\mathbf{x}}_{k|k} = \Phi_{k,0}\hat{\mathbf{x}}_{0|k} \tag{2.48}$$

2.2.2 Extended Kalman Filter

The Kalman Filter has long been known as the most popular estimation algorithm. It is a recursive filtering method that is optimal and *efficient*[2] for linear time-invariant dynamic systems, as well as being computationally efficient due to its recursive nature. To deal with systems that have nonlinear dynamics or nonlinear measurement models several modifications to the Kalman Filter have been proposed. A few examples are the Linearized Kalman Filter, the Extended Kalman Filter (EKF), and the Unscented Kalman Filter (UKF). This section presents the Extended Kalman Filter for a system with nonlinear dynamics and a nonlinear measurement model and shows the close

[2]Achieves the Cramér-Rao Lower Bound

relationship between the EKF covariance and the Fisher Information Matrix.

We assume a nonlinear system whose dynamics are given by

$$\mathbf{x}_{k+1} = \mathbf{f}(\mathbf{x}_k) + \mathbf{w}_k \tag{2.49}$$

$$\mathbf{z}_k = \mathbf{h}(\mathbf{x}_k) + \mathbf{v}_k \tag{2.50}$$

where $\mathbf{f}(\mathbf{x}_k)$ and $\mathbf{h}(\mathbf{x}_k)$ are the nonlinear dynamics and measurement models of the system, and $\mathbf{w}_k$ and $\mathbf{v}_k$ are the process and measurement noises, which are assumed to be uncorrelated, Gaussian and white with zero mean and covariance $\mathbf{Q}_k$ and $\mathbf{R}_k$ respectively (i.e. $\mathbf{w}_k \sim \mathcal{N}(0, \mathbf{Q}_k)$ and $\mathbf{v}_k \sim \mathcal{N}(0, \mathbf{R}_k)$).

The EKF algorithm is composed of a prediction step and an update step. The prediction step involves developing a state and covariance estimate of the next time step based on the current estimates and the system dynamics model. The update state involves processing the new measurement and updating the prediction made using the new information. The equations for the EKF are shown below.

Prediction phase:

$$\hat{\mathbf{x}}_{k|k-1} = \mathbf{f}(\hat{\mathbf{x}}_{k-1|k-1}) \tag{2.51}$$

$$\hat{\mathbf{z}}_{k|k-1} = \mathbf{h}(\hat{\mathbf{x}}_{k|k-1}) \tag{2.52}$$

$$\mathbf{P}_{k|k-1} = \Phi_{k,k-1}\mathbf{P}_{k-1|k-1}\Phi_{k,k-1}^T + \mathbf{Q}_k \tag{2.53}$$

Kalman Gain:

$$\mathbf{K}_k = \mathbf{P}_{k|k-1}\mathbf{H}_k^T \left[\mathbf{H}_k\mathbf{P}_{k|k-1}\mathbf{H}_k^T + \mathbf{R}_k\right]^{-1} \tag{2.54}$$

where $\Phi_{k,k-1}$ and $\mathbf{H}_k$ are, respectively, the Jacobians of the system dynamics and measurement models with respect to the state, evaluated at the predicted state $\hat{\mathbf{x}}_{k|k-1}$. The equations for $\Phi_{k,k-1}$ and $\mathbf{H}_k$ are given by

$$\Phi_{k,k-1} = \mathbf{F}_k = \nabla_{\mathbf{x}_k}\mathbf{f}(\mathbf{x}_k) \tag{2.55}$$

$$\mathbf{H}_k = \nabla_{\mathbf{x}_k}\mathbf{h}(\mathbf{x}_k) \tag{2.56}$$

Update phase:

$$\nu_k = \mathbf{z}_k - \hat{\mathbf{z}}_{k|k-1} \tag{2.57}$$

$$\hat{\mathbf{x}}_{k|k} = \hat{\mathbf{x}}_{k|k-1} + \mathbf{K}_k \nu_k \tag{2.58}$$

$$\mathbf{P}_{k|k} = \mathbf{P}_{k|k-1} - \mathbf{P}_{k|k-1}\mathbf{H}_k^T \left[\mathbf{H}_k \mathbf{P}_{k|k-1}\mathbf{H}_k^T + \mathbf{R}_k\right]^{-1} \mathbf{H}_k \mathbf{P}_{k|k-1} \tag{2.59}$$

The equations for the EKF covariance propagation are computationally intensive since they involve taking the inverse of $\left[\mathbf{H}_k \mathbf{P}_{k|k-1}\mathbf{H}_k^T + \mathbf{R}_k\right]$. The calculations can be greatly simplified by propagating the inverse of the covariance matrix instead of the covariance, resulting in an algorithm known as the Information Filter. The equations for the covariance propagation in the Information Filter are given by

$$\mathbf{P}_{k|k-1}^{-1} = \left[\Phi_{k,k-1}\mathbf{P}_{k-1|k-1}\Phi_{k,k-1}^T + \mathbf{Q}_{k-1}\right]^{-1} \tag{2.60}$$

$$\mathbf{P}_{k|k}^{-1} = \mathbf{P}_{k|k-1}^{-1} + \mathbf{H}_k^T \mathbf{R}_k^{-1} \mathbf{H}_k \tag{2.61}$$

and can be obtained directly from equations (2.53) and (2.59), and the Matrix Inversion Lemma[3]. Combining equations (2.60) and (2.61) gives

$$\mathbf{P}_{k|k}^{-1} = \left[\Phi_{k,k-1}\mathbf{P}_{k-1|k-1}\Phi_{k,k-1}^T + \mathbf{Q}_{k-1}\right]^{-1} + \mathbf{H}_k^T \mathbf{R}_k^{-1} \mathbf{H}_k \tag{2.62}$$

which has the same form as equation (2.21). For the case where there is no process noise ($\mathbf{Q}_k = \mathbf{0}$), the inverse covariance propagation becomes

$$\mathbf{P}_{k|k}^{-1} = \left[\Phi_{k,k-1}^T\right]^{-1} \mathbf{P}_{k-1|k-1}\Phi_{k,k-1}^{-1} + \mathbf{H}_k^T \mathbf{R}_k^{-1} \mathbf{H}_k \tag{2.63}$$

which is identical to equation (2.22) for the computation of the Fisher Information Matrix (see [68], [69] and [64]). The major difference between equations (2.22) and (2.63) is that the former is evaluated at the true target state whereas the latter is evaluated using the estimated target state. In practice, however, the algorithm has no access to the true target state so the online computation of the FIM would have to be

[3]Matrix Inversion Lemma: $A - AB^T(BAB^T + C)^{-1}BA = (A^{-1} + B^T C^{-1} B)^{-1}$

executed using the estimated target state, leading to equation (2.63). The Information Filter shows that functionals based on the FIM make good objective functions for maneuver optimization since the FIM closely resembles the covariance of the EKF, which is widely accepted as the traditional measure of estimation performance.

2.2.3 Particle Filtering

A more recent algorithm than the classical least-squares and EKF approaches is the Particle Filter. Particle filtering, also known as Sequential Monte Carlo (SMC) estimation, is a suboptimal filtering technique that works by performing Monte Carlo integration on a set of particles that represent the probability distribution of the process at hand. Here, a "particle" is a sample drawn from an *a priori* distribution of the parameter to be estimated. The basic idea behind the particle filter is that a large number of particles or samples can be used to represent the distribution of the estimation. The larger the number of particles used, the more accurately the particle set will represent the prior distribution.

The particle filter is initialized by drawing N particles from the *a priori* distribution of the parameters to be estimated. The filtering algorithm involves propagating these particles through a system model and then weighting them using the information obtained by taking a measurement. The resulting particles and associated weights represent the *posterior* distribution of the estimation process. The cycle is repeated for each new measurement and the particle weights are updated to represent the new posterior distribution. One major problem with this traditional particle filtering approach is that it usually results in a few particles having very large weights and the rest having negligible weighting values, which leads to filter instability. This problem can be fixed by introducing a resampling step, where N new particles are drawn from the distribution represented by the old particles and weights. These new particles are then given equal weights and the algorithm continues. The estimation results are obtained by taking the sample mean (and covariance) over the set of particles. If the samples are independent, the sample mean is an unbiased estimate of the true mean and, given finite variance and using the law of large numbers, as the

number of samples increases the estimation error converges to a zero mean Gaussian process with the same finite variance [64].

Even though the particle filter is a suboptimal filter, as the number of samples goes to infinity the algorithm approaches the optimal Bayesian estimator. Therefore it is desirable to have as many particles as possible to represent the process. Unfortunately this comes at the cost of increased computation, leading to a tradeoff between algorithm accuracy and speed of computation. The number of particles must therefore be selected based on the demands of the estimation problem at hand. Another consideration for tuning the particle filter is setting the resampling threshold. As mentioned before, resampling is an important step in particle filtering and without it the filter will eventually end up with one particle having a heavy weight while the others are almost negligible, degenerating the algorithm. The idea is that if the weights get too uneven and a resampling threshold is reached, the particles with low weights are thrown out and the remaining set forms the new probability density from which new samples can be taken. The choice of this resampling threshold presents a tradeoff where resampling too soon causes the filter to be overly sensitive to noise and resampling too late causes filter divergence. The other main design choice for the filter is the selection of a proper *importance density*. If it is difficult to sample from the posterior density, an approximation of the probability density function can be used instead, under certain conditions (see [64]). This process is called importance sampling and the choice of the importance density function affects the performance of the filter. An issue with choosing the importance density is that it has to be a function from which one can sample. The optimal choice of importance density is given by $p(\mathbf{x}_k|\mathbf{x}_{k-1}^i, \mathbf{z}_k)$, however, in general this is a difficult function to sample from. A suboptimal choice of importance density is the transitional prior which is given by the conditional probability of the target state given the previous set of particles, $p(\mathbf{x}_k|\mathbf{x}_{k-1}^i)$. This importance density relies on a model of the target dynamics to propagate the target state. It greatly simplifies the calculation of the particle weights, is commonly used in the literature, and is used in this work, giving the weighting equation shown in the algorithm below. The generic particle filtering

algorithm is summarized as follows:

1. To initialize, draw N particles from an *a priori* distribution $p(\mathbf{x}_0)$. Set all weights to be normalized and equal.

$$\begin{aligned} \mathbf{x}_0^i &\sim p(\mathbf{x}_0), \quad i = 1:N \\ m_0^i &= \frac{1}{N}, \quad i = 1:N \end{aligned} \tag{2.64}$$

2. Propagate the particle set according to a process model of the target dynamics.

$$\mathbf{x}_k^i = \mathbf{f}(\mathbf{x}_{k-1}^i) + \mathbf{w}_{k-1}^i, \quad i = 1:N \tag{2.65}$$

   Here $\mathbf{f}(\mathbf{x}_{k-1}^i)$ is the dynamics model and $\mathbf{w}_{k-1}^i$ is the noise.

3. Update the particle weights based on the received measurement $\mathbf{z}_k$ and the likelihood function (or conditional probability) of receiving that measurement given the current particle value.

$$m_k^i = m_{k-1}^i \, p(\mathbf{z}_k|\mathbf{x}_k^i), \quad i = 1:N \tag{2.66}$$

4. Normalize the weights.

$$m_k^i = \frac{m_k^i}{\sum_{i=1}^N m_k^i} \tag{2.67}$$

5. Compute the effective sample size. The bounds on the effective sample size are given by $1 \leq N_{eff} \leq N$.

$$N_{eff} = \frac{1}{\sum_{i=1}^N (m_k^i)^2} \tag{2.68}$$

6. Compare N_{eff} to the resampling threshold. Resample if necessary.

$$\begin{aligned} N_{eff} &< N_{thr} \longrightarrow \text{RESAMPLE AND GO TO STEP 2} \\ N_{eff} &\geq N_{thr} \longrightarrow \text{GO TO STEP 2} \end{aligned} \tag{2.69}$$

In this algorithm N_{eff} is used to determine if the particles are unevenly distributed. If a few particles have heavy weighting and the rest have comparatively low weighting values, N_{eff} will be close to 1. If all the particles have equal weighting values, N_{eff} will be equal to N. The resampling threshold can be tuned so that if N_{eff} becomes too low the particles can be resampled. The resampling step involves approximating the density of the estimation process based on the current particles and their weights. N new particles are then drawn at random from this distribution and their weights are set to be equal. At any time step, the value of the estimate is formed by computing the sample mean,

$$\bar{\mathbf{x}}_k = \sum_{i=1}^{N} \mathbf{x}_k^i m_k^i \tag{2.70}$$

The covariance can be computed using

$$\mathbf{P}_k = \sum_{i=1}^{N} (\mathbf{x}_k^i - \bar{\mathbf{x}}_k)^2 m_k^i \tag{2.71}$$

For an example of a particle filtering algorithm see Appendix B. For a complete tutorial on particle filters see [64].

One consideration to keep in mind while using particle filters is the insufficiency of the CRLB in assessing the complete performance of the PF algorithm. As mentioned before, the CRLB provides a lower bound on the mean-squared error of the estimation. For the particle filtering algorithm the mean and covariance of the estimation can be computed for comparison with the CRLB, which for Gaussian processes is enough. However, using the particle filtering algorithm, the posterior densities obtained for the nonlinear filtering problem are usually non-Gaussian, requiring higher

order moments to characterize the density. The CRLB is therefore theoretically insufficient for providing a limit on the accuracy of particle filters [64]. For many estimation problems, however, the probability distribution of the estimation can be approximated by a Gaussian distribution, in which case the CRLB can be used to provide an indication of the expected performance of the estimation. As mentioned before, the CRLB is based on the physical and geometrical aspects of the estimation problem and, since any filter can only do as well as the information provided, in most cases the CRLB is still a good indicator of the performance of the PF algorithm. This can be seen in the following section, especially by noting the similar performance of the PF and EKF algorithms for the constant velocity target scenario, which shows that the estimation performance is highly dependent on the vehicle trajectory and the information provided by the measurements.

2.3 Vision-Based Target Localization

This section explores the problem of target localization using vision-only measurements obtained from a UAV flying above the target. As described in Section 1.2.3, the images from the vision sensors can be converted into bearings-only measurements, which can be used to determine the location of the target. The filtering algorithms presented in this section consider this bearings-only target estimation problem. Two filter designs are implemented for the simplified two dimensional scenario and the full three dimensional case. The first method uses the EKF algorithm described in Section 2.2.2 and the second uses the Particle Filtering algorithm (Section 2.2.3). The target dynamics considered assume a stationary target and a slow stochastic target that is free to move in the ground plane but for which no prior motion model is known. For this slow moving target case, several different scenarios are considered, such as a random walk trajectory, a constant velocity trajectory and a semi-circular target trajectory. The UAV flight path is predefined, and for the 3-D case, is assumed to be a circular trajectory orbiting the target at a constant altitude. This trajectory was shown in Section 1.2.4 to be the best ad-hoc trajectory for the stationary target

case, resulting in the lowest error mean and variance for the target location estimation. Chapter 3 will further explore the problem of trajectory design. The following sections describe the estimation performance for the target localization problem using vision measurements, and show the information obtained from the measurements using the chosen vehicle trajectory.

2.3.1 EKF for Bearings-Only Target Localization

Here we apply the EKF algorithm discussed in section 2.2.2 to the target localization problem using bearings-only measurements. The details of the filtering algorithm are discussed in this section. The target dynamics model is assumed to be linear but the measurement model is still nonlinear, giving the following system dynamics,

$$\mathbf{x}_{k+1} = \Phi_{k+1,k}\mathbf{x}_k + \mathbf{w}_k \tag{2.72}$$

$$\mathbf{z}_k = \mathbf{h}(\mathbf{x}_k) + \mathbf{v}_k \tag{2.73}$$

where $\Phi_{k+1,k}$ is the state transition matrix of the system from time k to $k+1$ and $\mathbf{w}_k$ and $\mathbf{v}_k$ are the process and measurement noises, which are uncorrelated, Gaussian and white with zero mean and covariance $\mathbf{Q}_k$ and $\mathbf{R}_k$ respectively (i.e. $\mathbf{w}_k \sim \mathcal{N}(0, \mathbf{Q}_k)$ and $\mathbf{v}_k \sim \mathcal{N}(0, \mathbf{R}_k)$).

Recall the filter equations for the EKF are,

Prediction phase:

$$\hat{\mathbf{x}}_{k|k-1} = \Phi_{k,k-1}\hat{\mathbf{x}}_{k-1|k-1} \tag{2.74}$$

$$\hat{\mathbf{z}}_{k|k-1} = \mathbf{h}(\hat{\mathbf{x}}_{k|k-1}) \tag{2.75}$$

$$\mathbf{P}_{k|k-1} = \Phi_{k,k-1}\mathbf{P}_{k-1|k-1}\Phi_{k,k-1}^T + \mathbf{Q}_k \tag{2.76}$$

Kalman Gain:

$$\mathbf{K}_k = \mathbf{P}_{k|k-1}\mathbf{H}_k^T \left[\mathbf{H}_k\mathbf{P}_{k|k-1}\mathbf{H}_k^T + \mathbf{R}_k\right]^{-1} \tag{2.77}$$

where

$$\mathbf{H}_k = \nabla_{\mathbf{x}_k} \mathbf{h}(\mathbf{x}_k) \tag{2.78}$$

Update phase:

$$\begin{aligned} \nu_k &= \mathbf{z}_k - \hat{\mathbf{z}}_{k|k-1} && (2.79) \\ \hat{\mathbf{x}}_{k|k} &= \hat{\mathbf{x}}_{k|k-1} + \mathbf{K}_k \nu_k && (2.80) \\ \mathbf{P}_{k|k} &= \mathbf{P}_{k|k-1} - \mathbf{P}_{k|k-1}\mathbf{H}_k^T \left[\mathbf{H}_k \mathbf{P}_{k|k-1} \mathbf{H}_k^T + \mathbf{R}_k\right]^{-1} \mathbf{H}_k \mathbf{P}_{k|k-1} && (2.81) \end{aligned}$$

For the 2-D target localization case the measurement is of the bearing angle between the vehicle and the target, as described in Section 1.2.3 and shown in Figure 1-4. The measurement model is given by

$$\beta = \tan^{-1}\left(\frac{p_x - t_x}{p_y - t_y}\right) = \tan^{-1}\left(\frac{r_x}{r_y}\right) \tag{2.82}$$

where $\mathbf{p}_k = \begin{bmatrix} p_x & p_y \end{bmatrix}_k^T$ is the position of the vehicle, $\mathbf{t}_k = \begin{bmatrix} t_x & t_y \end{bmatrix}_k^T$ is the position of the target and $\mathbf{r}_k = \begin{bmatrix} r_x & r_y \end{bmatrix}_k^T$ is the relative vector between the vehicle and the target. The state to be estimated is $\mathbf{x}_k = \mathbf{t}_k = \begin{bmatrix} t_x & t_y \end{bmatrix}_k^T$. The measurement model is given by

$$\mathbf{h}(\mathbf{x}_k) = \tan^{-1}\left(\frac{r_x}{r_y}\right) \tag{2.83}$$

and its Jacobian with respect to the target is

$$\mathbf{H}_k = \begin{bmatrix} -\frac{r_y}{r_x^2 + r_y^2} & \frac{r_x}{r_x^2 + r_y^2} \end{bmatrix}_k \tag{2.84}$$

For the stationary target case the target position is assumed invariant between

time-steps. Therefore the state transition matrix and the process noise are given by

$$\Phi_{k,k-1} = \begin{bmatrix} 1 & 0 \\ 0 & 1 \end{bmatrix}, \quad \mathbf{Q}_k = \begin{bmatrix} 0 & 0 \\ 0 & 0 \end{bmatrix} \tag{2.85}$$

The sensor noise is assumed to have a constant variance which gives

$$\mathbf{R}_k = \sigma^2 \tag{2.86}$$

A simulation of the target localization problem, created in MATLAB, is used to analyze the target estimation performance. One hundred bearing measurements are taken by a vehicle following a circular trajectory around a target located at the origin. The position is measured in feet and the standard deviation of the sensor noise is assumed to be $\sigma = 5\,\text{deg}$ which is fairly typical for commercially available bearing sensors. The following values are used to initialize the simulation

$$\mathbf{x}_0 = \begin{bmatrix} 0 \\ 0 \end{bmatrix}, \quad \hat{\mathbf{x}}_0 = \begin{bmatrix} 30 \\ 30 \end{bmatrix}, \quad \mathbf{P}_0 = \begin{bmatrix} 200 & 0 \\ 0 & 200 \end{bmatrix} \tag{2.87}$$

Figure 2-1 shows the vehicle trajectory and the target estimation ground track on the left, the estimation performance for both axes on the right, and the Fisher Information for the trajectory on the bottom. The vehicle trajectory begins at $\mathbf{p}_0 = \begin{bmatrix} 100 & 0 \end{bmatrix}^T$ and circles counter clockwise around the target. An interesting result is that the estimation performance of the Y coordinate is initially much better than that of the X coordinate, as seen by the mean and standard deviation results. This is because, due to the vehicle trajectory, the information gained in the Y direction is initially more than in the X direction, leading to reduced uncertainty in the Y dimension. The information plot in Figure 2-1 shows that the information about the Y axis increases more rapidly than the X axis initially. At 25 measurements, the UAV completes a quarter circle around the target and the information about the X and Y axes is the same, as shown in the information plot. Note that at 25 measurement, the covariance of the X and Y axes also become the same as seen by standard deviation lines in

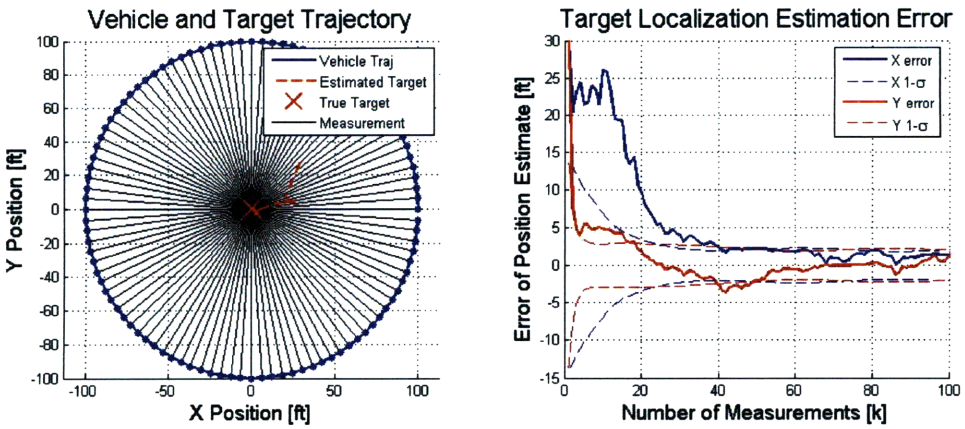

(a) Target Location Estimation

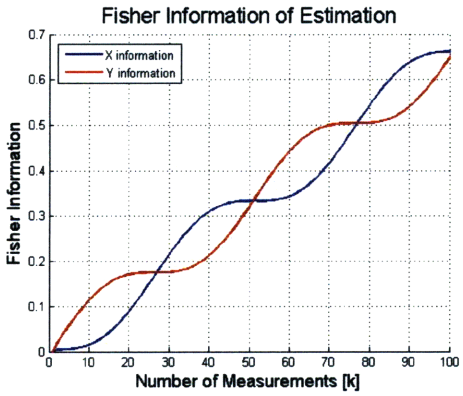

(b) Fisher Information

Figure 2-1: Target localization using EKF algorithm in 2-D

the estimation error plot. As the vehicle circles the target, increased information and observability are gained in the X and Y directions in a sinusoidal pattern corresponding to the circular UAV trajectory. After the full circle is completed, the estimation has the same information in both dimension yielding equal performance for both coordinates.

The scenario is extended to the three dimensional case. Here the target state to be estimated is $\mathbf{x}_k = \mathbf{t}_k = \begin{bmatrix} t_x & t_y & t_z \end{bmatrix}_k^T$. The measurements are of two bearings (described in Section 1.2.3 and shown in Figure 1-4)

$$\begin{aligned} \beta &= \tan^{-1}\left(\frac{p_x - t_x}{p_y - t_y}\right) = \tan^{-1}\left(\frac{r_x}{r_y}\right) \\ \phi &= \tan^{-1}\left(\frac{p_z - t_z}{\sqrt{(p_x - t_x)^2 + (p_y - t_y)^2}}\right) = \tan^{-1}\left(\frac{r_z}{\sqrt{r_x^2 + r_y^2}}\right) \end{aligned} \tag{2.88}$$

where $\mathbf{p}_k = \begin{bmatrix} p_x & p_y & p_z \end{bmatrix}_k^T$ is the position of the vehicle, $\mathbf{t}_k = \begin{bmatrix} t_x & t_y & t_z \end{bmatrix}_k^T$ is the position of the target and $\mathbf{r}_k = \begin{bmatrix} r_x & r_y & r_z \end{bmatrix}_k^T$ is the relative vector between the vehicle and the target. The measurement model is given by

$$\mathbf{h}(\mathbf{x}_k) = \begin{bmatrix} \tan^{-1}\left(\frac{r_x}{r_y}\right) \\ \tan^{-1}\left(\frac{r_z}{\sqrt{r_x^2+r_y^2}}\right) \end{bmatrix} \tag{2.89}$$

The Jacobian of the measurement with respect to the target is

$$\mathbf{H}_k = \begin{bmatrix} -\frac{r_y}{r_x^2+r_y^2} & \frac{r_x}{r_x^2+r_y^2} & 0 \\ \frac{r_x r_z}{(r_x^2+r_y^2+r_z^2)\sqrt{r_x^2+r_y^2}} & \frac{r_y r_z}{(r_x^2+r_y^2+r_z^2)\sqrt{r_x^2+r_y^2}} & -\frac{\sqrt{r_x^2+r_y^2}}{(r_x^2+r_y^2+r_z^2)} \end{bmatrix}_k = \begin{bmatrix} \mathbf{H}_\beta \\ \mathbf{H}_\phi \end{bmatrix}_k \tag{2.90}$$

Several target tracking cases using the EKF are considered, involving stationary and slow moving targets. The main scenarios described in this section include: a stationary target, a target exhibiting random walk behavior, a constant velocity target, and a target following a semi-circular trajectory. This section shows the EKF performance for these different cases and the results for all are summarized in Table 2.1. The data provided in Table 2.1 includes: the end estimation error for each axis as well as the norm of the estimation error, the ending variance of the estimation error for each axis and the total sum of the variances, and the Fisher Information obtained about each axis as well as the total sum of information over all axes. An additional case involving a fast target is presented at the end of the section.

To begin, the case of a stationary target located at the origin is considered first. For this scenario, the process noise is zero since the target position is constant, so the filter parameters for the EKF are given by

$$\Phi_{k,k-1} = \begin{bmatrix} 1 & 0 & 0 \\ 0 & 1 & 0 \\ 0 & 0 & 1 \end{bmatrix}, \quad \mathbf{Q}_k = \begin{bmatrix} 0 & 0 & 0 \\ 0 & 0 & 0 \\ 0 & 0 & 0 \end{bmatrix}, \quad \mathbf{R}_k = \begin{bmatrix} \sigma^2 & 0 \\ 0 & \sigma^2 \end{bmatrix} \tag{2.91}$$

A 3-D simulation is used to test the EKF algorithm. As mentioned before, the

vehicle trajectory is chosen to be a constant altitude circle above the target. Again the standard deviation of the noise is set to $\sigma = 5\,\text{deg}$. The simulation is initialized using the following values,

$$\mathbf{x}_0 = \begin{bmatrix} 0 \\ 0 \\ 0 \end{bmatrix}, \quad \hat{\mathbf{x}}_0 = \begin{bmatrix} 20 \\ 20 \\ 20 \end{bmatrix}, \quad \mathbf{P}_0 = \begin{bmatrix} 200 & 0 & 0 \\ 0 & 200 & 0 \\ 0 & 0 & 200 \end{bmatrix} \tag{2.92}$$

The initialization values shown above were selected arbitrarily. In practice, one can use a least squares approach with the first two measurements to develop an initial estimate of the target for the EKF initialization. Since the first two measurements are taken from locations very close to one another this will give a pretty bad initial estimate of the target location. This is because the information provided by two measurements that are close to each other is similar and therefore the second measurement does not provide much new information. Another approach would be to use other available data. For example one could use the UAV altitude, one measurement, and an assumption that the target is on the ground to develop an initial target estimate. This approach will usually have better geometry than the case of initialization with two subsequent measurements and will yield a more accurate initial target estimate. A third approach is to use an *a priori* distribution model for the target if one is available. This is the most accurate initialization method but it requires an initial distribution on the target location.

The EKF results are presented in Figure 2-2. The plot on the upper right shows the vehicle and target trajectories with the measurement line-of-sight vectors drawn in. The plot on the upper left shows the ground track for the target trajectory, along with the target location estimation results. The lower left plot shows the target trajectory and the estimation results for each axis, and the lower right plot shows the estimation error and standard deviation for each axis. The bottom plot shows the information obtained in each axis as a function of the number of measurements. The plots in Figure 2-2 once again show that the Y axis estimation results improve faster than the X axis due to the larger information provided initially by the trajectory in

that dimension. At 25 measurements the information about the X and Y dimensions is equal and the covariance of both dimensions also becomes the same. As the UAV circles around the target the X and Y information is increased in a sinusoidal manner due to the geometry of the vehicle trajectory. The Z axis estimation performance remains the worst throughout as can be seen by looking at the standard deviation bounds on the lower right plot and the low amount of Z information on the Fisher Information plot. This is because the UAV must remain above the target at all times. If it were allowed to go below the target, the information about the Z dimension would increase and, correspondingly, the uncertainty about this axis would decrease, improving the estimate. However, for obvious reasons, this is not an option and the Z axis estimation remains the worst throughout. The same trend can be seen in the problem of GPS navigation, where altitude is usually the most inaccurate value since the GPS satellites are always above the user.

The next cases explored involve moving targets. The motion of the target, however, is unknown and no prior behavior models about the target are available. The targets are therefore treated using a stochastic model which assumes a stationary process, but allows for unknown target motion by adjusting the assumptions on the process noise $\mathbf{Q}_k$. This is the most practical approach if no prior information is available about the target or the environment.

The first stochastic target behavior explored is the random walk. The target is chosen to move on the ground according to a random walk model. The filter parameters for this case are given by

$$\Phi_{k,k-1} = \begin{bmatrix} 1 & 0 & 0 \\ 0 & 1 & 0 \\ 0 & 0 & 1 \end{bmatrix}, \quad \mathbf{Q}_k = \begin{bmatrix} 13 & 0 & 0 \\ 0 & 13 & 0 \\ 0 & 0 & 0 \end{bmatrix}, \quad \mathbf{R}_k = \begin{bmatrix} \sigma^2 & 0 \\ 0 & \sigma^2 \end{bmatrix} \tag{2.93}$$

Here the nonzero process noise values for the X and Y variances represent the uncertainty in the motion of the target in these two directions. The Z variance is still chosen to be zero since the target is assumed to remain on the ground. This is a reasonable assumption for ground targets traveling on fairly level terrain. If the ter-

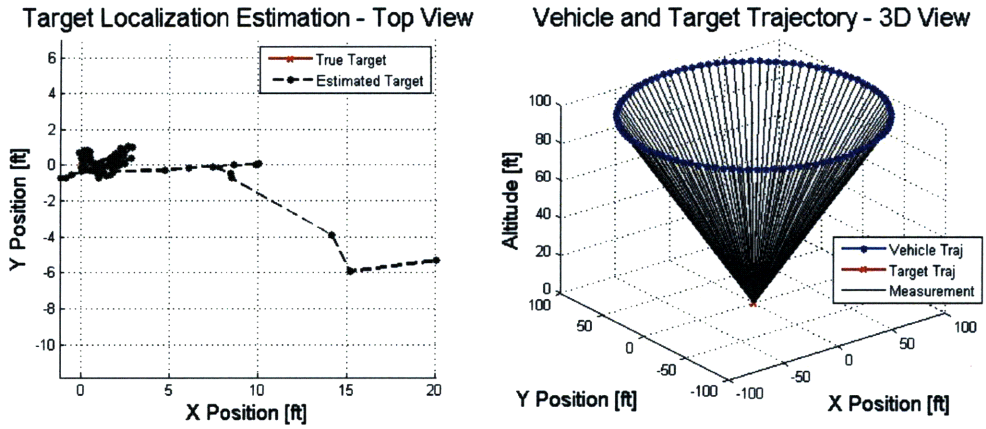

(a) Vehicle and Target Trajectories

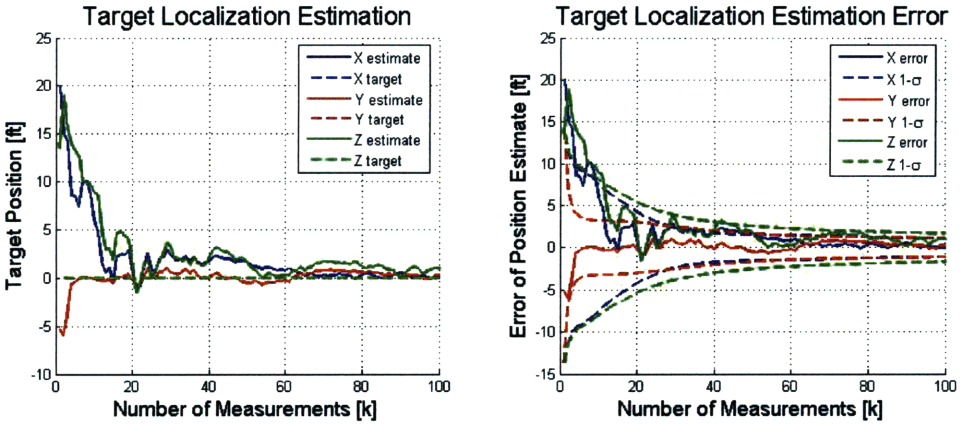

(b) Target Localization Estimation Results

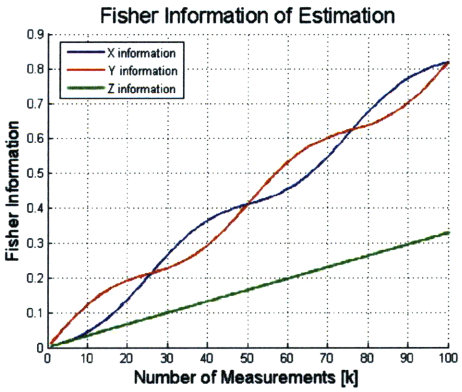

(c) Fisher Information

Figure 2-2: Localization of a stationary target using EKF algorithm in 3-D

rain is more varied then some process noise may be added, but in general the motion along the Z axis is expected to be considerably less than in the other directions. The actual values for the variances were selected as shown above for this specific case. In general the process noise selection represents a tradeoff, larger process noise values increase stability but decrease the accuracy of the estimation. For the random walk case the initialization conditions for the simulation are the same as those for the stationary case. Results for this scenario are presented in Figure 2-3 and show good tracking performance for the EKF (less than 5 feet of error). It is interesting to note that although the EKF provides proper results, it also exhibits occasional unstable behavior, especially when lower values of process noise are used. This is due to the nonlinearity in the bearings-only measurement model and the lack of good observability in the estimation process which tend to promote premature covariance collapse [6].

The next case considered involves a target moving with constant velocity. Since the objective is to estimate targets with no prior information or behavior model, it is important to note that the estimation algorithm does not know that the target is moving with constant velocity. The best it can do is assume that the target is stochastic and is moving somehow in the 2-D ground plane. Like the random walk case, this is handled by adjusting the process noise to account for the stochastic nature of the target. The parameters used for the EKF algorithm in this case are

$$\Phi_{k,k-1} = \begin{bmatrix} 1 & 0 & 0 \\ 0 & 1 & 0 \\ 0 & 0 & 1 \end{bmatrix}, \quad \mathbf{Q}_k = \begin{bmatrix} 1 & 0 & 0 \\ 0 & 1 & 0 \\ 0 & 0 & 0 \end{bmatrix}, \quad \mathbf{R}_k = \begin{bmatrix} \sigma^2 & 0 \\ 0 & \sigma^2 \end{bmatrix} \tag{2.94}$$

The simulation is initialized as before and the results for this scenario are presented in Figure 2-4. It is interesting to note the biased behavior of the estimation before the vehicle has finished circling the target and obtained measurements from all directions. This clearly shows the lack of proper information and estimation observability due to the vehicle trajectory. The estimation results obtained using the particle filtering algorithm in Section 2.3.2 display this same behavior and will be discussed further in

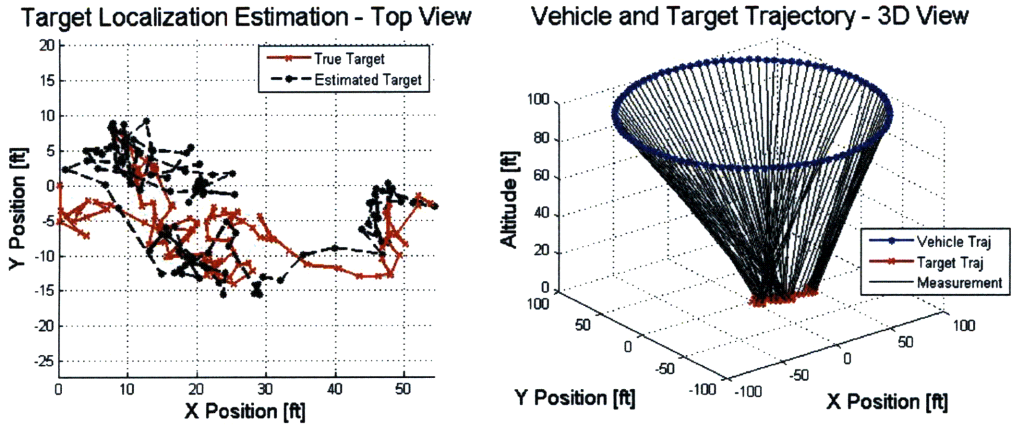

(a) Vehicle and Target Trajectories

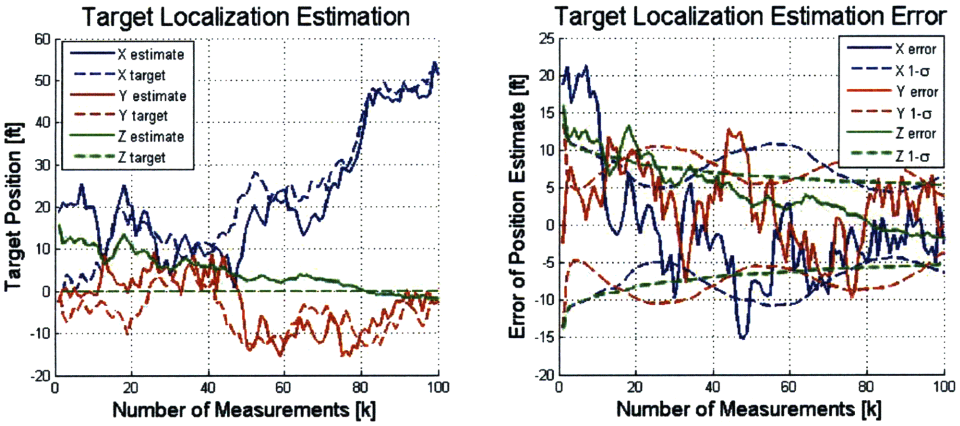

(b) Target Localization Estimation Results

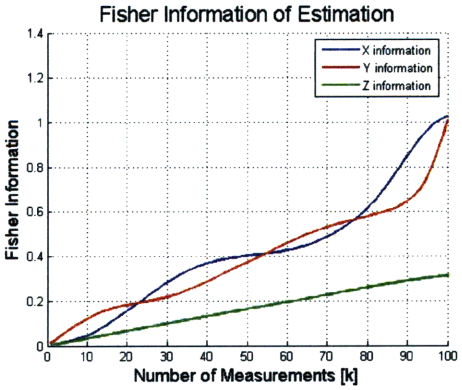

(c) Fisher Information

Figure 2-3: Localization of a target with random walk motion using EKF algorithm in 3-D

the following section. By the end of the circular trajectory, however, the estimation results converge to within the standard deviation bounds and the tracking performance is within 5 feet. Note the sharper information increase towards the end of the trajectory. This increase corresponds to the point where the UAV is closest to the target and the relative range between the UAV and the target is the lowest. This sensitivity of the Fisher Information to the relative range is more pronounced in the 3-D bearings-only case than in the 2-D case and is discussed further in Chapter 3.

The last slow moving target case considered in this section is a target following a semi-circular trajectory. The target begins at the origin and moves around a semi-circular trajectory with a radius of 20 ft. Again the estimation has no knowledge of the target's behavior and considers it to be stochastic. The process noise can be tuned accordingly and the EKF parameters are chosen to be

$$\Phi_{k,k-1} = \begin{bmatrix} 1 & 0 & 0 \\ 0 & 1 & 0 \\ 0 & 0 & 1 \end{bmatrix}, \quad \mathbf{Q}_k = \begin{bmatrix} 7 & 0 & 0 \\ 0 & 7 & 0 \\ 0 & 0 & 0 \end{bmatrix}, \quad \mathbf{R}_k = \begin{bmatrix} \sigma^2 & 0 \\ 0 & \sigma^2 \end{bmatrix} \tag{2.95}$$

For this scenario, the process noise can be tuned to provide accurate estimation without causing filter instability. The simulation is initialized as before and the results for the curved target trajectory case are shown in Figure 2-5. The tracking performance is shown to be within 7 ft of the actual target trajectory. For this scenario, the EKF diverges more often due to the nonlinearity of the target trajectory. The estimation results are noisier and the variance for this scenario is much higher than that of the other cases (see Table 2.1). It is interesting to note the close relationship between the Fisher Information and the covariance of the estimation. The information plot of Figure 2-5 shows that the Fisher Information about the X and Y coordinates increases in a sinusoidal pattern. This same sinusoidal pattern is seen in the 1-σ bounds of the X and Y axis shown in the estimation error plot. The variance of the estimation oscillates but does not improve much even if more measurements are taken. This is because of the nonlinear target motion and the assumption of stochastic target dynamics in the filter. It is also due to the fact that the older measurements do

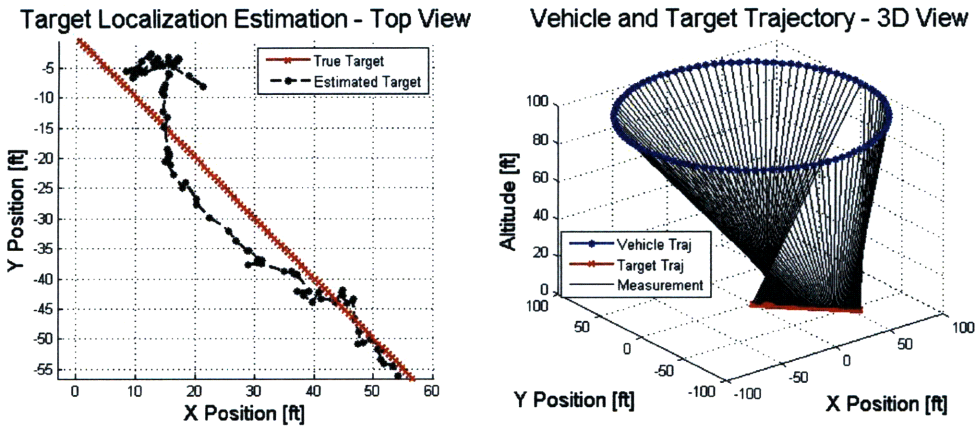

(a) Vehicle and Target Trajectories

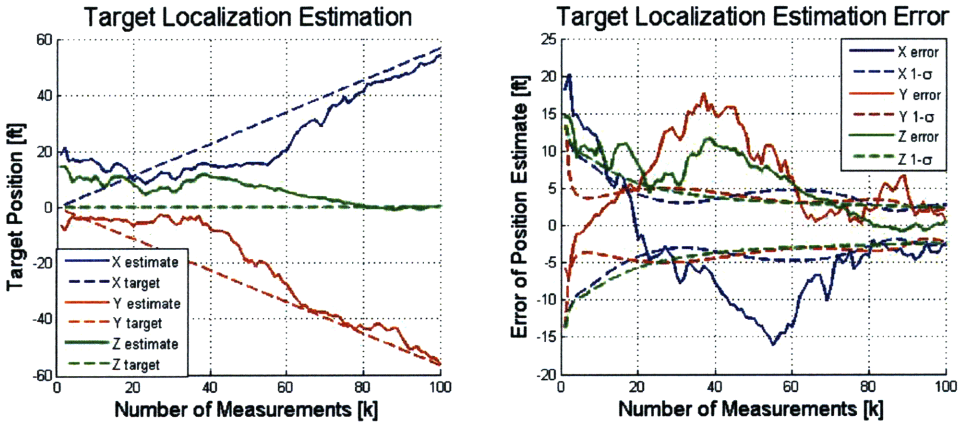

(b) Target Localization Estimation Results

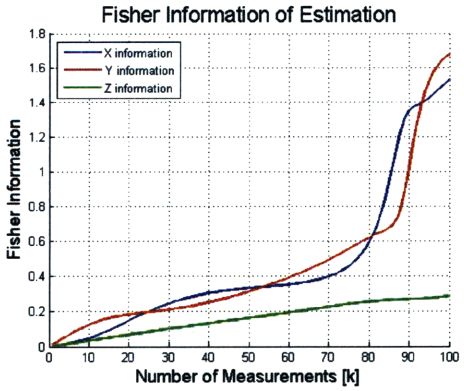

(c) Fisher Information

Figure 2-4: Localization of a constant velocity target using EKF algorithm in 3-D

Table 2.1: Summary of results for 3-D EKF Estimation

Target Dynamics		Estimation Error	Estimation Variance	Fisher Information
Stationary	x	0.05	1.20	0.82
	y	0.31	1.18	0.82
	z	0.97	2.82	0.33
	Total	1.02	5.19	1.97
Random Walk	x	-2.54	38.79	1.03
	y	0.18	10.22	1.01
	z	-1.79	28.03	0.31
	Total	3.11	77.04	2.35
Constant Velocity	x	-2.40	7.75	1.53
	y	0.54	5.72	1.68
	z	0.56	5.74	0.28
	Total	2.52	19.21	3.49
Semi-circular	x	4.17	80.89	0.88
	y	5.26	30.66	0.89
	z	1.85	16.78	0.32
	Total	6.96	128.33	2.09

not accurately represent the newer target position, however, the filter assumes a stationary target model and therefore does not properly discount older measurements. If the target motion model were known the filter performance could be improved, leading to increased accuracy in the target estimation and increased filter stability. However, since the target motion is unknown, the best assumption is that the target is stationary and the uncertainty in the process is high.

An additional case considered involves tracking a fast moving target using the predefined UAV trajectory and the EKF estimation algorithm. For this scenario the target velocity is chosen to be 22 ft/sec, which is half the cruise velocity of the UAV. The EKF parameters are given by,

$$\Phi_{k,k-1} = \begin{bmatrix} 1 & 0 & 0 \\ 0 & 1 & 0 \\ 0 & 0 & 1 \end{bmatrix}, \quad \mathbf{Q}_k = \begin{bmatrix} 1 & 0 & 0 \\ 0 & 1 & 0 \\ 0 & 0 & 0 \end{bmatrix}, \quad \mathbf{R}_k = \begin{bmatrix} \sigma^2 & 0 \\ 0 & \sigma^2 \end{bmatrix} \tag{2.96}$$

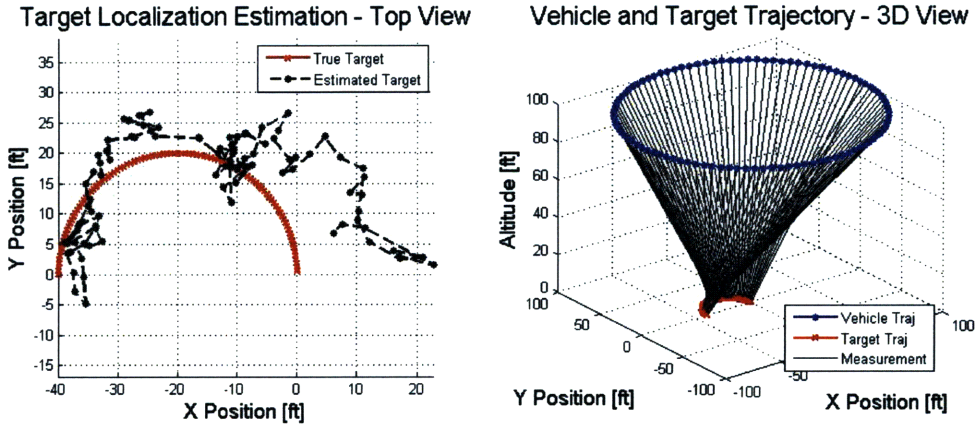

(a) Vehicle and Target Trajectories

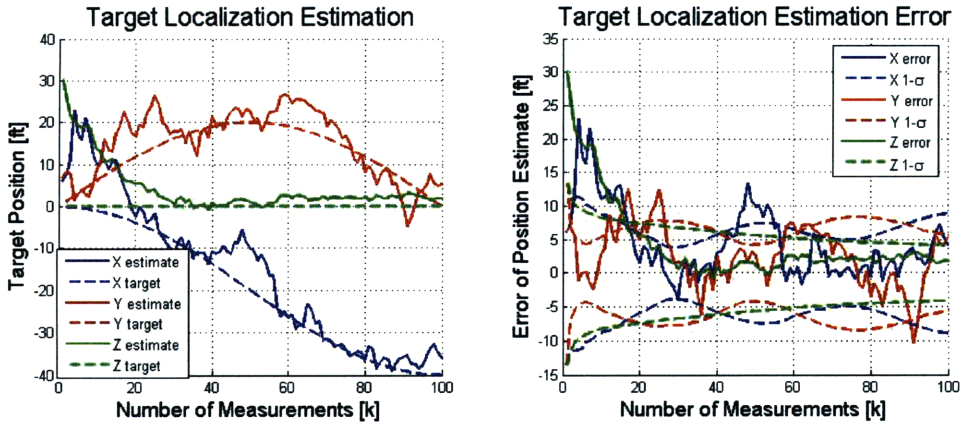

(b) Target Localization Estimation Results

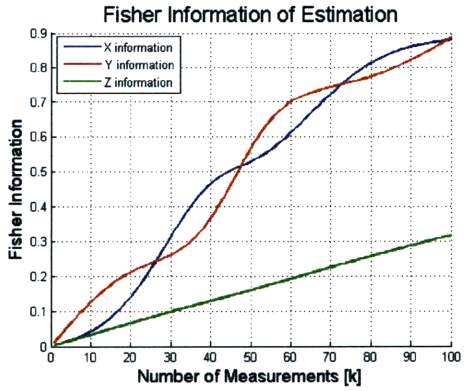

(c) Fisher Information

Figure 2-5: Localization of a turning target using EKF algorithm in 3-D

and the results for this case are presented in Figure 2-6. As seen in the plots, the EKF cannot track the target and the filter diverges. The motion of the target is too extreme, and even with several different values of process noise variance, the filter cannot localize the target properly. The information plot (bottom plot of Figure 2-6 shows that the information content of the measurements provided by the ad-hoc circular trajectory is low, and that as the target moves further away the information tends to level off indicating that the new measurements are not providing much new information.

Using an EKF with a stochastic target model produces promising results for different types of target trajectories in all but the most extreme cases. Even though no initial model of target behavior is known the EKF is able to track the target and the resulting estimation error is usually within 5 feet. The approach taken in most past literature is to assume a model for the target behavior (typically stationary or moving with a constant velocity). If a correct model of target behavior is assumed, the filtering results for the EKF would be more accurate than those obtained with this stochastic version of target behavior and the filter would diverge less often, however, the tradeoff is the obvious lack of flexibility. Since in practice it is rare to have a model of target behavior, especially for small UAVs used in areas in which the user has no prior information about the terrain or the targets it may encounter, it is of more value to have a filtering algorithm that is flexible enough to handle several types of target behaviors. Even though this approach works well for stationary and slow moving target, the EKF with a stochastic target model cannot handle fast moving targets. Using an ad-hoc vehicle trajectory, the EKF algorithm is incapable of tracking the fast target and the filter diverges. The relationship between the information content of the set of measurements and the filer performance is shown in all of the above cases, motivating the development of vehicle trajectories that increase the amount of information provided by the measurements. Chapter 3 explains the process of developing such information-based UAV trajectories for 3-D bearings-only target localization and Chapter 4 revisits the cases presented above using a simultaneous target estimation and vehicle trajectory optimization approach.

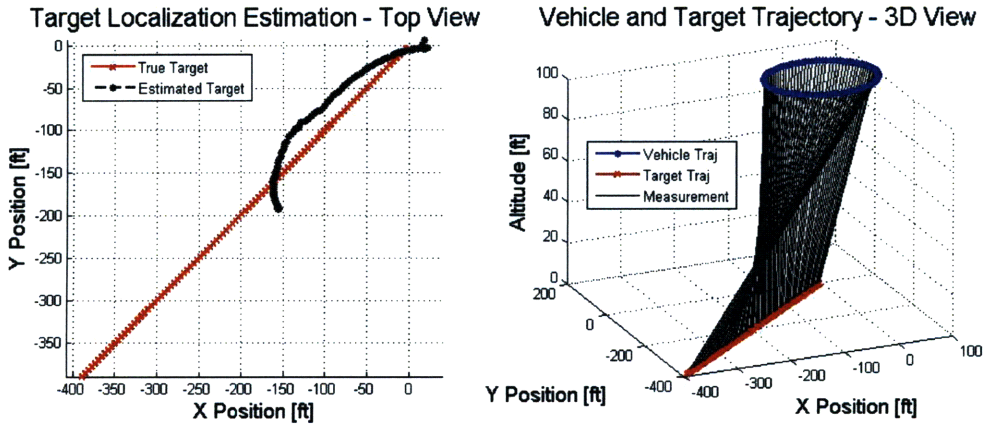

(a) Vehicle and Target Trajectories

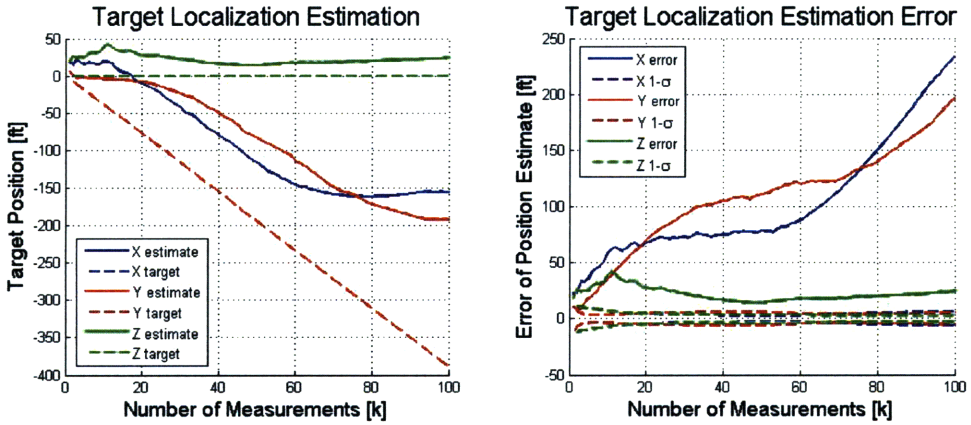

(b) Target Localization Estimation Results

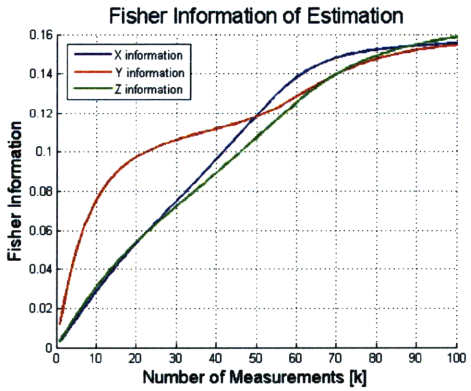

(c) Fisher Information

Figure 2-6: Localization of a fast constant velocity target using EKF algorithm in 3-D

2.3.2 Particle Filter for Bearings-Only Target Localization

The next filtering algorithm explored for the problem of target localization with vision based measurements is the particle filter. The particle filtering algorithm, described in Section 2.2.3, is implemented first in a simplified 2-D version of the estimation problem. The number of particles is set to $N = 500$, which is usually low for a particle filter, but which provides adequate estimation results in real-time (less than a second). The vehicle trajectory, target location, and initialization parameters are the same as those used in the EKF problem. The sample particles for the 2-D case are initialized from a Gaussian distribution $p(\mathbf{x}_0) = \mathcal{N}(\hat{\mathbf{x}}_0, \mathbf{P}_0)$ with mean and covariance given by

$$\hat{\mathbf{x}}_0 = \begin{bmatrix} 30 \\ 30 \end{bmatrix}, \quad \mathbf{P}_0 = \begin{bmatrix} 200 & 0 \\ 0 & 200 \end{bmatrix} \tag{2.97}$$

The particle propagation model is assumed to be constant with a noise model given by $\mathbf{w}_k \sim \mathcal{N}(0, \sigma_w)$. Selecting the particle filter tuning parameters is important for determining the performance of the algorithm. Increasing the value of σ_w speeds up the response and convergence of the particle filter, however, it increases the overall variance and the estimate is noisier. The resampling threshold N_{thr} affects the overall stability of the algorithm. If N_{thr} is too high the algorithm degenerates and diverges and if it is too low then the resampling is based on noisy processing of measurements and not on a true significant change in probability distribution. For the 2-D stationary target case the tuning parameters are set to

$$\sigma_w = 1.5 \tag{2.98}$$

$$N_{thr} = 10 \tag{2.99}$$

The measurement likelihood function is Gaussian and is defined by

$$p(\mathbf{z}_k|\mathbf{x}_k^i) = \frac{1}{\sqrt{2\pi\sigma^2}} \exp\left\{-\frac{1}{\sigma^2}\left[\mathbf{z}_k - \mathbf{h}(\mathbf{x}_k^i)\right]^2\right\} \tag{2.100}$$

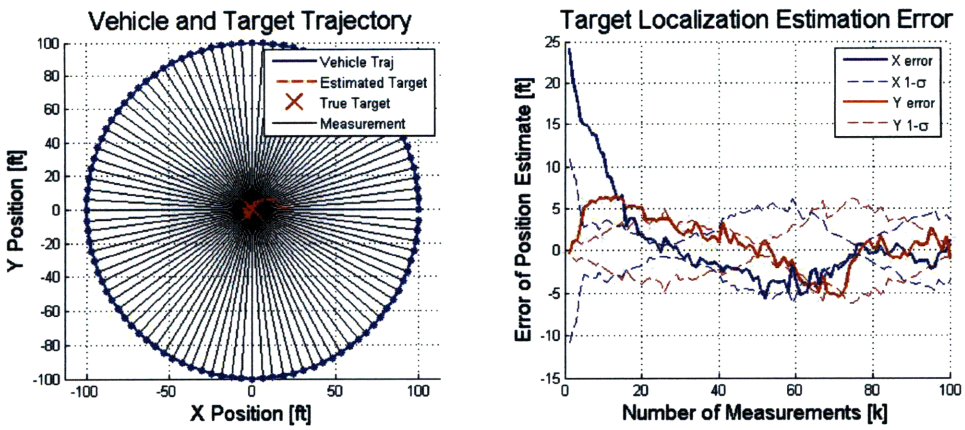

(a) Target Location Estimation

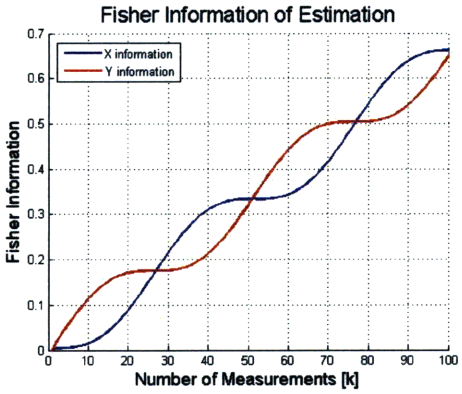

(b) Fisher Information

Figure 2-7: Target localization using a particle filtering algorithm in 2-D

Here $\mathbf{h}(\mathbf{x}_k^i)$ is the measurement model evaluated at the particle $\mathbf{x}_k^i$ and is given by

$$\mathbf{h}(\mathbf{x}_k^i) = \tan^{-1}\left(\frac{p_{k_x} - \mathbf{x}_{k_x}^i}{p_{k_y} - \mathbf{x}_{k_y}^i}\right) = \tan^{-1}\left(\frac{r_{k_x}}{r_{k_y}}\right) \tag{2.101}$$

which is the measurement model described previously for the EKF. The results for the 2-D particle filtering algorithm are shown in Figure 2-7. Note that, once again, the initial Y axis performance is much better than that of the X axis due to the sharper initial increase in information in the Y direction.

The particle filtering algorithm is extended to the 3-D target localization case. The UAV trajectory is chosen to be a circle of 100 ft radius, orbiting the target at a constant altitude of 100 ft, which is the same vehicle trajectory used in the previous section. The particle filter sample set is initialized using a Gaussian distribution

$p(\mathbf{x}_0) = \mathcal{N}(\hat{\mathbf{x}}_0, \mathbf{P}_0)$ with mean and covariance given by

$$\hat{\mathbf{x}}_0 = \begin{bmatrix} 20 \\ 20 \\ 20 \end{bmatrix}, \quad \mathbf{P}_0 = \begin{bmatrix} 200 & 0 & 0 \\ 0 & 200 & 0 \\ 0 & 0 & 200 \end{bmatrix} \tag{2.102}$$

The particle filter algorithm is used on the following scenarios: a stationary target, a target exhibiting random walk behavior, a constant velocity target and a target following a semi-circular trajectory. The results for these cases are summarized in Table 2.2, which provides the same data described in the previous section for the EKF results table. An additional case for a fast moving target is considered as well and presented last.

For the stationary target case, the particle propagation model is assumed to be constant. The noise model is given by $\mathbf{w}_k \sim \mathcal{N}(0, \sigma_w)$ and the tuning parameters are set to

$$\sigma_w = 0.5 \tag{2.103}$$

$$N_{thr} = 30 \tag{2.104}$$

The measurement likelihood function for the 3-D case is based on two bearings measurements as before, and its equation is given by

$$p(\mathbf{z}_k|\mathbf{x}_k^i) = \frac{1}{\sqrt{2\pi\sigma^2}} \exp\left\{-\frac{1}{\sigma^2}\left[\mathbf{z}_k - \mathbf{h}(\mathbf{x}_k^i)\right]^T \left[\mathbf{z}_k - \mathbf{h}(\mathbf{x}_k^i)\right]\right\} \tag{2.105}$$

where $\mathbf{z}_k = \begin{bmatrix} \beta & \phi \end{bmatrix}_k^T$ (see equation (2.88)) and the measurement model is

$$\mathbf{h}(\mathbf{x}_k^i) = \begin{bmatrix} \tan^{-1}\left(\frac{p_{k_x} - \mathbf{x}_{k_x}^i}{p_{k_y} - \mathbf{x}_{k_y}^i}\right) \\ \tan^{-1}\left(\frac{p_{k_z} - \mathbf{x}_{k_z}^i}{\sqrt{(p_{k_x} - \mathbf{x}_{k_x}^i)^2 + (p_{k_y} - \mathbf{x}_{k_y}^i)^2}}\right) \end{bmatrix} = \begin{bmatrix} \tan^{-1}\left(\frac{r_{k_x}}{r_{k_y}}\right) \\ \tan^{-1}\left(\frac{r_{k_z}}{\sqrt{r_{k_x}^2 + r_{k_y}^2}}\right) \end{bmatrix} \tag{2.106}$$

The PF results for the stationary target case are presented in Figure 2-8. The final estimation error is 0.46 ft, but the variance is still high (see Table 2.2). More accurate

results can be obtained if the number of particles is increased. However, for real-time use onboard a UAV the computational cost required for processing more particles is too high. For instance the PF algorithm with 500 particles takes under a second to run whereas with 5000 particles the run-time is two orders of magnitude higher.

The next case considered is for a stochastic target pursuing a random walk behavior. For this case the particle propagation model is once again considered constant, but the variance of the process noise is increased to account for the added uncertainty due to the target motion. The filter tuning parameters for the random walk case are set to

$$\sigma_w = 2.0 \tag{2.107}$$

$$N_{thr} = 20 \tag{2.108}$$

The results are given in Figure 2-9. The filter successfully tracks the random walk and the estimation error is within 5 feet.

A constant velocity target is explored next. No prior behavior model for the target dynamics is assumed so the particle propagation model is once again constant and the process noise is adjusted accordingly to account for the target motion. The tuning parameters for the constant velocity target case are

$$\sigma_w = 1.5 \tag{2.109}$$

$$N_{thr} = 30 \tag{2.110}$$

The results for the estimation of the constant velocity target are presented in Figure 2-10. It is interesting to note that the performance of the estimation for the particle filtering algorithm is very similar to that of the EKF shown in the previous section (see Figure 2-4). Once again there are biases in both the X and Y axes until the vehicle completes a circle above the target and obtains measurements from all sides. Furthermore, the drastic improvement in estimation performance seen in the error plot of Figure 2-10 corresponds to the increase in information observed in the

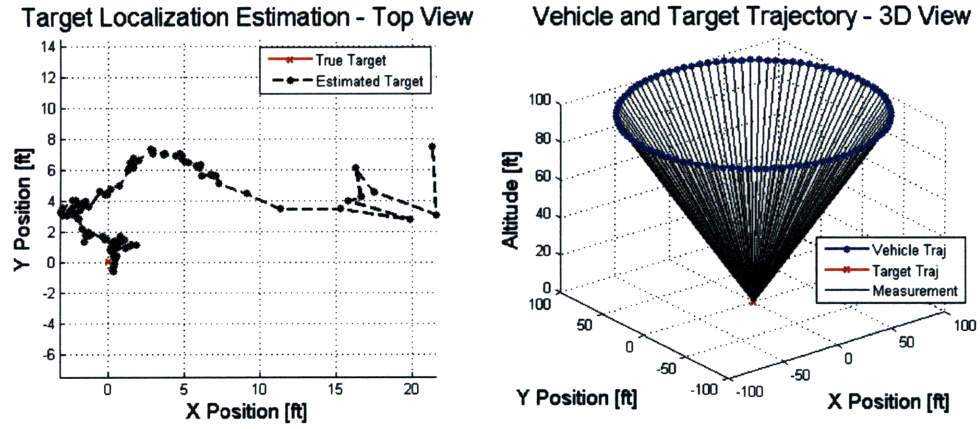

(a) Vehicle and Target Trajectories

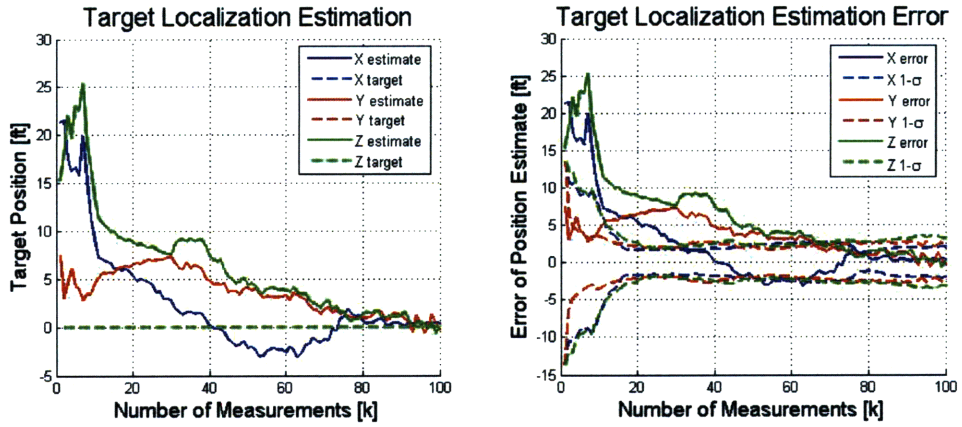

(b) Target Localization Estimation Results

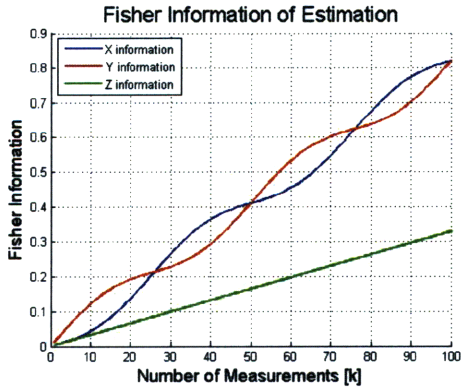

(c) Fisher Information

Figure 2-8: Localization of a stationary target using a particle filtering algorithm in 3-D

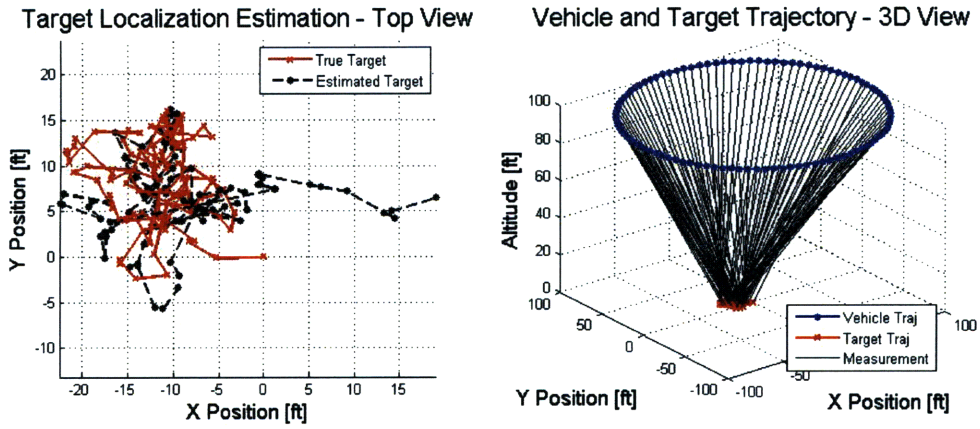

(a) Vehicle and Target Trajectories

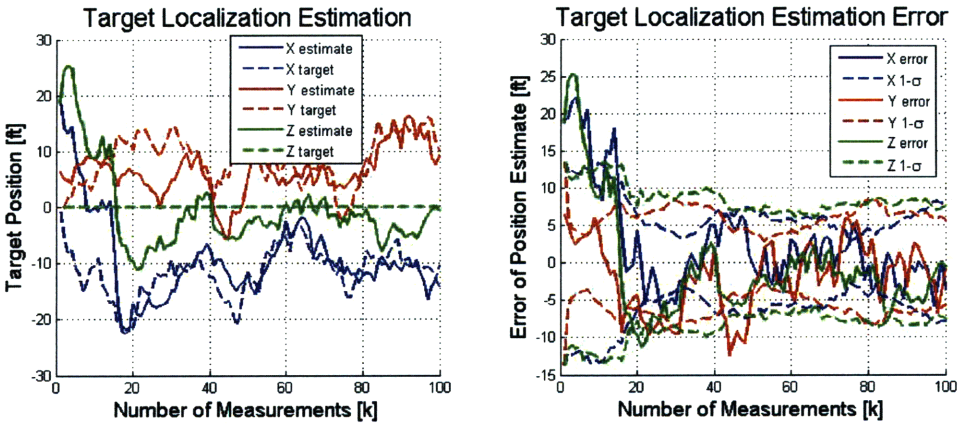

(b) Target Localization Estimation Results

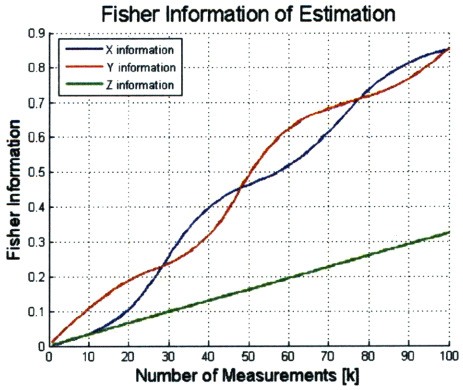

(c) Fisher Information

Figure 2-9: Localization of a target with random walk motion using a particle filtering algorithm in 3-D

Fisher Information plot. This shows the dependence of the estimation performance on the vehicle trajectory and illustrates the importance of selecting a trajectory that maximizes the information provided by the measurements.

The last slow moving target case considered is for a target starting at the origin and following a semi-circular trajectory. The particle propagation model for this case is also assumed constant and the tuning parameters are set as follows

$$\sigma_w = 1.2 \tag{2.111}$$

$$N_{thr} = 20 \tag{2.112}$$

The results for the target following a semi-circular trajectory are presented in Figure 2-11. The estimation convergence properties for the PF are better than those of the EKF and the filter diverges less often. The tracking performance however is noisier and the estimation error is about 9 ft with a variance of 70.5 (see Table 2.2). Decreasing σ_w would make the PF results less noisy, but for this moving target case, lower values of σ_w would decrease the stability of the filter.

An additional case of a fast moving constant velocity target is considered as well and the results are presented in Figure 2-12. The target velocity is 22 ft/sec, half the cruise speed of the UAV, and the UAV trajectory is predefined as before. The results show that the particle filter is incapable of tracking the fast target. For several values of the tuning parameters σ_w and N_{thr} the filter still diverges. The information provided by the ad-hoc UAV trajectory, shown in the bottom plot of Figure 2-12, is very low compared to the other scenarios, and, as in the case using the EKF, the information tends to level off showing that the new measurements are not providing much new information.

Overall, the particle filtering algorithm performs as desired yielding good tracking performance for the stationary target case and for the cases of slow moving targets with unknown target dynamics, even though tracking in the fast moving target case is not achievable. In general, the particle filtering algorithm is more stable than the EKF and is less prone to filter collapse or algorithm degeneration. It is also able to

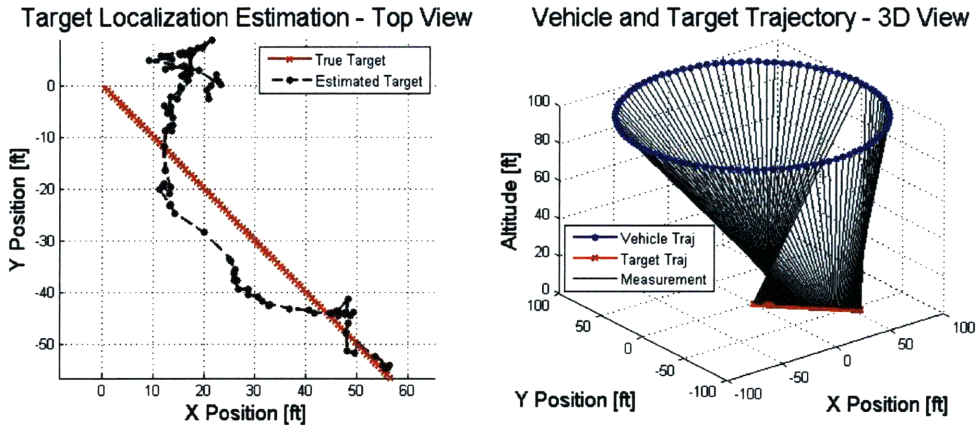

(a) Vehicle and Target Trajectories

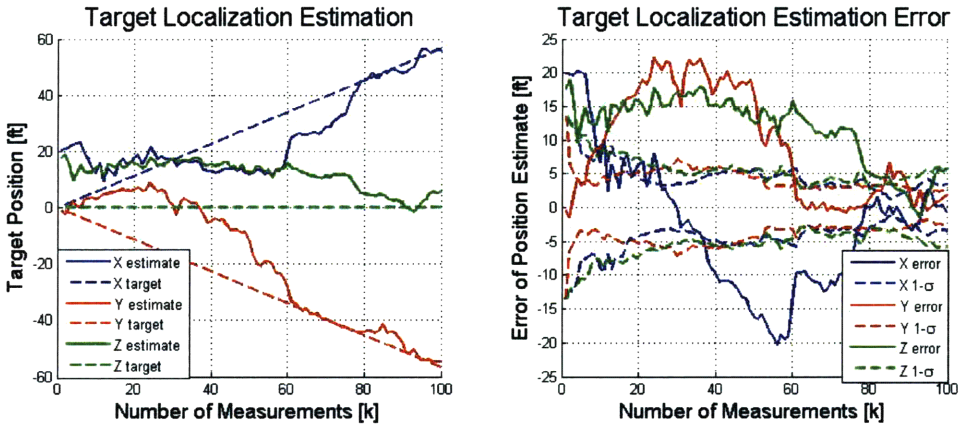

(b) Target Localization Estimation Results

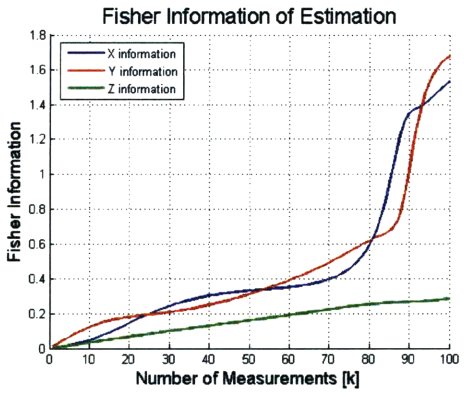

(c) Fisher Information

Figure 2-10: Localization of a constant velocity target using a particle filtering algorithm in 3-D

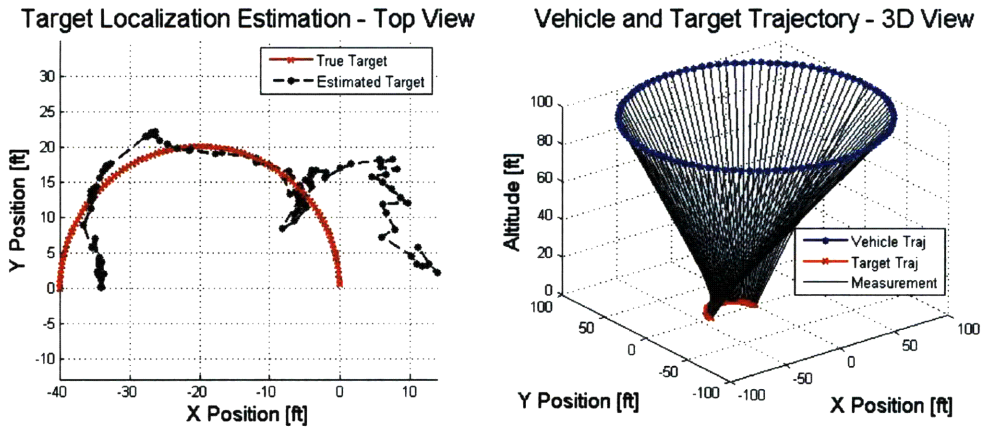

(a) Vehicle and Target Trajectories

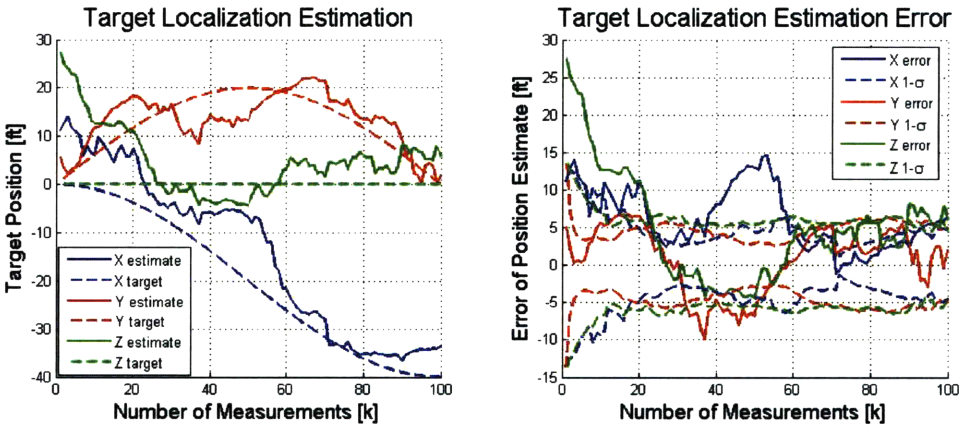

(b) Target Localization Estimation Results

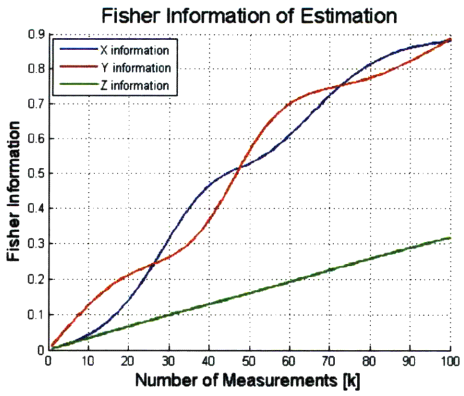

(c) Fisher Information

Figure 2-11: Localization of a turning target using a particle filtering algorithm in 3-D

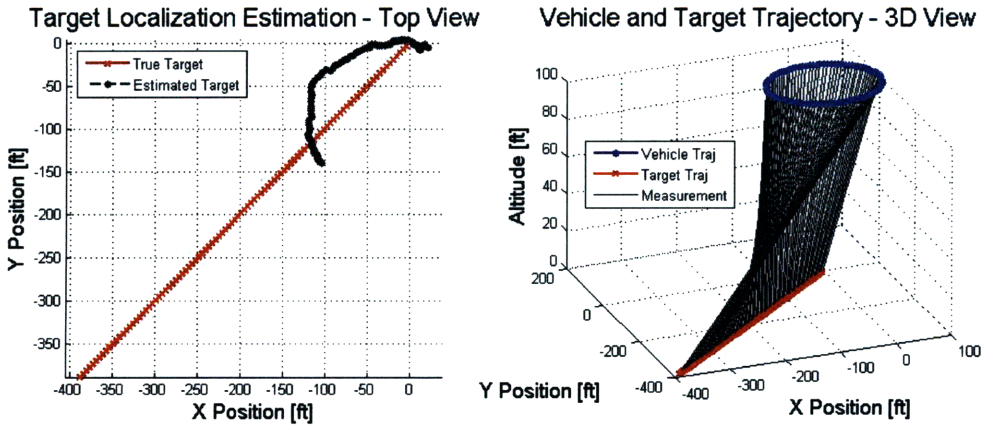

(a) Vehicle and Target Trajectories

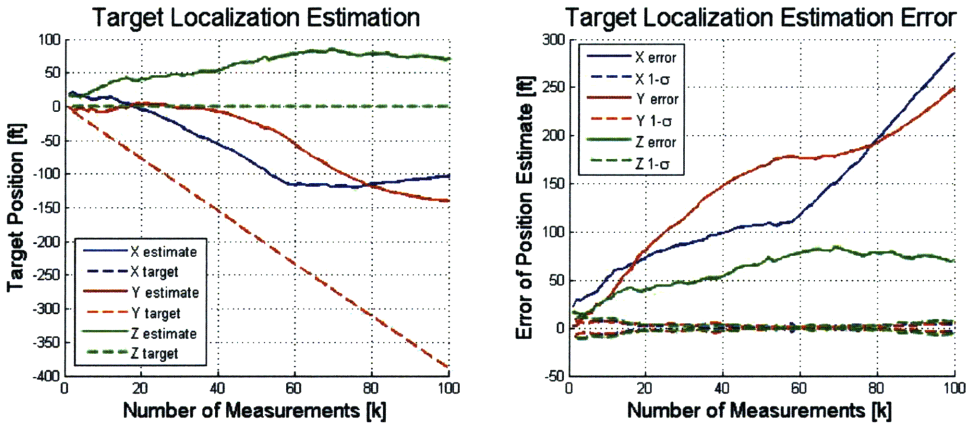

(b) Target Localization Estimation Results

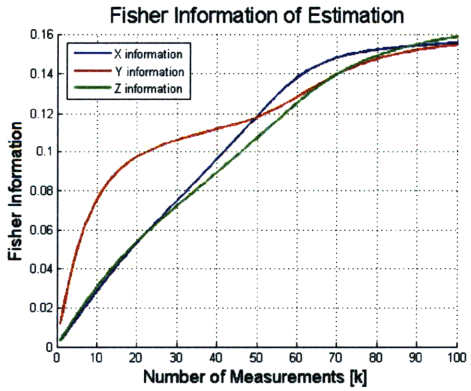

(c) Fisher Information

Figure 2-12: Localization of a fast constant velocity target using a particle filtering algorithm in 3-D

Table 2.2: Summary of results for 3-D Particle Filter Estimation

Target Dynamics		Estimation Error	Estimation Variance	Fisher Information
Stationary	x	0.34	4.55	0.82
	y	-0.31	4.80	0.82
	z	0.04	12.30	0.33
	Total	0.46	21.65	1.97
Random Walk	x	-3.68	69.38	0.85
	y	-0.85	34.75	0.85
	z	-0.73	56.45	0.32
	Total	3.84	160.59	2.02
Constant Velocity	x	-0.72	12.58	1.53
	y	1.90	9.42	1.68
	z	5.75	32.20	0.28
	Total	6.10	54.21	3.49
Semi-circular	x	6.34	23.58	0.88
	y	2.08	20.65	0.89
	z	6.02	26.26	0.32
	Total	8.99	70.49	2.09

handle the nonlinear, non-Gaussian distribution better and, given enough particles, leads to a more accurate estimation of the target motion (although at the cost of higher computational requirements). On the other hand, the particle filter is more sensitive to its tuning parameters, requiring more design effort to properly select these parameters, and, in many cases, it is not obvious what the best selection of these should be.

The most interesting result though is observing the similarities between the algorithms' performances. This is especially noted in the constant velocity target scenario, where both algorithms have similar biased estimation results and poor performance in the same axes during the same time spans, until enough information and proper estimation observability is provided by the UAV coming close to the target and by completing the circle. For all of the scenarios shown above, using an ad-hoc UAV trajectory provides the same information to the EKF and the PF, and the estimation performance for both algorithms is shown to be highly dependent on the information contained in the measurements, illustrating the need for proper trajectory generation

algorithms that focus on increasing the information provided by the measurements. The next chapter focuses on designing trajectories that maximize the information for the 3-D bearings-only target location estimation problem, and Chapter 4 revisits the estimation problem for the cases shown above using the optimized vehicle trajectory.

THIS PAGE INTENTIONALLY LEFT BLANK

Chapter 3

Vehicle Trajectory Optimization

Optimizing the trajectory of the vehicle is a necessary step in improving estimation performance. The previous chapters explained and illustrated the dependance of the estimation performance on the vehicle trajectory. This is an especially big concern for the problem of target localization using vision based measurements, since the measurement model is highly nonlinear, and the estimation results become severely biased if the measurements do not provide much new information and proper estimation observability is not obtained. This chapter explores the problem of trajectory design and optimization for the bearings-only target location estimation problem. The first sections revisit the concept of the Fisher Information Matrix and show how this performance measure can be used to produce an objective function for the trajectory optimization problem. The following sections show the optimization results for the sensor placement case and the problem of trajectory design with motion constraints. The sensor placement case analyzes the problem of determining the best locations from which to take measurements, without considering vehicle motion constraints that restrict the distance between subsequent measurement locations. This scenario is applicable to a target localization problem without a strict time limit or to the case of target localization using multiple UAVs. The results for the sensor placement case provide intuition about the expected trajectory shape and are useful in testing and comparing different objective functions. The next scenario examined is that of trajectory optimization with vehicle constraints. Here the motion of the vehicle is

restricted between subsequent measurements based on the vehicle's capabilities and constraints. The resulting trajectories are applicable to the case of target localization using a single UAV.

It is important to note that the results in this chapter are obtained assuming that the true target location is known. Since the problem at hand is to estimate the location of the target, this is obviously a very limiting assumption. The dependence of the optimization solution on the true target location has been one of the biggest problems associated with vehicle trajectory optimization, usually leading to a highly nonlinear problem if the estimation and optimization are solved simultaneously (see [72]). Nevertheless, exploring the theoretical results for trajectory optimization using the true target location leads to results which provide intuition about the expected performance of the trajectory optimizer. Chapter 4 addresses the problem of uncertainty in the target location and provides ways to deal with this issue by combining the optimization and estimation problems.

3.1 Objective Function Selection

As described in Section 2.1, the Fisher Information Matrix captures the physical and geometrical properties of the estimation problem and provides a good baseline for quantifying the performance of the estimation process. Since all measurements differ in the information contained about the estimation process, an information-theoretic framework provides a way of selecting which measurements bring the most additional or new information, thus increasing the overall information content and enhancing the performance of the estimation. In addition to being related to the accuracy of the estimation, the FIM enjoys several useful properties which make it a good framework for the trajectory optimization problem. These properties include being symmetric and positive-definite (or at least positive semi-definite), having a recursive form for computation, and being additive across multiple sensors and time-steps (the overall FIM from many sensors over time is the sum of the FIM's for the individual sensors, or the FIM over many time steps is the sum of the FIM's for each time step). The

FIM is the inverse of the CRLB which is a lower bound on the covariance achievable by the estimation algorithm. Since the objective is to minimize the covariance of the estimation, it is desirable to make the FIM as large as possible.

The FIM is a function of the sensor locations, among other things, suggesting that the sensor locations can be optimized to maximize the value of the FIM. In a strict sense this amounts to finding a configuration for the sensors, $\mathbf{p}^\star$, such that $\mathbf{J}(\mathbf{p}^\star) \geq \mathbf{J}(\mathbf{p})$ where $\mathbf{J}$ is the FIM and $\mathbf{p}$ is any other sensor configuration. This is equivalent to requiring the matrix defined by $\mathbf{J}(\mathbf{p}^\star) - \mathbf{J}(\mathbf{p})$ to be at least positive semi-definite. In general $\mathbf{p}^\star$ is not likely to exist except under very special circumstances and even then it is difficult to find [72]. It is therefore desirable to find a scalar real-valued function based on the FIM over which the optimization can be performed. Since going from a matrix to a scalar results in a loss of information, this leads to a weaker optimization metric, but simplifies the process enough to produce successful trajectory results. An analysis of different possible functions is provided in Section 3.1.2.

Another main problem with the FIM is its dependence on the true value of the parameter to be estimated, in this case, the true target location. Chapter 4 will look at this issue in more detail. The form of the FIM for the bearings-only target localization problem is derived in Section 3.1.1. The equations show the dependence of the FIM on both the vehicle measurement locations and the true target position.

3.1.1 Fisher Information Matrix for Bearings-Only Target Localization

The equations for the Fisher Information Matrix are given in Section 2.1.1. The recursive form of the FIM is provided by

$$\begin{aligned} \mathbf{J}_k &= [\Phi_{k,k-1}^T]^{-1}\mathbf{J}_{k-1}\Phi_{k,k-1}^{-1} + \mathbf{H}_k^T\mathbf{R}_k^{-1}\mathbf{H}_k \\ &= \sum_{\imath=1}^{k} \Phi_{k,\imath}^T\mathbf{H}_\imath^T\mathbf{R}_\imath^{-1}\mathbf{H}_\imath\Phi_{k,\imath} \end{aligned} \tag{3.1}$$

Here $\Phi_{k,i}$ is the state transition matrix of the estimation process from time i to k, $\mathbf{R}_k$ is the measurement noise covariance, and $\mathbf{H}_k$ is the Jacobian of the measurement model defined by $\mathbf{H}_k = \nabla_{\mathbf{x}_k}\mathbf{h}(\mathbf{x}_k)$.

To derive the Fisher Information Matrix for the 2-D bearings-only estimation problem, the measurement model used is

$$\mathbf{h}(\mathbf{x}_k) = \beta = \tan^{-1}\left(\frac{p_x - t_x}{p_y - t_y}\right) = \tan^{-1}\left(\frac{r_x}{r_y}\right) \tag{3.2}$$

where $\mathbf{p}_k = \begin{bmatrix} p_x & p_y \end{bmatrix}_k^T$ is the position of the vehicle, $\mathbf{t}_k = \begin{bmatrix} t_x & t_y \end{bmatrix}_k^T$ is the position of the target and $\mathbf{r}_k = \begin{bmatrix} r_x & r_y \end{bmatrix}_k^T$ is the relative vector between the vehicle and the target. The state to be estimated is $\mathbf{x}_k = \mathbf{t}_k = \begin{bmatrix} t_x & t_y \end{bmatrix}_k^T$, so the Jacobian of the measurement model is given by

$$\mathbf{H}_k = \begin{bmatrix} -\frac{r_y}{r_x^2+r_y^2} & \frac{r_x}{r_x^2+r_y^2} \end{bmatrix}_k \tag{3.3}$$

Using a constant process model and constant sensor noise variance gives

$$\Phi_{k,i} = \begin{bmatrix} 1 & 0 \\ 0 & 1 \end{bmatrix}, \quad \mathbf{R}_k = \sigma^2 \tag{3.4}$$

and the FIM reduces to

$$\mathbf{J}_k = \frac{1}{\sigma^2}\sum_{i=1}^{k} \mathbf{H}_i^T\mathbf{H}_i \tag{3.5}$$

For the 2-D case $\mathbf{H}^T\mathbf{H}$ becomes

$$\mathbf{H}^T\mathbf{H} = \begin{bmatrix} \frac{r_y^2}{(r_x^2+r_y^2)^2} & -\frac{r_x r_y}{(r_x^2+r_y^2)^2} \\ -\frac{r_x r_y}{(r_x^2+r_y^2)^2} & \frac{r_x^2}{(r_x^2+r_y^2)^2} \end{bmatrix} \tag{3.6}$$

which gives

$$\mathbf{J}_k = \frac{1}{\sigma^2}\sum_{\imath=1}^{k}\begin{bmatrix} \frac{r_{\imath y}^2}{(r_{\imath x}^2+r_{\imath y}^2)^2} & -\frac{r_{\imath x}r_{\imath y}}{(r_{\imath x}^2+r_{\imath y}^2)^2} \\ -\frac{r_{\imath x}r_{\imath y}}{(r_{\imath x}^2+r_{\imath y}^2)^2} & \frac{r_{\imath x}^2}{(r_{\imath x}^2+r_{\imath y}^2)^2} \end{bmatrix} = \frac{1}{\sigma^2}\sum_{i=1}^{k}\frac{1}{|\mathbf{r}_i|^4}\begin{bmatrix} r_{\imath y}^2 & -r_{\imath x}r_{\imath y} \\ -r_{\imath x}r_{\imath y} & r_{\imath x}^2 \end{bmatrix} \tag{3.7}$$

To calculate the Fisher Information Matrix for the 3-D case, the measurement model consisting of two bearing angles is used (see Figure 3-1),

$$\mathbf{h}(\mathbf{x}_k) = \begin{bmatrix}\beta \\ \phi\end{bmatrix} = \begin{bmatrix} \tan^{-1}\left(\frac{p_x-t_x}{p_y-t_y}\right) \\ \tan^{-1}\left(\frac{p_z-t_z}{\sqrt{(p_x-t_x)^2+(p_y-t_y)^2}}\right)\end{bmatrix} = \begin{bmatrix} \tan^{-1}\left(\frac{r_x}{r_y}\right) \\ \tan^{-1}\left(\frac{r_z}{\sqrt{r_x^2+r_y^2}}\right)\end{bmatrix} \tag{3.8}$$

where $\mathbf{p}_k = \begin{bmatrix} p_x & p_y & p_z \end{bmatrix}_k^T$ is the position of the vehicle, $\mathbf{t}_k = \begin{bmatrix} t_x & t_y & t_z \end{bmatrix}_k^T$ is the position of the target and $\mathbf{r}_k = \begin{bmatrix} r_x & r_y & r_z \end{bmatrix}_k^T$ is the relative vector between the vehicle and the target. The Jacobian of the measurement model with respect to the target is then given by

$$\mathbf{H}_k = \begin{bmatrix} -\frac{r_y}{r_x^2+r_y^2} & \frac{r_x}{r_x^2+r_y^2} & 0 \\ \frac{r_x r_z}{(r_x^2+r_y^2+r_z^2)\sqrt{r_x^2+r_y^2}} & \frac{r_y r_z}{(r_x^2+r_y^2+r_z^2)\sqrt{r_x^2+r_y^2}} & -\frac{\sqrt{r_x^2+r_y^2}}{(r_x^2+r_y^2+r_z^2)} \end{bmatrix}_k = \begin{bmatrix}\mathbf{H}_\beta \\ \mathbf{H}_\phi\end{bmatrix}_k \tag{3.9}$$

Since the target is stationary or stochastic with a stationary process model the state transition matrix is constant. The noise is assumed to be uncorrelated and with constant covariance giving

$$\Phi_{k,\imath} = \begin{bmatrix} 1 & 0 & 0 \\ 0 & 1 & 0 \\ 0 & 0 & 1 \end{bmatrix}, \quad \mathbf{R}_k = \begin{bmatrix} \sigma^2 & 0 \\ 0 & \sigma^2 \end{bmatrix} \tag{3.10}$$

and the FIM reduces to

$$\mathbf{J}_k = \frac{1}{\sigma^2}\sum_{\imath=1}^{k}\mathbf{H}_\imath^T\mathbf{H}_\imath \tag{3.11}$$

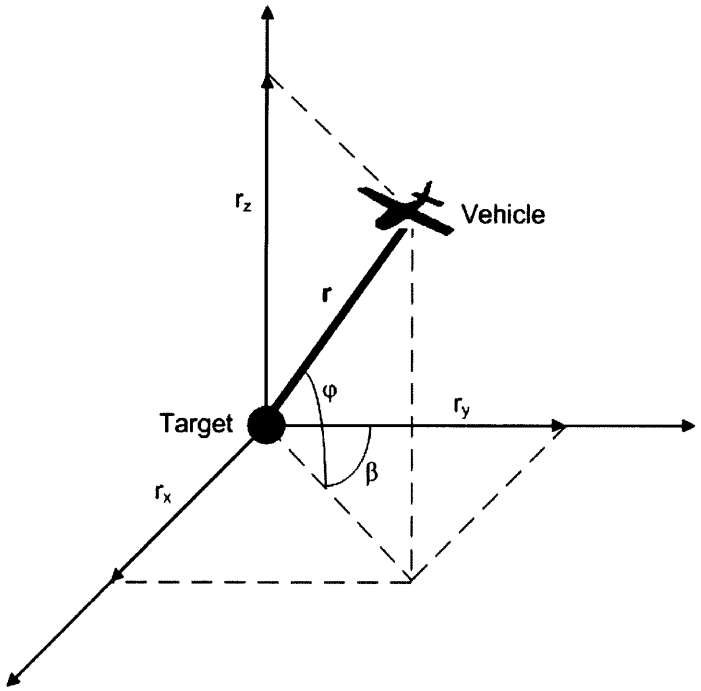

Figure 3-1: Azimuth (β) and elevation (ϕ) between vehicle and target

In the 3-D case $\mathbf{H}^T\mathbf{H}$ becomes

$$\begin{aligned}
\mathbf{H}^T\mathbf{H} &= \begin{bmatrix} \frac{r_y^2}{(r_x^2+r_y^2)^2} + \frac{r_x^2 r_z^2}{(r_x^2+r_y^2+r_z^2)^2(r_x^2+r_y^2)} & -\frac{r_x r_y}{(r_x^2+r_y^2)^2} + \frac{r_x r_y r_z^2}{(r_x^2+r_y^2+r_z^2)^2(r_x^2+r_y^2)} & -\frac{r_x r_z}{(r_x^2+r_y^2+r_z^2)^2} \\ -\frac{r_x r_y}{(r_x^2+r_y^2)^2} + \frac{r_x r_y r_z^2}{(r_x^2+r_y^2+r_z^2)^2(r_x^2+r_y^2)} & \frac{r_x^2}{(r_x^2+r_y^2)^2} + \frac{r_y^2 r_z^2}{(r_x^2+r_y^2+r_z^2)^2(r_x^2+r_y^2)} & -\frac{r_y r_z}{(r_x^2+r_y^2+r_z^2)^2} \\ -\frac{r_x r_z}{(r_x^2+r_y^2+r_z^2)^2} & -\frac{r_y r_z}{(r_x^2+r_y^2+r_z^2)^2} & \frac{(r_x^2+r_y^2)}{(r_x^2+r_y^2+r_z^2)^2} \end{bmatrix} \\
&= \begin{bmatrix} \frac{r_y^2}{(r_x^2+r_y^2)^2} & -\frac{r_x r_y}{(r_x^2+r_y^2)^2} & 0 \\ -\frac{r_x r_y}{(r_x^2+r_y^2)^2} & \frac{r_x^2}{(r_x^2+r_y^2)^2} & 0 \\ 0 & 0 & 0 \end{bmatrix} + \begin{bmatrix} \frac{r_x^2 r_z^2}{(r_x^2+r_y^2+r_z^2)^2(r_x^2+r_y^2)} & \frac{r_x r_y r_z^2}{(r_x^2+r_y^2+r_z^2)^2(r_x^2+r_y^2)} & -\frac{r_x r_z}{(r_x^2+r_y^2+r_z^2)^2} \\ \frac{r_x r_y r_z^2}{(r_x^2+r_y^2+r_z^2)^2(r_x^2+r_y^2)} & \frac{r_y^2 r_z^2}{(r_x^2+r_y^2+r_z^2)^2(r_x^2+r_y^2)} & -\frac{r_y r_z}{(r_x^2+r_y^2+r_z^2)^2} \\ -\frac{r_x r_z}{(r_x^2+r_y^2+r_z^2)^2} & -\frac{r_y r_z}{(r_x^2+r_y^2+r_z^2)^2} & \frac{(r_x^2+r_y^2)}{(r_x^2+r_y^2+r_z^2)^2} \end{bmatrix} \\
&= \mathbf{H}_\beta^T\mathbf{H}_\beta + \mathbf{H}_\phi^T\mathbf{H}_\phi \qquad (3.12)
\end{aligned}$$

which gives

$$\mathbf{J}_k = \frac{1}{\sigma^2}\sum_{\imath=1}^{k} \begin{bmatrix} \frac{r_{\imath y}^2}{(r_{\imath x}^2+r_{\imath y}^2)^2} + \frac{r_{\imath x}^2 r_{\imath z}^2}{(r_{\imath x}^2+r_{\imath y}^2+r_{\imath z}^2)^2(r_{\imath x}^2+r_{\imath y}^2)} & -\frac{r_{\imath x} r_{\imath y}}{(r_{\imath x}^2+r_{\imath y}^2)^2} + \frac{r_{\imath x} r_{\imath y} r_{\imath z}^2}{(r_{\imath x}^2+r_{\imath y}^2+r_{\imath z}^2)^2(r_{\imath x}^2+r_{\imath y}^2)} & -\frac{r_{\imath x} r_{\imath z}}{(r_{\imath x}^2+r_{\imath y}^2+r_{\imath z}^2)^2} \\ -\frac{r_{\imath x} r_{\imath y}}{(r_{\imath x}^2+r_{\imath y}^2)^2} + \frac{r_{\imath x} r_{\imath y} r_{\imath z}^2}{(r_{\imath x}^2+r_{\imath y}^2+r_{\imath z}^2)^2(r_{\imath x}^2+r_{\imath y}^2)} & \frac{r_{\imath x}^2}{(r_{\imath x}^2+r_{\imath y}^2)^2} + \frac{r_{\imath y}^2 r_{\imath z}^2}{(r_{\imath x}^2+r_{\imath y}^2+r_{\imath z}^2)^2(r_{\imath x}^2+r_{\imath y}^2)} & -\frac{r_{\imath y} r_{\imath z}}{(r_{\imath x}^2+r_{\imath y}^2+r_{\imath z}^2)^2} \\ -\frac{r_{\imath x} r_{\imath z}}{(r_{\imath x}^2+r_{\imath y}^2+r_{\imath z}^2)^2} & -\frac{r_{\imath y} r_{\imath z}}{(r_{\imath x}^2+r_{\imath y}^2+r_{\imath z}^2)^2} & \frac{(r_{\imath x}^2+r_{\imath y}^2)}{(r_{\imath x}^2+r_{\imath y}^2+r_{\imath z}^2)^2} \end{bmatrix}$$

The FIM for this 3-D case can also be written as

$$\mathbf{J}_k = \frac{1}{\sigma^2}\sum_{\imath=1}^{k}\mathbf{H}_\imath^T\mathbf{H}_\imath = \frac{1}{\sigma^2}\sum_{\imath=1}^{k}\left(\mathbf{H}_{\imath_\beta}^T\mathbf{H}_{\imath_\beta} + \mathbf{H}_{\imath_\phi}^T\mathbf{H}_{\imath_\phi}\right) = \mathbf{J}_{k_\beta} + \mathbf{J}_{k_\phi} \tag{3.13}$$

showing that the FIM is additive and that the FIM contributions of each sensor can be computed separately (assuming that the sensors are independent and uncorrelated). This is a very valuable property because it allows for the inclusion of multiple sensors with different characteristics or sensors providing measurements at different times.

To obtain a better physical intuition of what the equations of the FIM shown above mean, it is advantageous to make the substitutions given below. The magnitude of the vector for the 2-D top-view projection corresponding to the measurement of β can be written as (see Figure 3-1)

$$|\mathbf{r}_a| = \sqrt{r_x^2 + r_y^2} \tag{3.14}$$

The overall magnitude of the relative measurement vector is given by

$$|\mathbf{r}| = \sqrt{r_x^2 + r_y^2 + r_z^2} \tag{3.15}$$

The following trigonometric substitutions can be made

$$\begin{aligned} \sin\beta &= \frac{r_x}{|\mathbf{r}_a|} \\ \cos\beta &= \frac{r_y}{|\mathbf{r}_a|} \\ \sin\phi &= \frac{r_z}{|\mathbf{r}|} \\ \cos\phi &= \frac{|\mathbf{r}_a|}{|\mathbf{r}|} \end{aligned} \tag{3.16}$$

Using these substitutions, the FIM components $\mathbf{H}_\beta^T\mathbf{H}_\beta$ and $\mathbf{H}_\phi^T\mathbf{H}_\phi$ can be rewritten

as,

$$\mathbf{H}_\beta^T \mathbf{H}_\beta = \frac{1}{|\mathbf{r}_a|^2} \begin{bmatrix} \cos^2\beta & -\sin\beta\cos\beta & 0 \\ -\sin\beta\cos\beta & \sin^2\beta & 0 \\ 0 & 0 & 0 \end{bmatrix}$$

$$\mathbf{H}_\phi^T \mathbf{H}_\phi = \frac{1}{|\mathbf{r}|^2} \begin{bmatrix} \sin^2\beta\sin^2\phi & \sin\beta\cos\beta\sin^2\phi & -\sin\beta\sin\phi\cos\phi \\ \sin\beta\cos\beta\sin^2\phi & \cos^2\beta\sin^2\phi & -\cos\beta\sin\phi\cos\phi \\ -\sin\beta\sin\phi\cos\phi & -\cos\beta\sin\phi\cos\phi & \cos^2\phi \end{bmatrix}$$

and the overall equation for the FIM is given by

$$\mathbf{J}_k = \frac{1}{\sigma^2} \sum_{\imath=1}^{k} \left(\frac{1}{|\mathbf{r}_{i_a}|^2} \begin{bmatrix} \cos^2\beta_\imath & -\sin\beta_\imath\cos\beta_\imath & 0 \\ -\sin\beta_\imath\cos\beta_\imath & \sin^2\beta_\imath & 0 \\ 0 & 0 & 0 \end{bmatrix} + \ldots \right.$$
$$\left. \frac{1}{|\mathbf{r}_\imath|^2} \begin{bmatrix} \sin^2\beta_\imath\sin^2\phi & \sin\beta_\imath\cos\beta_\imath\sin^2\phi & -\sin\beta_\imath\sin\phi\cos\phi \\ \sin\beta_\imath\cos\beta_i\sin^2\phi & \cos^2\beta_\imath\sin^2\phi & -\cos\beta_\imath\sin\phi\cos\phi \\ -\sin\beta_\imath\sin\phi\cos\phi & -\cos\beta_\imath\sin\phi\cos\phi & \cos^2\phi \end{bmatrix} \right) \quad (3.17)$$

The equation above shows that the range and bearing information are separable in the FIM. It is convenient to rewrite the FIM using these trigonometric substitutions, especially when computing norms of the FIM, to preserve this separation between range and angular information. This form of the matrix suggests that maximization of the FIM involves lowering the range to the target and increasing the angular separation between measurements, which supports the intuition developed in Section 1.2.4.

3.1.2 Selection of an Objective Function Based on Matrix Measures

Since maximizing the Fisher Information Matrix is a difficult task, it is necessary to find a real-valued scalar function based on the FIM to serve as an objective function

in the trajectory optimization problem. Going from a matrix to a scalar function results in a loss or compression of information, leading to a weaker optimization metric. Careful analysis of different possible functions is necessary to ensure that the information of interest to the estimation problem is properly captured. The optimization algorithm will find an "optimal" trajectory based on minimizing the chosen objective function, and if the objective function does not capture the desired trajectory behavior, this "optimal" trajectory will not produce the desired results. Furthermore, it is desirable to choose a function that is well structured for optimization (contains the fewest local extrema, is equally sensitive to all optimization variables, etc). As mentioned before, the FIM is symmetric and at least positive semi-definite, therefore its eigenvalues are real and positive (or zero). The eigenvalues of the FIM are related to the uncertainty ellipsoid of the target estimation, since the FIM is related to the estimation error covariance. More specifically, the length of each axis of the uncertainty ellipsoid is given by one over an eigenvalue squared for each eigenvalue of the FIM. Therefore, maximizing the eigenvalues of the FIM leads to a smaller uncertainty ellipsoid and a more accurate estimation.

A few of the most common matrix measures are described below. The first function is based on the determinant of the FIM and is known as the D-optimality criterion. Its equation is given by

$$f(\mathbf{J}) = -\log\det\{\mathbf{J}\} \tag{3.18}$$

The determinant of a symmetric positive definite matrix is given by the multiplication of its eigenvalues so the D-optimality criterion results in the minimization of the volume of the uncertainty ellipsoid. The determinant is a very popular choice of matrix measure and is used widely in the literature. One advantage of the D-optimality criterion is that it is invariant for parameter scale changes and linear transformations [72]. A drawback of using the determinant is that it is not a monotonic function, resulting in several local minimums and maximums in the objective function. This makes the optimization quite sensitive to initial conditions and may cause the optimizer to get

stuck in a local maximum if not initialized properly. Furthermore, calculating the determinant of a matrix is more computationally intensive than many other matrix norms. The next function considered is the E-optimality condition which uses the maximum eigenvalue of the inverse of the FIM and is given by

$$f(\mathbf{J}) = \max_i \{\text{eig}(\mathbf{J}^{-1})\} \tag{3.19}$$

Optimizing using the E-optimality criterion leads to the minimization of the length of the largest axis of the uncertainty ellipsoid. A third function is the A-optimality criterion which involves computing the trace of the inverse of the FIM. Its equation is given by

$$f(\mathbf{J}) = \text{Tr}\{\mathbf{J}^{-1}\} \tag{3.20}$$

and it is designed to minimized the average variance of the estimates. The last function considered is the sensitivity criterion given by

$$f(\mathbf{J}) = -\text{Tr}\{\mathbf{J}\} \tag{3.21}$$

This criterion involves maximizing the trace of the FIM, which for a symmetric positive definite matrix, is the sum of the eigenvalues. The sensitivity criterion is the easiest to compute and provides a monotonic optimization function, however, it is not stable and could result in a singular FIM. It is typically used only to initialize the optimization problem. These are the most widely used matrix measures. Uciński provides a complete discussion on possible matrix measures for the FIM [72].

A sensor placement exercise serves as a benchmark for testing and comparing several functions of the Fisher Information Matrix. The algorithm is based on numerical optimization techniques and uses a gradient descent method to find a set of N optimal UAV measurement locations in 3-D space with a fixed altitude constraint. Section 3.2.1 shows more detail for the results of the sensor placement optimization scenario. The sensor placement case is used to test the performance of the functions

described above in order to determine which is the one best suited to the problem. The selected objective function must capture the dependence of the estimation on the angular separation between measurement locations and the relative range to the target (as described above and in Section 1.2.4). The first function, based on the determinant of the FIM, is very sensitive to changes in range but exhibits far less sensitivity to changes in angular separation. The optimization tends to bring the measurement locations together to reduce the range as much as possible, resulting in a sensor configuration that places all the points directly above the target (since, for a fixed altitude, this is the position of lowest relative range). This result is obviously undesirable since it leads to an unobservable estimation for the bearings-only estimation problem. Another test performed on the determinant function, but holding the range fixed, shows that the optimization algorithm separates the points properly. This confirms that the determinant function does contain information about the angular dependence between the measurements, but due to the high sensitivity of the determinant function to the relative range, this angular dependence is essentially ignored. In addition to being overly sensitive to range, the determinant function has many local extrema and, if not initialized properly, the optimization gets stuck in a local minimum and returns a suboptimal configuration. It is important to state that the determinant function is not dismissed lightly. In general, the D-optimality criterion does capture most of the essential dependencies of the estimation on the measurement locations and is widely used in literature as the optimization function of choice. Furthermore, analytically computing the determinant of the FIM for the two-dimensional bearings-only target localization problem gives

$$\begin{aligned} \det\{\mathbf{J}_N\} &= \frac{1}{\sigma^4}\left[\left(\sum_{\imath=1}^{N}\frac{r_{\imath y}^2}{(r_{\imath x}^2+r_{\imath y}^2)^2}\right)\left(\sum_{\imath=1}^{N}\frac{r_{\imath x}^2}{(r_{\imath x}^2+r_{\imath y}^2)^2}\right)-\left(\sum_{\imath=1}^{N}\frac{r_{\imath x}r_{\imath y}}{(r_{\imath x}^2+r_{\imath y}^2)^2}\right)^2\right] \\ &= \frac{1}{2\sigma^4}\sum_{\imath,\jmath}^{N}\left[\frac{\mathbf{r}_\imath\times\mathbf{r}_\jmath}{|\mathbf{r}_\imath|^2|\mathbf{r}_\jmath|^2}\right]^2 \end{aligned} \tag{3.22}$$

where the cross product in the numerator shows the need for increased orthogonality between the measurement vectors and the magnitude of the range in the denominator

shows that the determinant is maximized when the range to the target is as low as possible. Most of the literature uses the D-optimality criterion in a two dimensional setting, however, for the 3-D case, the sensitivity to range and the problem of local maximums makes optimization quite difficult.

Next the sensitivity criterion involving the trace of the FIM is explored as an optimization function. The trace function results in a configuration which completely ignores the angular separation between measurements and optimizes only the range. Even when the range is held constant the bearing angles do not change at all. Again, as in the case of the determinant function, the sensor placement optimization places all the measurement points directly overhead the target. This sensor configuration results in an unobservable estimation for the bearings-only estimation problem and is therefore undesirable, showing that the trace of the FIM does not capture the dependencies of interest in this problem. Furthermore, analytically deriving the trace of the FIM and simplifying the expression gives

$$\mathrm{Tr}\{\mathbf{J}\} = \mathbf{J}_k = \frac{1}{\sigma^2}\sum_{i=1}^{k}\left(\frac{1}{|\mathbf{r}_{t_a}|^2} + \frac{1}{|\mathbf{r}_i|^2}\right) \tag{3.23}$$

showing that the information about the dependence of the estimation on the angular separation between measurements is completely lost.

The remaining functions, the E-optimality and the A-optimality criteria, result in very similar measurement configurations. They both return sets of measurement locations that are evenly spaced in a circular pattern above the target. This circular sensor configuration shows the tradeoff between reducing the range to the target, while still maintaining as much orthogonality between measurements as possible. Furthermore, both the A-optimality and E-optimality criteria exhibit faster convergence and higher stability in the optimization. Since the A-optimality criterion involves all the eigenvalues of the inverse of the FIM, it represents the uncertainty in all dimensions equally and is therefore chosen over the E-optimality criterion as the best optimization

function. It is interesting to note that the expression for the A-optimality criterion,

$$f(\mathbf{J}) = \mathrm{Tr}\{\mathbf{J}^{-1}\} \tag{3.24}$$

closely resembles the expression for geometric dilution of precision (GDOP), which is commonly exploited in GPS navigation to select the configuration of satellites that gives the most accurate position estimate, showing that the A-optimality criterion captures the geometric system dependencies. Furthermore, the A-optimality criterion is the most physically significant function for the estimation problem since it is based on minimizing the individual variances of the estimates. The following sections show the results for the optimization of UAV measurement locations for several different scenarios using the A-optimality criterion.

3.2 Trajectory Optimization

For the problem of optimizing the trajectory of a UAV performing target localization two main scenarios are considered. The first case examines the problem of finding the best sensing locations for a fixed number of measurements. This scenario is applicable to a UAV with a limit on the amount of measurements it can take (due to bandwidth or storage constraints, for example). It can also be used for the case of placing multiple UAVs which can collaborate to provide a vehicle estimate. The second scenario looks at the problem of trajectory optimization for a single UAV with motion constraints. The rate at which measurements are taken is fixed and the motion constraints limit the amount the vehicle can travel and turn between measurements. The optimization for both scenarios is implemented using a gradient descent numerical method with the objective function based on the A-optimality criterion. The gradient descent algorithm uses a polar coordinate approach, varying the range to the target and the angular separation between the measurement locations. The results are provided in the following sections.

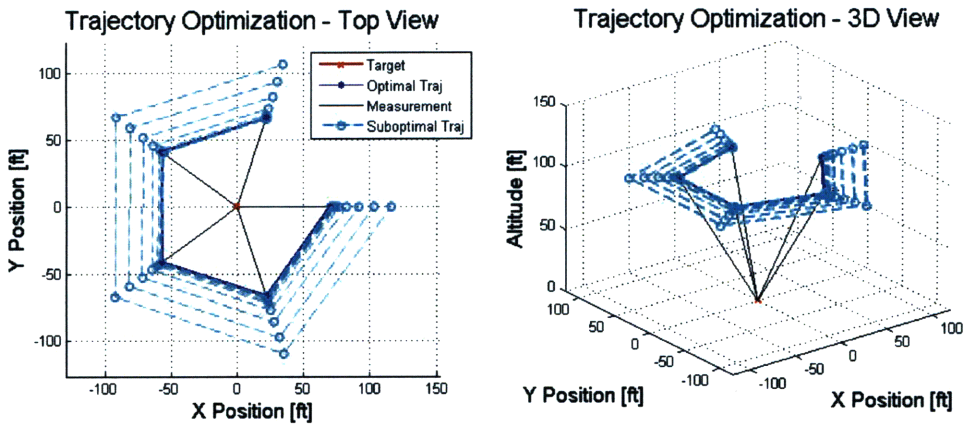

Figure 3-2: Optimization of vehicle trajectory using sensor placement techniques

3.2.1 Optimization of Measurement Locations Using Sensor Placement Techniques

This section describes the case of trajectory optimization for a UAV flying at a fixed altitude above a stationary target taking a fixed number of measurements (N) of the target. The optimization uses a gradient descent method which numerically computes the derivative with respect to the range and bearing for each measurement location, using a finite difference method, and updates the positions by taking steps proportional to the computed derivative. The optimal sensor placement configuration is given by the measurement locations evenly spaced around a circle directly above the target. This is not a surprising result since a circular trajectory is widely accepted in literature as the optimal trajectory and, as described in Section 1.2.4, is the path that makes the most sense intuitively. The UAV trajectory is obtained by joining the measurement locations and the results are shown in Figure 3-2 for the case of $N = 5$. The cyan lines show the suboptimal trajectories tried by the optimization routine and the blue line shows the final optimal UAV trajectory.

The optimization was performed for several different values of N. Figure 3-3 shows the resulting trajectories for $N = 5$, $N = 10$, and $N = 15$. As the number of measurements increases the trajectory approaches a circle at a fixed altitude centered on the target. An interesting result is that the ratio of the radius of the circular trajectory to the altitude above the target is always close to 0.7 (± 0.02) regardless

of the number of measurements. This demonstrates the tradeoff between minimizing the relative range to the target and maintaining proper angular separation between measurements. If the range only is considered, all the measurements would be taken directly above the target, since this is the closest point within the altitude constraint, leading to a radius to altitude ratio of zero. If the angular separation is the only consideration the measurement vectors would be chosen to be orthogonal and the ratio between the radius and the altitude would be 1. Since the optimal radius is 0.7, this shows that there is a compromise between proximity to the target and angular separation of the measurements. These results scale with altitude and the 0.7 ratio remains the same for several different altitudes.

The task of simultaneously optimizing N measurement locations has several issues. The first is that the optimization is a multimodal problem of high dimensionality. The objective function is dependent upon all N measurements and for the general 3-D case the gradient vector has $3N$ terms ($2N$ with a fixed altitude constraint). As N increases, the computational load required to perform the optimization increases as well. Another complication is that as N gets larger, the dependencies of the objective function on the measurement locations become more complex making the optimization quite difficult. For the bearings-only case the optimal configuration is not unique since the spacing between the measurements is important and not the actual bearing locations, leading to infinitely many optimal configurations. This can be remedied by fixing the bearing information for one of the measurement locations and optimizing over the rest. Furthermore, as N increases the objective function has a growing number of local extrema causing severe sensitivities to initialization and often leading to suboptimal solutions if not initialized properly. This is the most difficult issue to deal with since, unless there is some prior insight about the problem, it is often unclear what a proper choice of initial measurement configuration should be. Another issue with improper initialization of the optimization is that the algorithm tends to cluster the measurement locations. An example of this suboptimal configuration is shown in Figure 3-4, where the five-point trajectory optimization results in clusters of two points on each end of a line and one point in the center. The cyan lines show the

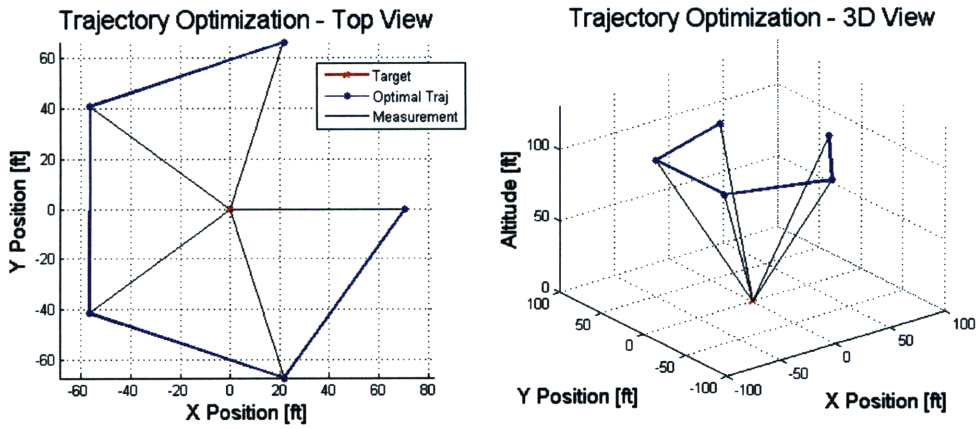

(a) 5 point trajectory

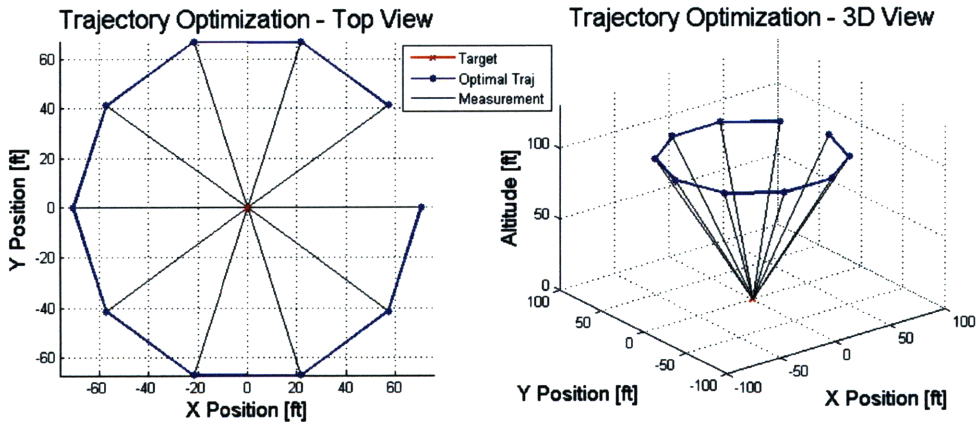

(b) 10 point trajectory

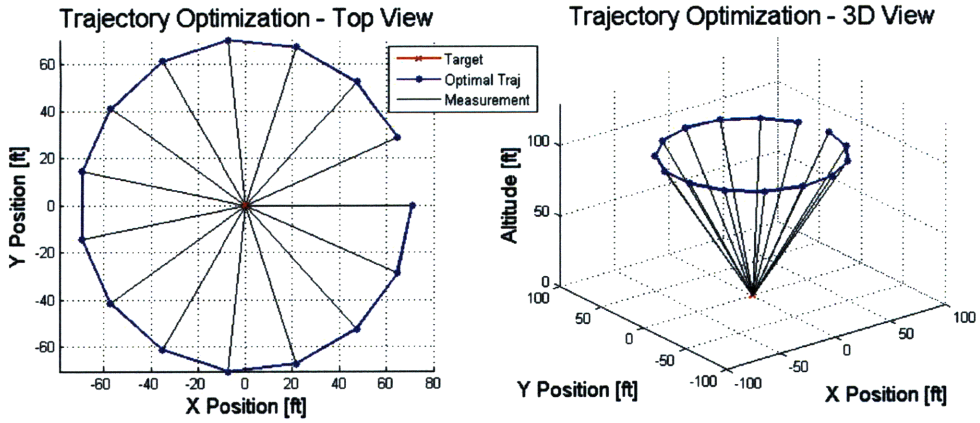

(c) 15 point trajectory

Figure 3-3: Optimal vehicle trajectories using sensor placement techniques

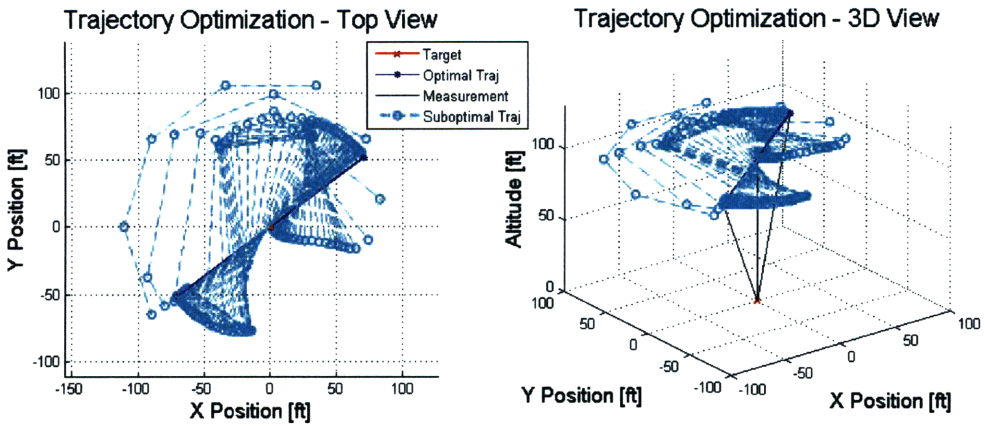

Figure 3-4: Sensor clustering due to improper initialization

progress of the optimization and the straight blue line shows the resulting "optimal" trajectory. This suboptimal solution occurs because of the assumption that the noise between the different measurements is spatially uncorrelated [72]. This result is not practical and can be avoided by properly initializing the optimization.

The intuition about the problem and the insight provided by the sensor placement case with low values of N suggest that the optimal solution tends to a circle above the target with the measurement locations evenly distributed around it. This measurement configuration is used to initialize the optimization and the algorithm can then be executed to find the optimal relative range value for the radius of the circle. Overall, the sensor placement case is a useful benchmark for providing intuition about the problem and for determining which objective function is best suited to the trajectory optimization task. The next section explores the inclusion of vehicle motion constraints to provide trajectories for a single UAV that account for the vehicle's limitations.

3.2.2 Trajectory Optimization With Vehicle Motion Constraints

In this section, motion constraints on the vehicle are incorporated into the optimization of the UAV trajectory. The platform vehicle considered is the fixed-wing Raven UAV, whose performance limitations are described in Section 1.2.1. The motion con-

straints for the UAV include a fixed velocity of 44 ft/sec and a maximum turn rate of 12 deg/sec, which are within the operating specifications of the Raven. The measurement rate is fixed to 2 Hz and the vehicle motion between measurement locations is restricted based on the UAV's maneuverability. The imaging sensors are assumed to be mounted on gimbals, which can be controlled to keep the target in the field of view. Therefore, field of view constraints are not considered in this section. The optimization is initialized with a starting vehicle position and uses the A-optimality criterion to determine the subsequent trajectory points that maximize the amount of information while remaining within the vehicle's velocity and turn rate constraints. The optimization algorithm used in this section works by determining the optimal trajectory points one at a time and updating the Fisher Information Matrix recursively. This optimization method provides the next best immediate decision based on all prior information. Other optimization strategies could consider looking ahead and finding the next N optimal trajectory points. The resulting trajectories using a forward looking strategy would be better, providing a higher total amount of information. However, optimization of N points suffers from the same issues mentioned in the previous section. The major problem is that optimizing over a large number of trajectory points produces local extrema and is likely to lead to suboptimal solutions. Furthermore, the computational resources required for a multi-point optimization is several orders of magnitude larger than for single point optimization and the resulting algorithm cannot be implement in real-time using onboard UAV computers. Therefore, for this work, a single point optimization strategy is considered and the optimization algorithm is used at each time step to find the next best UAV measurement location. The following sections show the resulting UAV trajectories for the stationary target case, the multiple target scenario, and several moving target cases.

Trajectory Optimization for Stationary Targets

Several cases of trajectory optimization are considered in this section. The first case assumes a stationary target located at the origin and a UAV initial position of

$\mathbf{p}_0 = \begin{bmatrix} 100 & 0 & 100 \end{bmatrix}^T$ with an initial heading of $\frac{\pi}{2}$ (North). These are the same initial conditions assumed in Chapter 2, where the UAV was made to fly a circular trajectory around the target. In this case, the trajectory is computed by the optimizer for 50 measurements and the results are presented in Figure 3-5. There are a few interesting points to be made about this case. The first is that, after the initial spiral, the UAV follows a circular orbit with a radius of approximately 70 ft. Since the altitude is 100 ft, this case illustrates the results from the previous section where the optimal radius to altitude ratio is found to be 0.7. Another interesting observation is that the information provided by this optimal trajectory in the X and Y axes is almost equivalent to the information provided by the ad-hoc circular UAV trajectory used in Chapter 2 (see Figure 2-2), however the number of measurements taken for the optimal trajectory is 50 whereas the ad-hoc trajectory required 100 measurements to reach this amount of information. This shows that by using a trajectory optimization algorithm and placing the measurement locations efficiently the number of measurements required to achieve a certain information threshold can be drastically reduced. Unfortunately, due to the poor geometry with respect to the Z axis, the information about this dimension cannot be increased much. The resulting Z information using the optimal trajectory is about half of that obtained with the ad-hoc circular trajectory, since only half the measurements are taken.

The next case considered places the UAV at an initial position which is farther from the target. For this scenario the target is stationary and at the origin and the UAV is initialized with a position of $\mathbf{p}_0 = \begin{bmatrix} 200 & 0 & 100 \end{bmatrix}^T$ and a heading of $\frac{\pi}{2}$. The resulting trajectory is shown in Figure 3-6. Here the UAV begins by spiralling toward the target, but instead of converging to a circular orbit it attempts to reduce the relative range to the target as much as possible. This behavior increases the amount of information provided in the X and Y dimensions as shown in the lower right plot of Figure 3-6. The UAV then circles around and returns to the target on a second spiral, once again passing close to it. The drastic increase in information around measurements 15 and 35 correspond to the points on the trajectory that are nearest to the target, showing the sensitivity of the Fisher Information to the relative range.

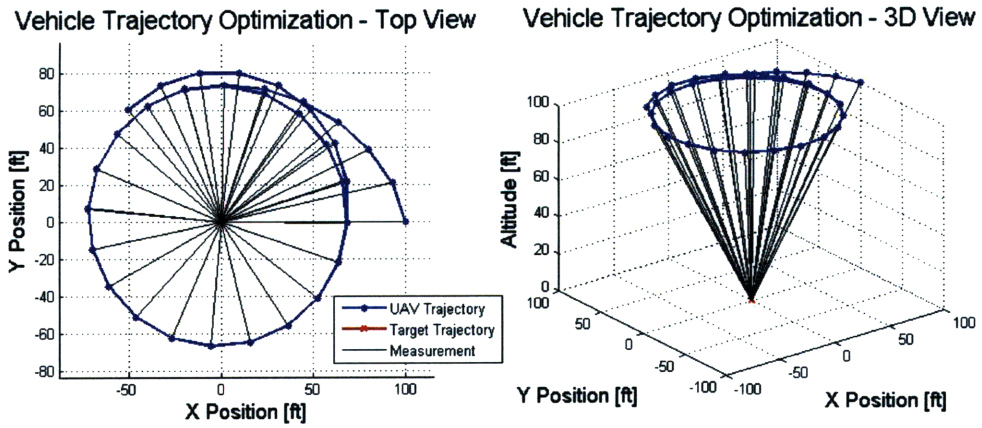

(a) Vehicle and Target Trajectories

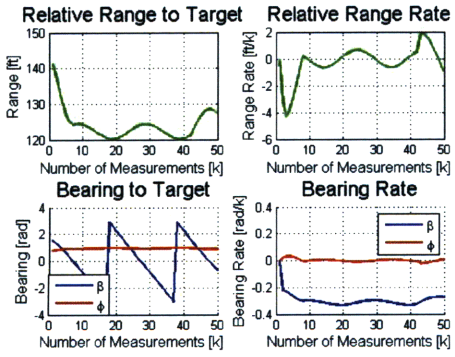

(b) Trajectory Parameters

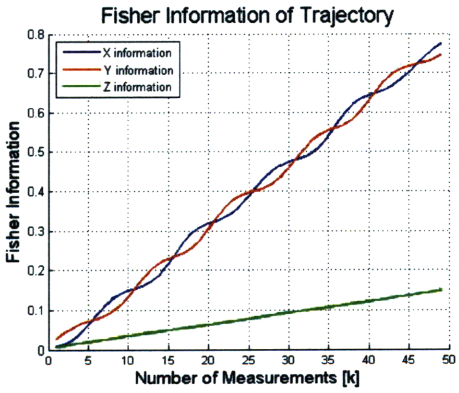

(c) Fisher Information

Figure 3-5: Trajectory optimization with motion constraints, stationary target, case 1

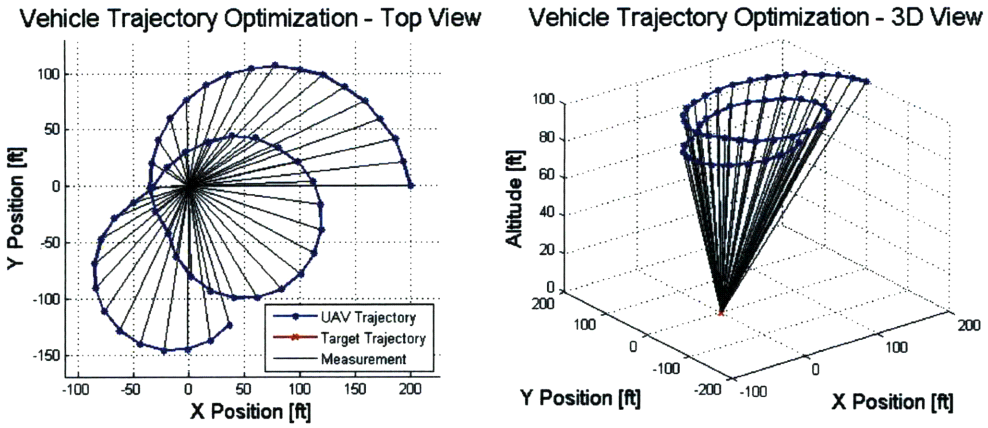

(a) Vehicle and Target Trajectories

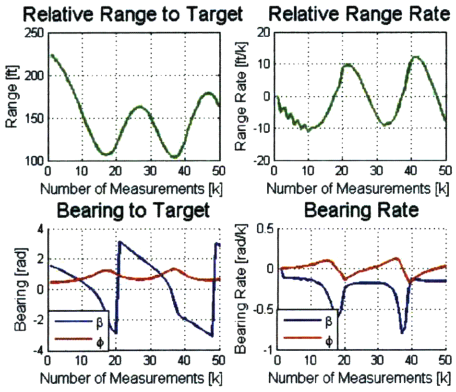

(b) Trajectory Parameters

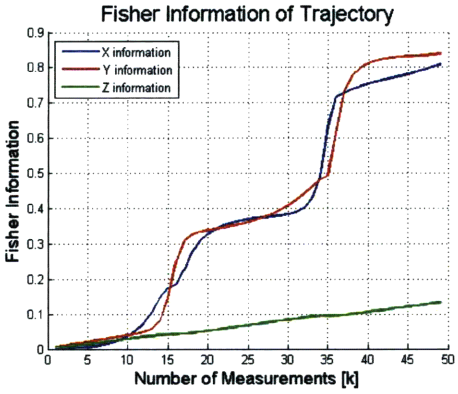

(c) Fisher Information

Figure 3-6: Trajectory optimization with motion constraints, stationary target, case 2

Even though the target is initially farther away than in the previous scenario, the total information for this trajectory is higher than that shown in Figure 3-5 since the UAV is able to pass close to the target.

The third case considered involves starting the UAV with a different heading. The UAV is initially at $\mathbf{p}_0 = \begin{bmatrix} 200 & 0 & 100 \end{bmatrix}^T$, as before, but its heading is π (West). The results for this scenario are provided in Figure 3-7. The vehicle begins by diverging from the straight path towards the target to provide better angular separation between the measurements. It then turns towards the target and passes close to it and finally loops back around to circle the target. Again a larger increase in information is observed when the UAV passes close to the target.

The next few cases study the effect of the UAV turn rate constraint. The trajectory

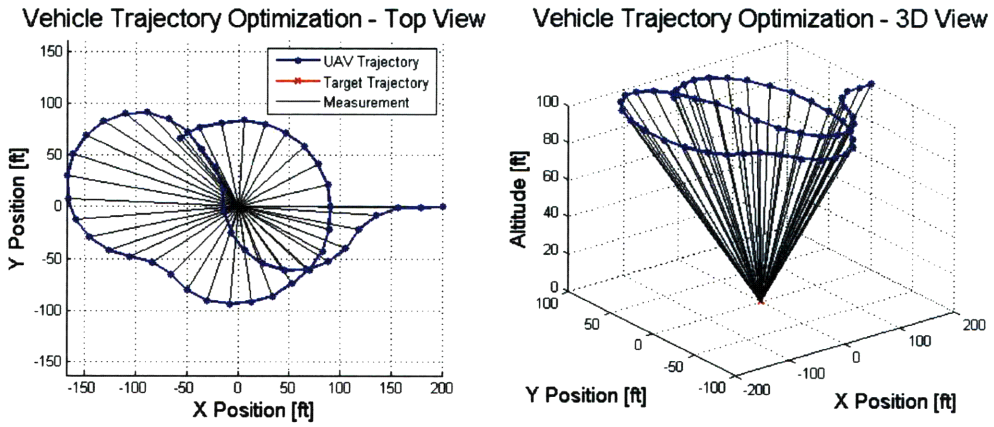

(a) Vehicle and Target Trajectories

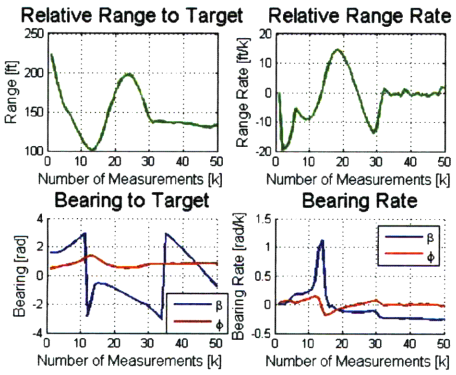

(b) Trajectory Parameters

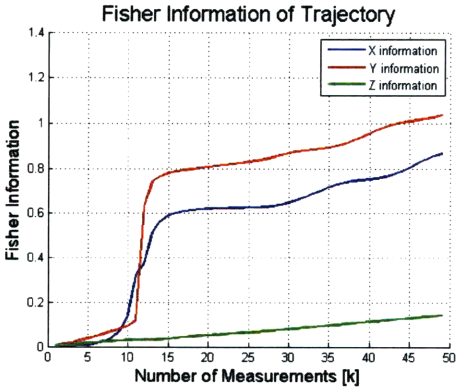

(c) Fisher Information

Figure 3-7: Trajectory optimization with motion constraints, stationary target, case 3

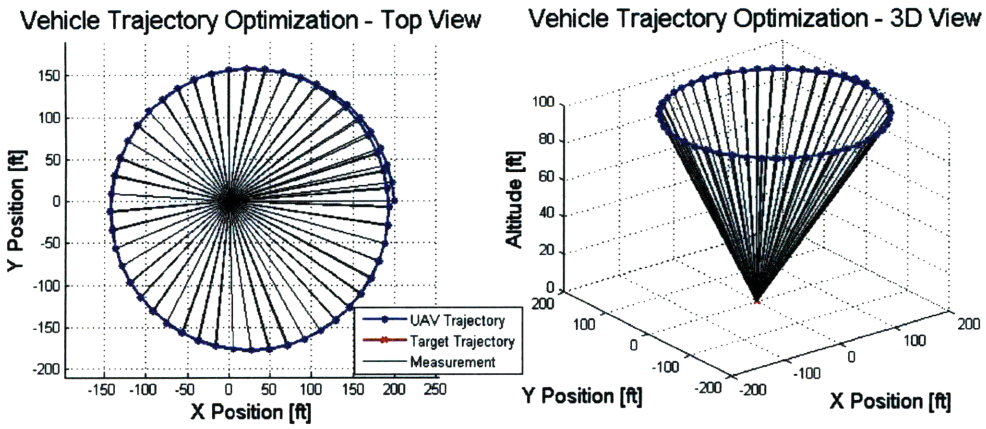

(a) Vehicle and Target Trajectories

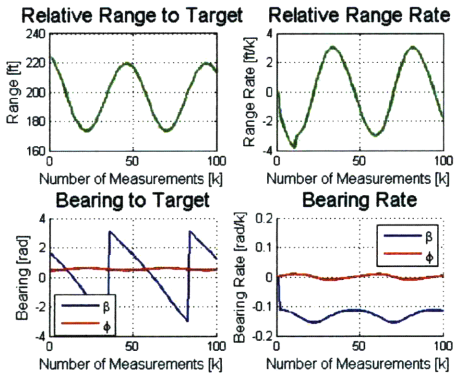

(b) Trajectory Parameters

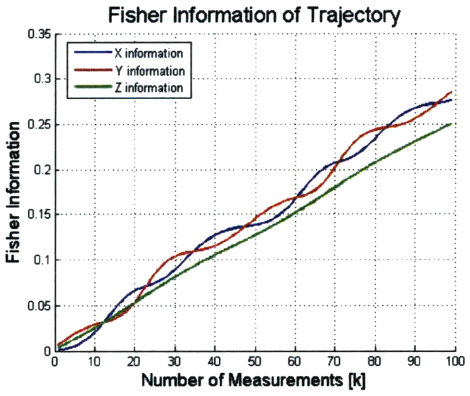

(c) Fisher Information

Figure 3-8: Trajectory optimization with turn constraint of 5 deg/sec

optimization is performed for a 100 measurement trajectory and the maximum UAV turn rate is varied. The first scenario uses a low maximum allowable turn rate, restricting the vehicle to maximum turns of 5 deg/sec. The resulting trajectory, shown in Figure 3-8, is an orbit around the target. An interesting observation is that the target is not in the center of the orbit, as seen by looking at the oscillations in the relative range and relative range rate plots on the lower right of Figure 3-8. Additionally, the information rate is higher and the increase in information is sharper when the vehicle passes closest to the target. This is because the error contribution of the vehicle orientation errors is lower when the relative range to the target is lower, as explained in Section 1.2.4, and correspondingly, the uncertainty in the estimation is reduced. Therefore the optimal information-theoretic move is to minimize the relative range to the target as much as possible within the vehicle turn rate constraints. The

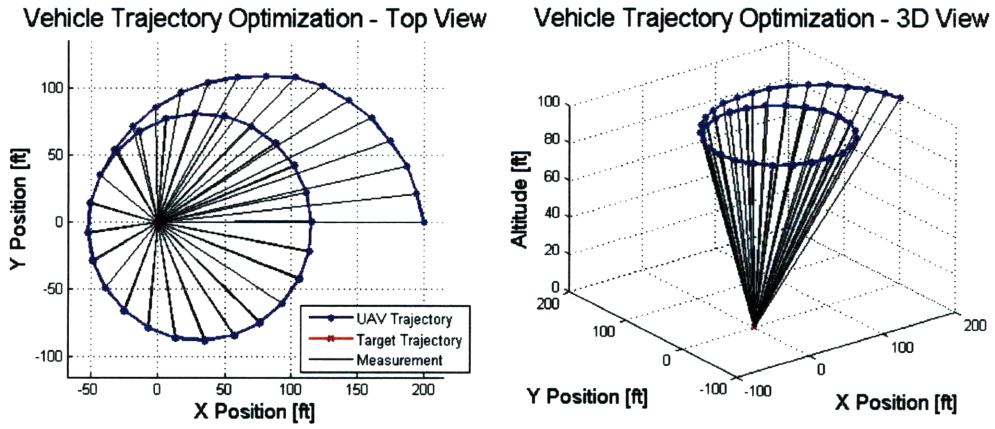

(a) Vehicle and Target Trajectories

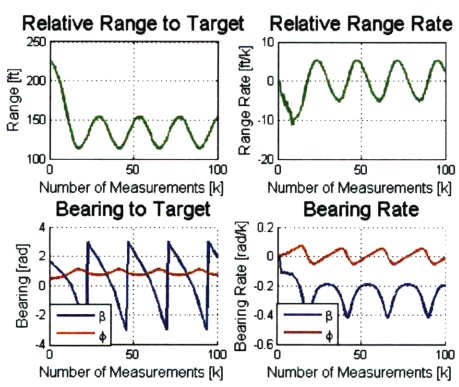

(b) Trajectory Parameters

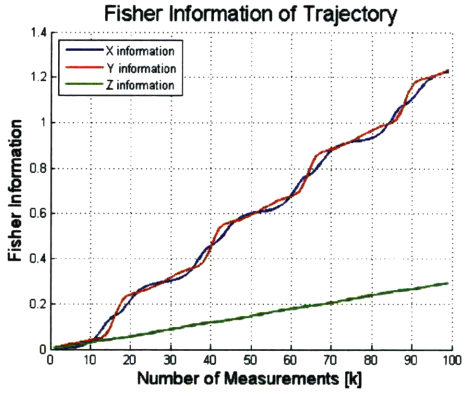

(c) Fisher Information

Figure 3-9: Trajectory optimization with turn constraint of 10 deg/sec

turn rate is then increased to 10 deg/sec and the trajectory optimization results for this case are shown in Figure 3-9. The UAV again begins by spiralling in to the target, reducing the relative range to the target while maintaining a heading which is nearly orthogonal to the line-of-sight vector to the target. The UAV trajectory converges on to an orbit around the target. Once again, the target is not in the center of the orbit as can be seen by looking at the relative range and range rate plots on the lower left of Figure 3-9. The plot on the lower right shows that the information increase is largest when the UAV is on the portion of the orbit that passes nearest to the target. The turn rate is increased to 15 deg/sec, which is the maximum allowable turn rate for the Raven. The resulting trajectory is provided in Figure 3-10 and is shown to spiral towards the target, reducing the relative range as much as possible. Since the trajectory passes so close to the target, the next best decision after passing the target

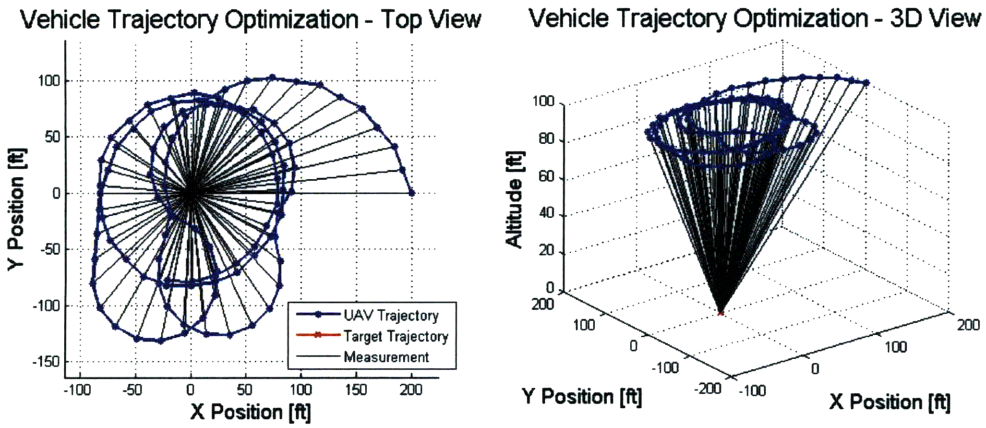

(a) Vehicle and Target Trajectories

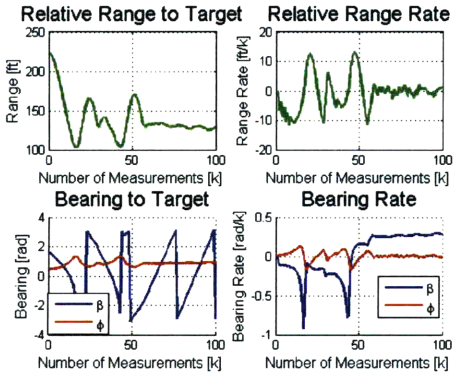

(b) Trajectory Parameters

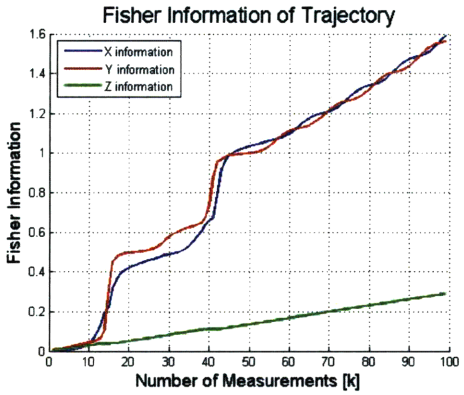

(c) Fisher Information

Figure 3-10: Trajectory optimization with turn constraint of 15 deg/sec

is to change directions and circle around again, coming in for a second pass. After these transients, the trajectory converges onto a circle around the target. This time the circle is centered on the target, as seen in the second half of the relative range and relative range rate plots. Again the two sharp increases in information correspond to when the UAV is nearest to the target. The final case considered is for a maximum turn rate of 20 deg/sec. The results for this scenario are shown in Figure 3-11. The UAV once again spirals into the target, this time passing almost directly overhead the target. The information is drastically increased during this first pass. The UAV then circles around and converges to a limit cycle centered on the target, where the information increases at a constant rate. Note that the total amount of information increases as the constraints are loosened. For the four turn rate cases considered, 5 deg/sec, 10 deg/sec, 15 deg/sec and 20 deg/sec, the average total information for the

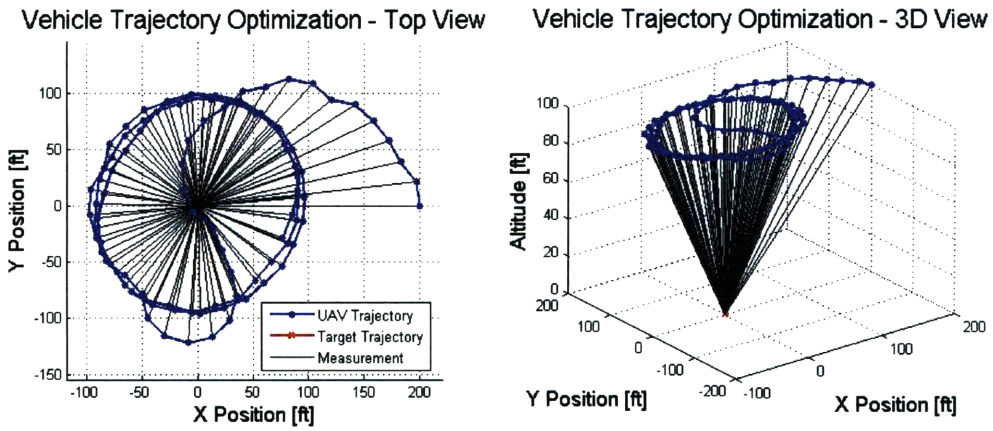

(a) Vehicle and Target Trajectories

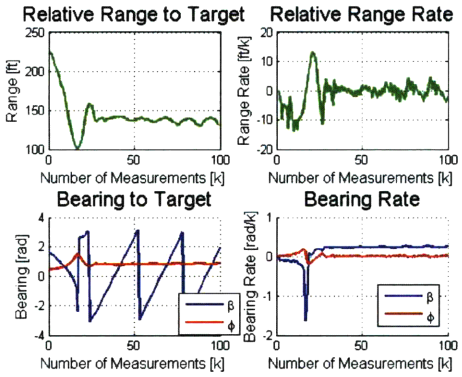

(b) Trajectory Parameters

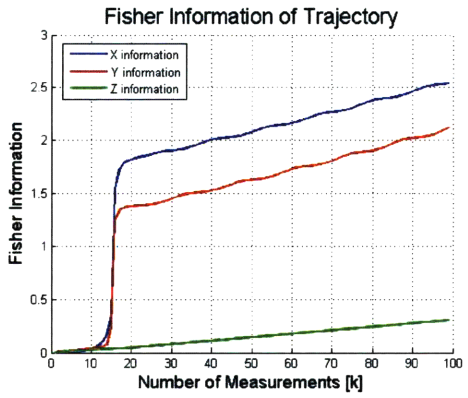

(c) Fisher Information

Figure 3-11: Trajectory optimization with turn constraint of 20 deg/sec

X and Y axes is 0.28, 1.22, 1.58, and 2.30, respectively. This shows that the more restricted the vehicle is, the less capable it is of obtaining the best possible trajectory, a result which makes intuitive sense. The maximum turn rate study shows that different UAV constraints cause different orbiting behavior, however, the information-theoretic framework produces trajectories that have the basic properties of reducing the relative range to the target as much as possible, within the vehicle constraints, and maintaining a heading that is nearly orthogonal to the line-of-sight to the target.

Trajectory Optimization for Multiple Targets

Since the FIM is additive, trajectory optimization for multiple target tracking can be performed using the same optimization framework. In this section the FIM contri-

butions of several stationary targets are added together and the UAV trajectory is optimized so that the average amount of information about the targets is maximized. The UAV is restricted to maintain a cruise speed of 44 ft/sec and has a maximum desired turn radius of 12 deg/sec. The starting position is $\mathbf{p}_0 = \begin{bmatrix} 200 & 0 & 100 \end{bmatrix}^T$ and the initial heading is $\frac{\pi}{2}$. The UAV is assumed to take measurements of all the targets at every measurement time-step. The resulting trajectories for tracking 2, 3 and 4 targets are provided in Figures 3-12, 3-13, and 3-14 respectively. The spiral behavior is present again and the UAV is shown to close in on each target, circle around, and then move onto the next target. As in the previous cases, the average information is shown to increase sharply when the UAV passes close to a target. It is interesting to note that the UAV trajectory optimization favors spiralling into a farther target instead of circling around a target which the UAV has already passed close to. This is because the unknown information about a farther target is greater than that of a close target, leading to a higher information rate for the farther target. Therefore the information increase obtained by reducing the range to a farther target is larger than that obtained by re-circling a close target. As mentioned before, this optimization assumes that all targets are measured at each time-step. A more realistic approach would involve selecting one target at every time-step to take a measurement of, and further optimization can be done to determine which target to look at in order to obtain the largest amount of total information.

Trajectory Optimization for Moving Targets

Trajectory optimization for moving targets is considered in this section. The first scenario involves targets moving with a constant velocity. The UAV constraints are the same as those described in the first example. The UAV is restricted to maintain a cruise speed of 44 ft/sec and has a maximum desired turn radius of 12 deg/sec. The starting position is $\mathbf{p}_0 = \begin{bmatrix} 200 & 0 & 100 \end{bmatrix}^T$ and the initial heading is $\frac{\pi}{2}$. The target starts at the origin and moves on the ground plane with a constant velocity of 2.8 ft/sec. The results for two constant velocity target cases are shown in Figures 3-15 and 3-16. The UAV trajectories still exhibit the spiral behavior as before, but adjust

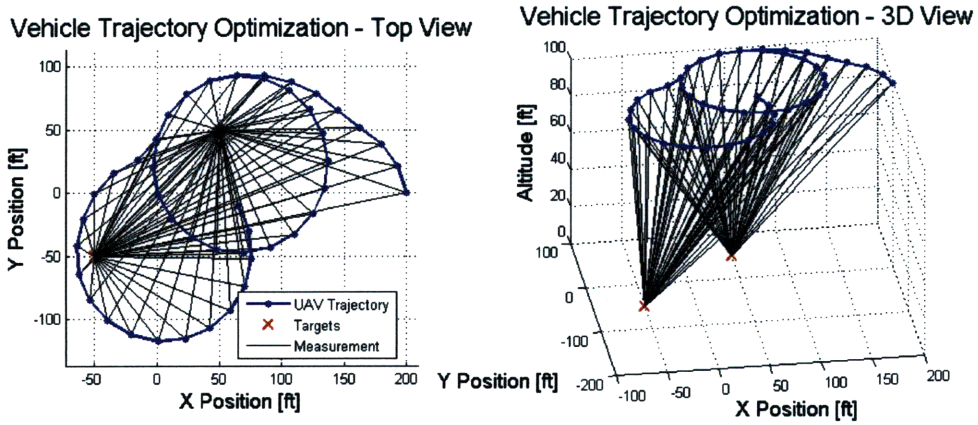

(a) Vehicle and Target Trajectories

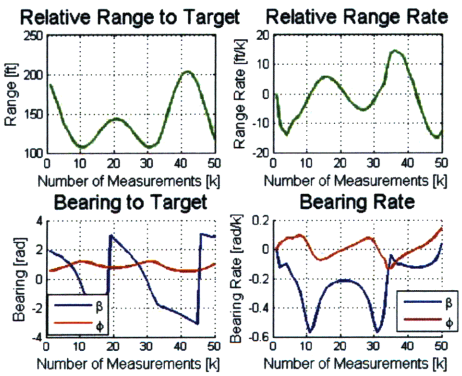

(b) Trajectory Parameters

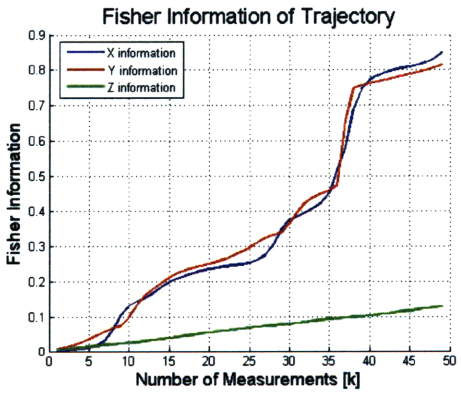

(c) Fisher Information

Figure 3-12: Trajectory optimization for tracking two targets

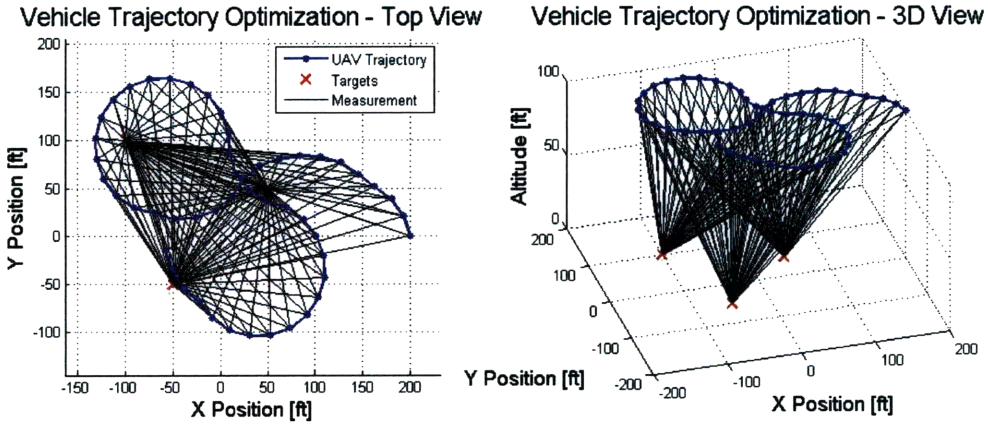

(a) Vehicle and Target Trajectories

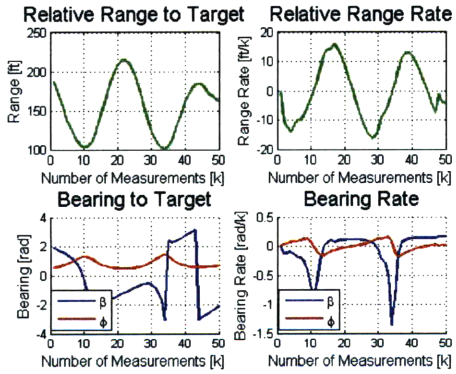

(b) Trajectory Parameters

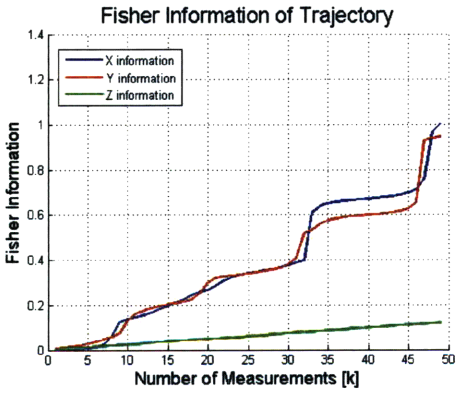

(c) Fisher Information

Figure 3-13: Trajectory optimization for tracking three targets

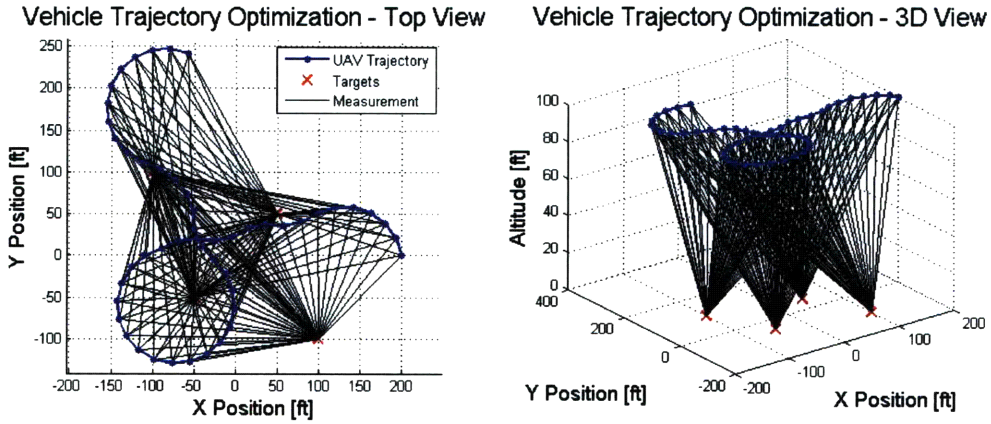

(a) Vehicle and Target Trajectories

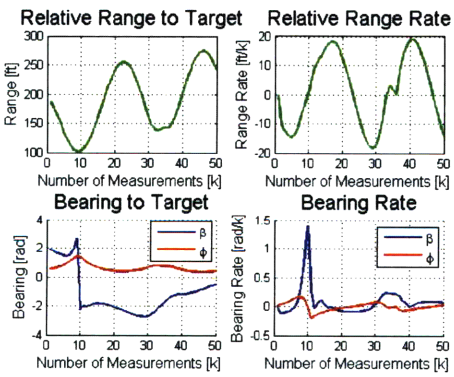

(b) Trajectory Parameters

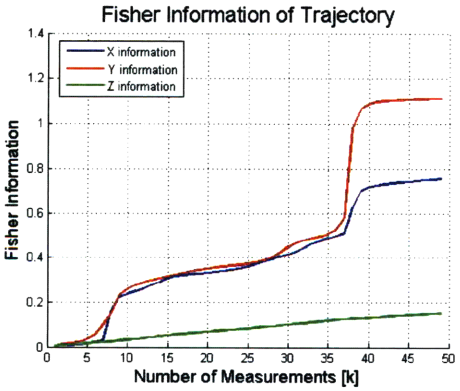

(c) Fisher Information

Figure 3-14: Trajectory optimization for tracking four targets

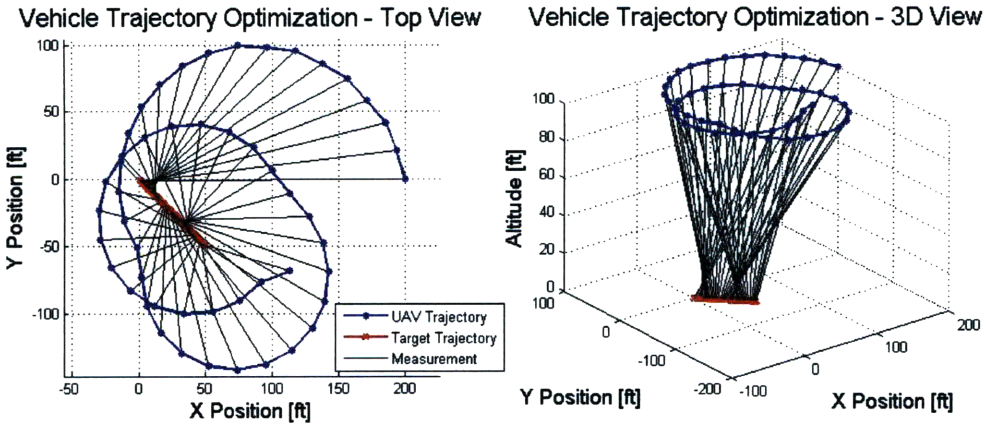

(a) Vehicle and Target Trajectories

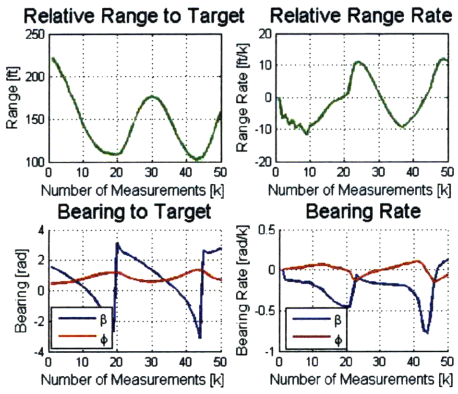

(b) Trajectory Parameters

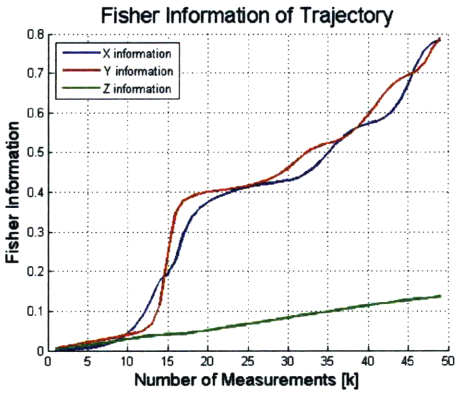

(c) Fisher Information

Figure 3-15: Trajectory optimization with motion constraints, constant velocity target, case 1

the shape of the trajectory to accommodate for the target's motion. The information gain is again largest when the vehicle is nearest to the target.

Another moving target scenario considered is for a target following a semi-circular trajectory. The target starts at the origin once again and is restricted to move in the ground plane following a semi-circular trajectory with a 20 ft radius. The UAV constraints on altitude and speed are the same as before and the UAV position is again initialized to $\mathbf{p}_0 = \begin{bmatrix} 200 & 0 & 100 \end{bmatrix}^T$ with a heading of $\frac{\pi}{2}$. The results for two semi-circular target trajectories are shown in Figures 3-17 and 3-18. Again the basic spiralling behavior is present, maintaining an orthogonal motion to the line-of-sight vector to the target while reducing relative range. As the UAV passes near the target the information is increased more rapidly, as before.

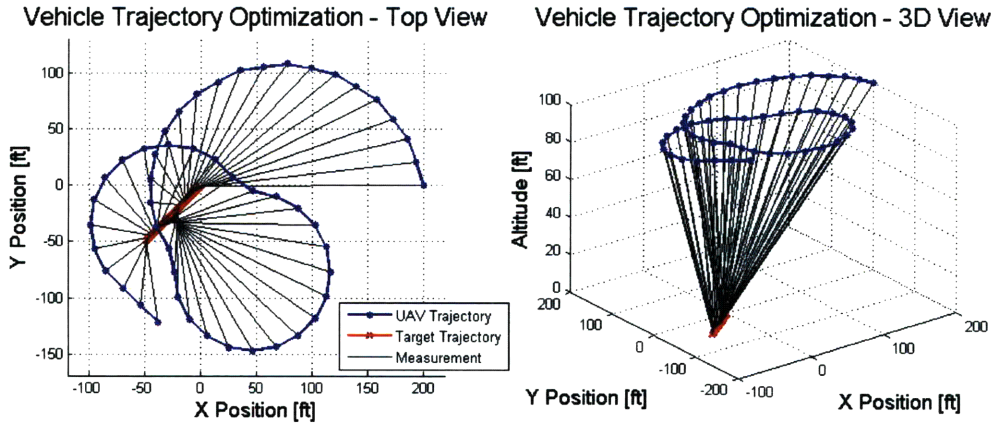

(a) Vehicle and Target Trajectories

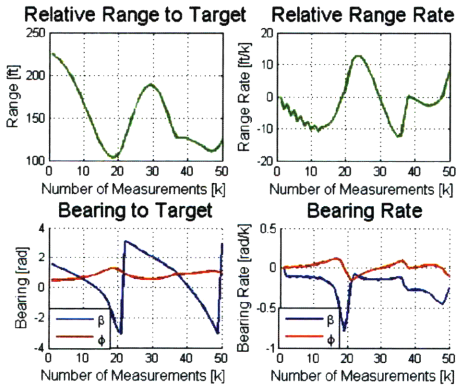

(b) Trajectory Parameters

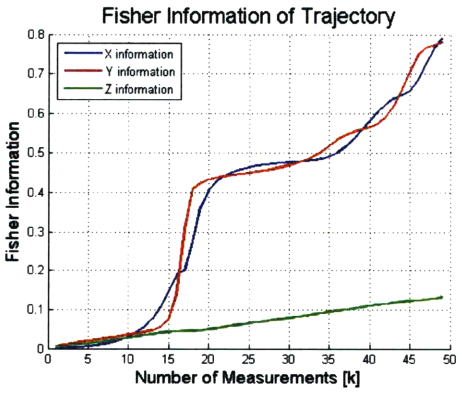

(c) Fisher Information

Figure 3-16: Trajectory optimization with motion constraints, constant velocity target, case 2

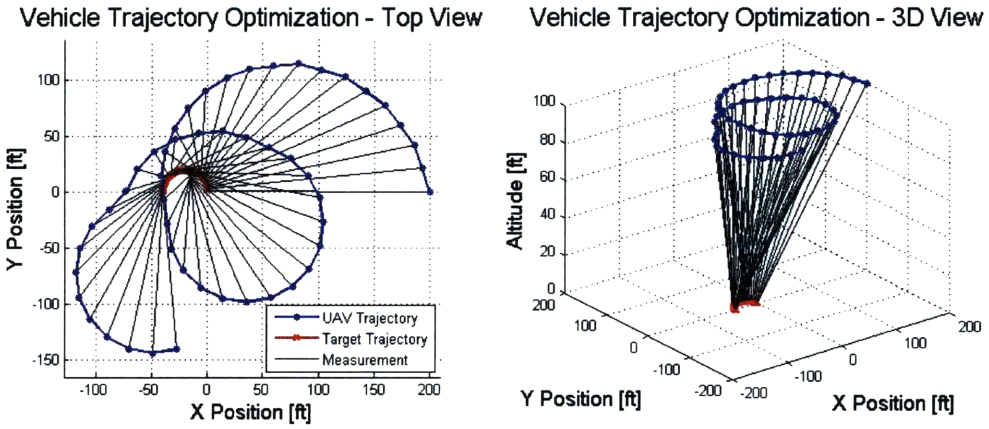

(a) Vehicle and Target Trajectories

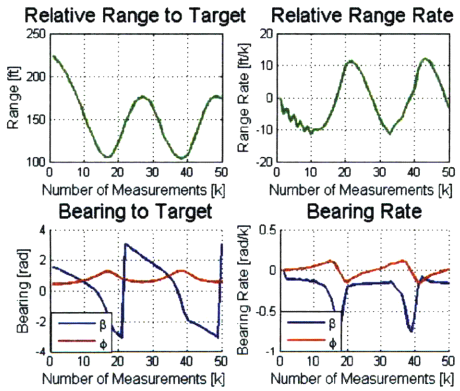

(b) Trajectory Parameters

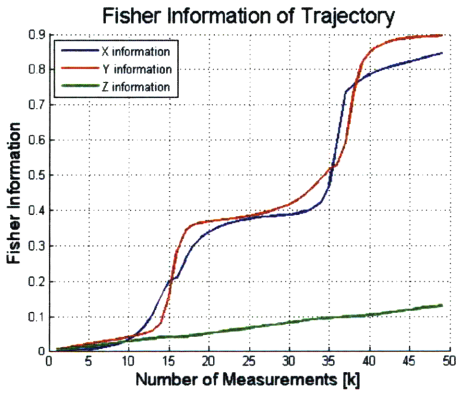

(c) Fisher Information

Figure 3-17: Trajectory optimization with motion constraints, turning target, case 1

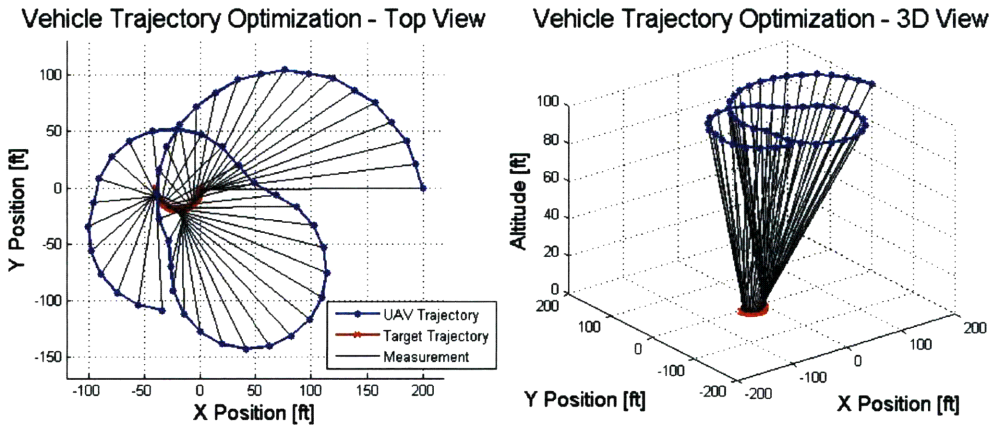

(a) Vehicle and Target Trajectories

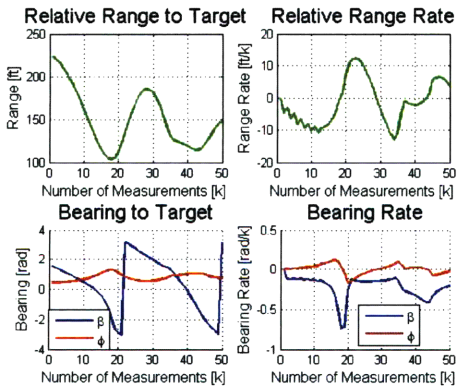

(b) Trajectory Parameters

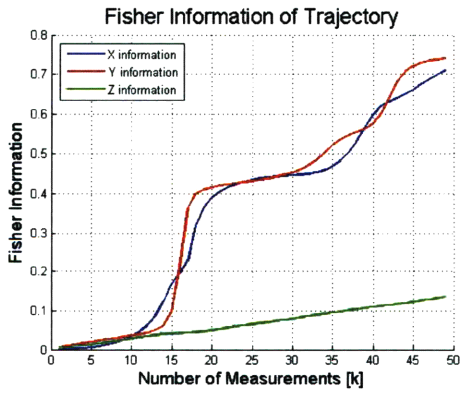

(c) Fisher Information

Figure 3-18: Trajectory optimization with motion constraints, turning target, case 2

A few cases of faster moving targets are considered. The first involves a constant velocity target moving at 22 ft/sec, which is half of the UAV velocity. The results for this case are shown in Figure 3-19 for the first 50 measurements and in Figure 3-20 for a 100 measurement UAV trajectory. Figure 3-19 shows that, in this case, the UAV spirals towards the target but cannot close in because of the fast target motion. It then moves alongside the target until it has passed it and finally spirals around to the other side. Note the sharp information increase obtained when the UAV crosses over the target. This is due to the reduction in uncertainty provided by the geometry of the measurements. Figure 3-20 shows the entire 100 measurement trajectory. After the first crossover, the UAV continues to move alongside the target and then, once it has passed it, circles around. The lower right plot of Figure 3-20 shows the slightly sharper information increases at around 55 measurements and 80 measurements corresponding to the second and third crossovers.

The second scenario for a fast moving target considers a target following a semi-circular trajectory with 100 ft radius and a UAV taking 50 measurements. The trends for this case are the same as before. The UAV begins by spiralling into the target, crosses over it and subsequently circles around it. The information about the X and Y dimensions is increased after the crossover.

One limitation of using the Fisher Information Matrix in the moving target scenarios is that the FIM is computed using the position of the target at the particular time the corresponding measurement is taken. The total information reflects the summation over all the measurements, however, since the target is moving and its position is changing, the information provided by the old measurements is not as useful as that of the new ones. The FIM framework accounts for this by using a proper transition matrix which represents the motion of the target. However, in our case, the behavior model of the target is unknown and therefore the transition matrix is assumed to be an identity matrix. The result of this inaccuracy is that the information provided by older measurements is not as valuable as the newer information and therefore the total information used in the problem misrepresents the reality of the situation. One way of fixing this could be by using an exponentially forgetting algorithm which discounts

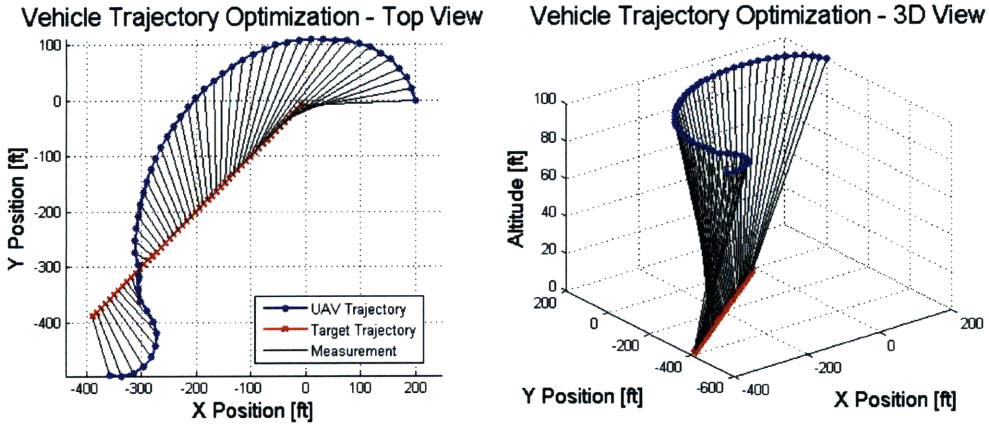

(a) Vehicle and Target Trajectories

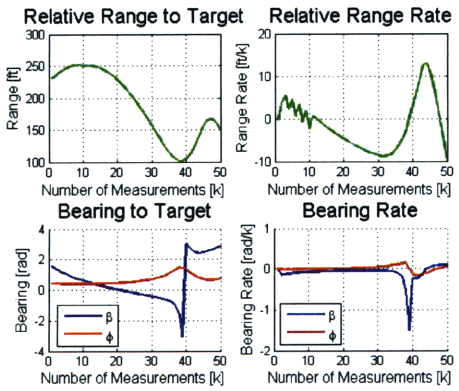

(b) Trajectory Parameters

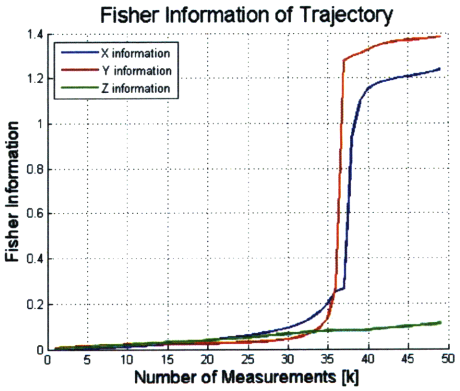

(c) Fisher Information

Figure 3-19: Trajectory optimization with motion constraints, fast constant velocity target, 50 measurements

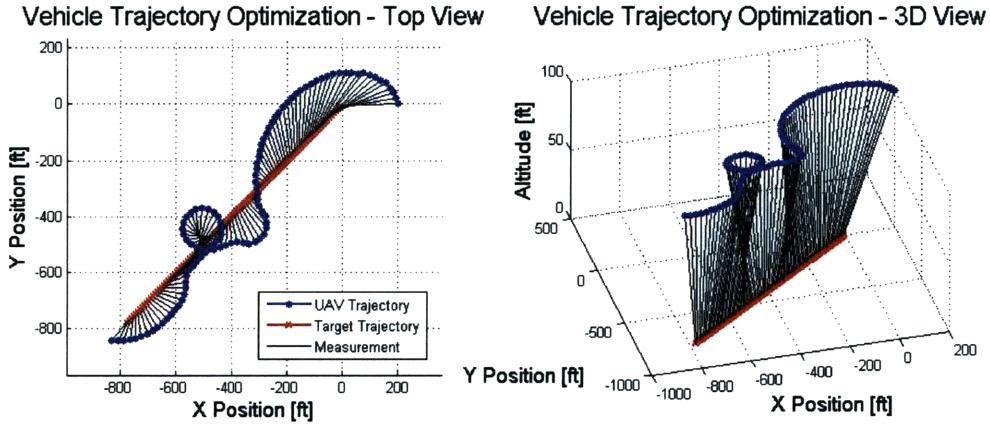

(a) Vehicle and Target Trajectories

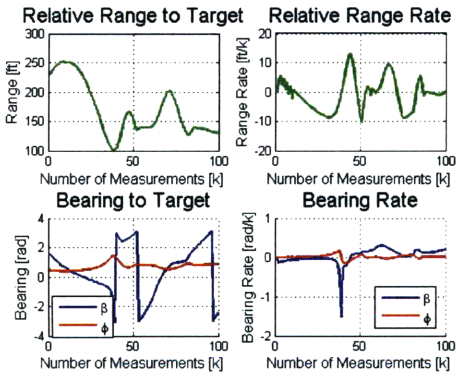

(b) Trajectory Parameters

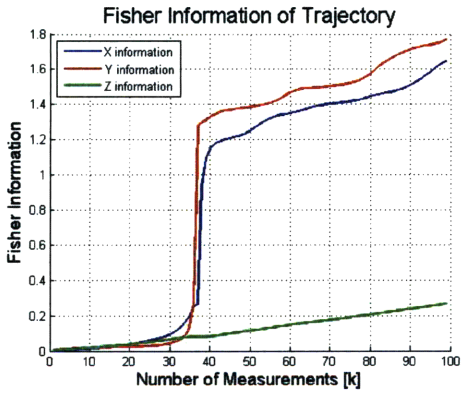

(c) Fisher Information

Figure 3-20: Trajectory optimization with motion constraints, fast constant velocity target, 100 measurements

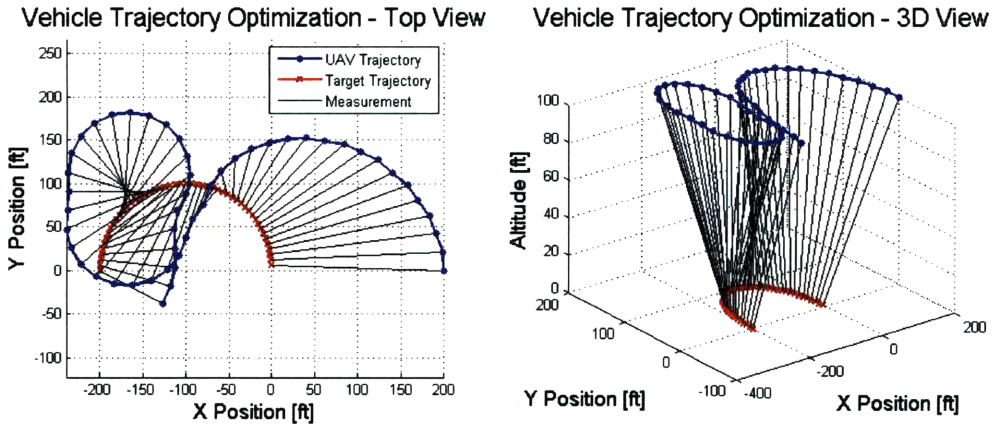

(a) Vehicle and Target Trajectories

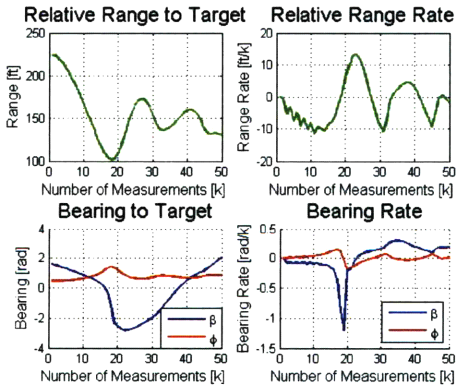

(b) Trajectory Parameters

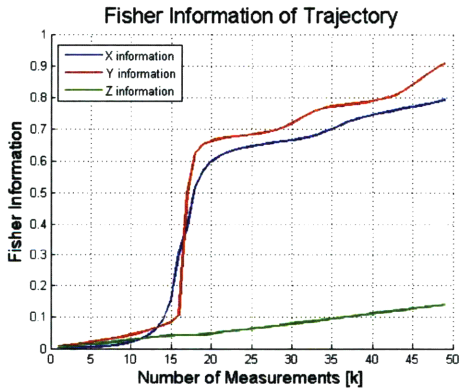

(c) Fisher Information

Figure 3-21: Trajectory optimization with motion constraints, fast turning target

passed measurements and weights newer ones more heavily.

The UAV trajectories presented in this chapter show that, even though the circular trajectory above the target is widely accepted as the optimal trajectory, it is better for a UAV with motion constraints to adopt a spiral trajectory that slowly reduces the range to the target. Most common approaches involve orbiting the target in a circular trajectory, or moving straight towards the target first and then following a circle of reduced range. These approaches do not produce the best information-based trajectories and the optimization objective functions used in these cases do not properly capture the physical and geometrical dependencies of the bearings-only estimation problem. The circling behavior is only optimal for the case of highly constrained UAV turn rate, and even then it is preferable for the circle or orbit to be offset from the target to ensure that some parts of the trajectory are as close to the target as possible. The spiral behavior shown in this section is based on maximizing the information and guides the UAV to get the most information out of each new measurement. Quigley et al. [61] address the problem of UAV trajectory planning at a constant altitude using Hopf bifurcation techniques. The resulting UAV trajectories for the stationary target case are spirals which converge to a constant limit cycle involving a circle of predefined radius. Even though their optimization approach is ad-hoc, the resulting trajectories show that the trends which improve estimation performance are captured. Using this approach, however, is limiting since it leads to fixed-shape spirals which are not well suited for dealing with randomly moving target scenarios or for the multi-target tracking case. For a UAV with a gimballed camera system, the optimal information-theoretic action is to minimize the relative range and close in on the target, while attempting to maintain a nearly orthogonal heading to the line-of-sight vector to the target. This behavior maximizes the information by reducing the relative range as much as possible instead of circling above the target where errors in the X and Y axes are improved but at a slower rate. The approach shown in this chapter provides a better way to design UAV trajectories, which is based on minimizing the estimation error and maximizing the information provided by each measurement, and which is modular enough to handle stationary

targets, multiple target tracking and several types of moving targets. As mentioned before, the main drawback to this trajectory optimization approach is that the Fisher Information Matrix is dependent upon the true target location, a quantity which is unfortunately unknown to the UAV. Chapter 4 addresses this problem and provides different approaches to handle the uncertainty in the target's location, solving the target estimation and vehicle trajectory optimization problems simultaneously.

Chapter 4

Vehicle Trajectory Optimization for Stochastic Targets

The main issue with information based optimization strategies is the dependence of the objective function on the parameters to be estimated. As shown in Chapter 3, the Fisher Information Matrix is a function of the parameters to be estimated, which in this case is the target location. This issue is prevalent throughout the literature and is best described by Cochran [15] as: "You tell me the value of θ and I promise to design the best experiment for estimating θ." Since in practice the trajectory planner has no access to the true target state, the best that can be done is to use an *a priori* distribution on the target location [52] and to perform the target estimation and vehicle trajectory optimization simultaneously. There are obvious limitations to this approach and, since combining the estimation and optimization usually leads to a highly nonlinear problem, convergence cannot be guaranteed. However, for the problem of 3-D bearings-only target tracking, if the estimation is initialized properly and the optimization is updated at a fast enough rate, the simultaneous estimation and optimization approach provides the desired performance, as will be shown in the following sections.

This chapter ties together the target localization estimation procedures described in Chapter 2 and the vehicle trajectory optimization from Chapter 3. The basic approach involves invoking the Certainty Equivalence Principle by using the estimation

results in place of the true target location for the trajectory optimization, and updating the estimation and optimization every time a measurement is taken. Section 4.1 describes the results and performance for the simultaneous trajectory planning and estimation problem using both the Extended Kalman Filter and Particle Filter algorithms. Another approach is to use a known distribution on the target instead of a single value (the estimation result), to represent the target location. This method was first considered by Mandic and Frazzoli in [52] for the task of localizing a stochastic target using acoustic measurements. Using the target distribution instead of the mean of the estimate gives a better representation of the target's location, but comes at the expense of higher computational costs since the expected value of the FIM must be taken over the entire target distribution instead of at a single value. The benefits and drawbacks of this approach are described in Section 4.2.

4.1 Simultaneous Trajectory Optimization and Target Estimation

This section explains the process of combining the target estimation and vehicle trajectory optimization algorithms, and shows the resulting UAV trajectories and estimation performance for several different cases. The two filters used for the estimation are the EKF and the Particle Filter described in Section 2.3. The trajectory optimization is performed by using the most current value of the target estimation to form the FIM, and then minimizing the trace of the inverse of the FIM (using the A-optimality criterion described in Section 3.1.2). Measurements are taken every 0.5 seconds and the estimation and optimization routines are run in sequence, updating both results at every time step. The processing time required to perform the computations for these two algorithms is usually well within the allotted time of 0.5 seconds (due to the stochastic nature of the problem, sometimes the optimization takes longer to converge but this is rare). The simultaneous estimation and optimization results show that the estimation performance achieved using the optimized

trajectory is similar to that obtained using the circular UAV trajectory presented in Chapter 2, however the number of measurements for the optimized trajectory is reduced by half. The total amount of information obtained using the optimized trajectory with half the measurements is also shown to be similar to the information gained over the ad-hoc trajectory presented in Chapter 2. Furthermore, both the EKF and particle filter show increased stability and faster convergence and tend to diverge less often. It is important to note that using this approach of simultaneous estimation and optimization does not guarantee convergence, however, for the cases described below, the initialization parameters are an order of magnitude larger than the expected estimation accuracy and both filters are very stable, exhibiting better convergence properties than in the case without an optimized trajectory. The results for each filter are presented and discussed in the following sections.

4.1.1 Trajectory Optimization with Extended Kalman Filter Estimation

Combining the trajectory optimization with the Extended Kalman Filter involves using the current value of the target estimation in the optimization as the best known target position. Several cases of target motion are analyzed, as in Section 2.3, and the results for all the cases are summarized in Table 4.1, which provides the same data as before. The stationary target scenario is considered first. The filter is initialized, as in Section 2.3, using

$$\mathbf{x}_0 = \begin{bmatrix} 0 \\ 0 \\ 0 \end{bmatrix}, \quad \hat{\mathbf{x}}_0 = \begin{bmatrix} 20 \\ 20 \\ 20 \end{bmatrix}, \quad \mathbf{P}_0 = \begin{bmatrix} 200 & 0 & 0 \\ 0 & 200 & 0 \\ 0 & 0 & 200 \end{bmatrix} \tag{4.1}$$

The UAV is operated at a fixed altitude with a velocity constraint of 44 ft/sec and a turn rate constraint of 12 deg/sec. The UAV initial position is given by $\mathbf{p}_0 = \begin{bmatrix} 200 & 0 & 100 \end{bmatrix}^T$, which is much farther than the initial position given in Chapter 2 of $\mathbf{p}_0 = \begin{bmatrix} 100 & 0 & 100 \end{bmatrix}^T$. The results for the simultaneous trajectory optimization

and target estimation for the stationary target case are provided in Figure 4-1. The UAV trajectory follows the initial spiral shape described in Chapter 3, passing close to the target and then circling around for a second pass. The convergence of the estimation is much faster, and the resulting mean and variance for the X and Y dimensions is much more accurate than the case presented in Chapter 2 (see Table 4.1), and using only half the measurements than before. Furthermore, the X and Y information are also shown to be higher than before. The estimation performance for the Z axis is worse however, since only half the measurements are used than before, and the trajectory optimization cannot drastically improve the information obtained about the Z axis. This can be seen by looking at the information plot of Figure 4-1. In practice though, terrain elevation data is usually available and could be used to improve the performance of the Z estimation. It is interesting to note that the information in the X and Y axes increases sharply when the UAV crosses over the target the second time, and, correspondingly, the estimation performance drastically improves. Overall, even though the UAV is farther away from the target than in the previous case and less measurements are taken, the estimation performance is better, since the optimized trajectory provides higher information, reducing the uncertainty in the estimation.

The next scenarios considered are for moving targets with no prior behavior model of the target motion, as described in Section 2.3. The first case involves a target exhibiting a random-walk behavior. The EKF parameters are initialized as in Section 2.3 and the UAV trajectory is optimized using the target estimation results. The results for this case are presented in Figure 4-2. The UAV trajectory produced by the optimizer closely resembles the results shown in Figure 3-6, and the UAV is shown to spiral in towards the target, passing over and then circling around for another pass. The information in the X and Y axes in significantly improved when the UAV passes over the target as seen in the information plot of Figure 4-2. Correspondingly, the X and Y estimation error and covariance decrease, but due to the random walk dynamics of the target, the estimation accuracy decreases as the UAV moves away again. The resulting estimation performance for the random walk case is slightly

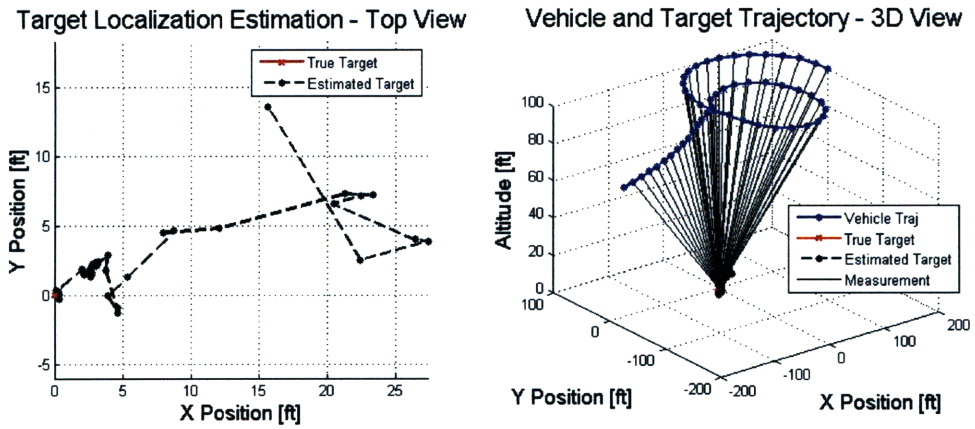

(a) Vehicle and Target Trajectories

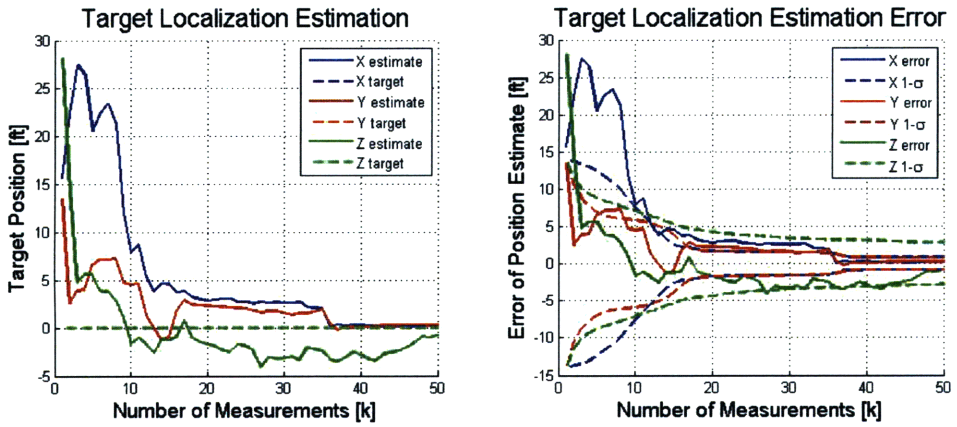

(b) Target Localization Estimation Results

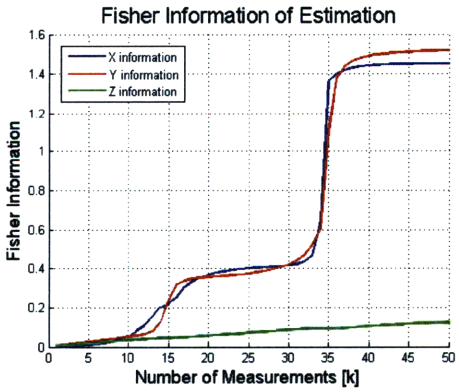

(c) Fisher Information

Figure 4-1: UAV trajectory optimization and EKF estimation results for stationary target localization

worse than that obtained in Chapter 2 but overall is quite similar even though only half the measurements are used.

The next moving target case considered is for a constant velocity target. As before, no target behavior model is assumed, and the EKF consists of a stochastic target model with constant propagation and increased process noise. The results for this scenario are presented in Figure 4-3. The resulting UAV trajectory is similar to that shown in Figure 3-15 exhibiting the same spiralling and circling behavior as before. The estimation performance for this case is worse than that of Section 2.3.1 and the estimation error and variance are about twice as much as before and the information is half as much. These results are shown in Table 4.1 and the particle filter algorithm also shows the same performance (described in the next Section). Since only 50 measurements as opposed to 100 from before are used, the estimation performance is about equal to that of Section 2.3.1. An interesting thing to note however, is that although the variance and estimation error remain noisy, the estimation is not biased as before and the optimal UAV trajectory is effective in eliminating the estimation bias by increasing the information rapidly (as evidenced by the increase in information after 10 measurements in Figure 4-3).

The final slow moving target case involves tracking a target following a semi-circular trajectory. The target is restricted to the ground plane and follows a semi-circular trajectory of 20 ft radius as before. Again, a stochastic model of the target is used in the EKF, since the estimation algorithm cannot assume that the target is turning. The results for the turning target case are provided in Figure 4-4. The UAV trajectory again resembles the results shown in Chapter 3. A sharp information gain can be seen as the UAV comes close to the target, around 15 measurements, causing a corresponding decrease in uncertainty and increase in estimation accuracy. The overall estimation performance is better than in Section 2.3.1, showing a lower error, much lower variance and increased information with only half the measurements (see Table 4.1).

An additional case involving a fast moving constant velocity target is considered as well. In this scenario the target has a velocity of 22 ft/sec which is half the speed

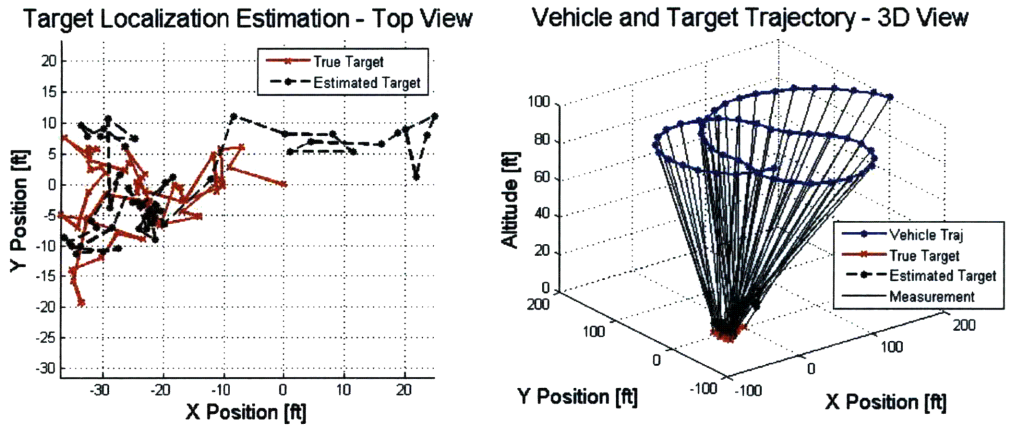

(a) Vehicle and Target Trajectories

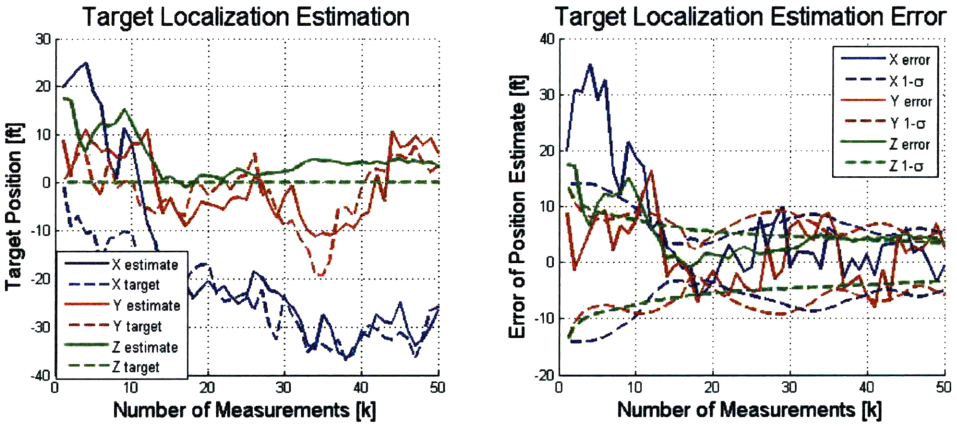

(b) Target Localization Estimation Results

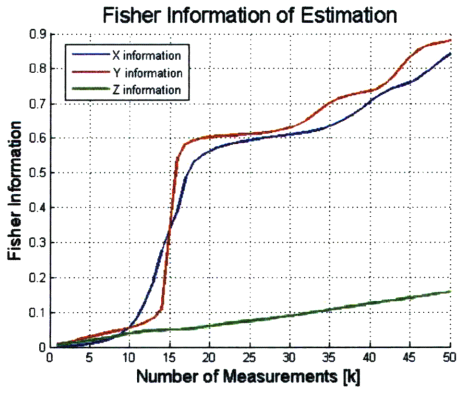

(c) Fisher Information

Figure 4-2: UAV trajectory optimization and EKF estimation results for a target with random walk behavior

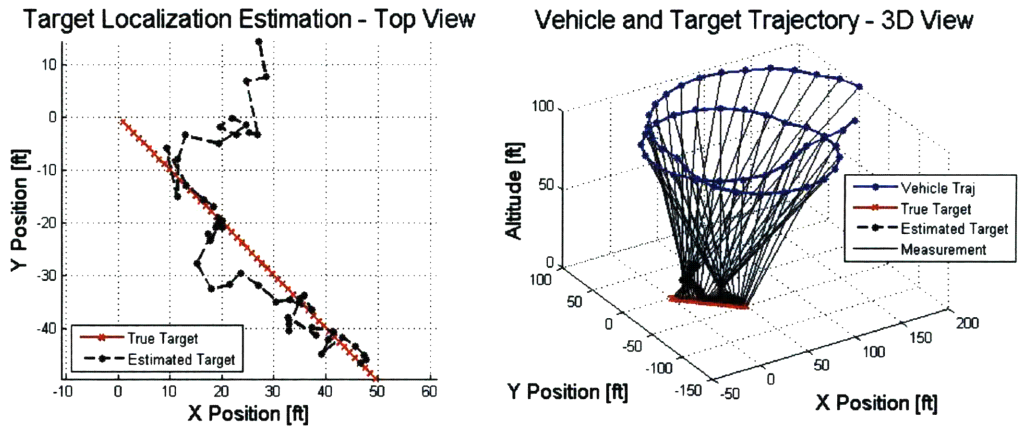

(a) Vehicle and Target Trajectories

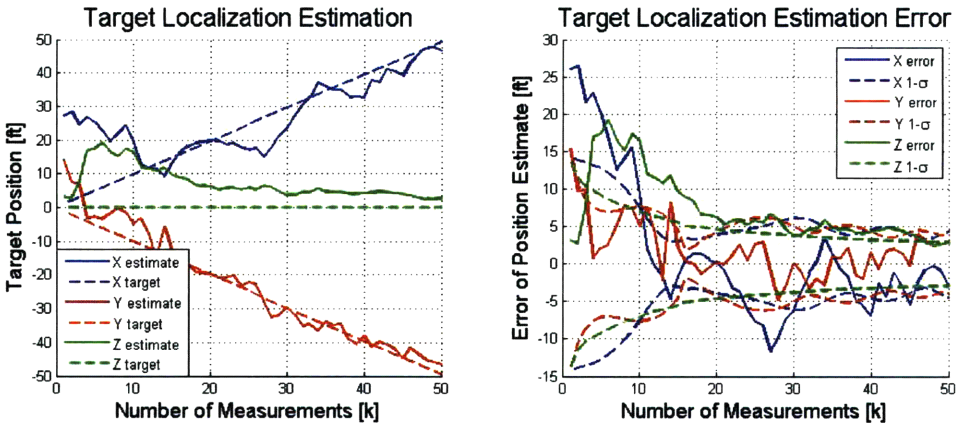

(b) Target Localization Estimation Results

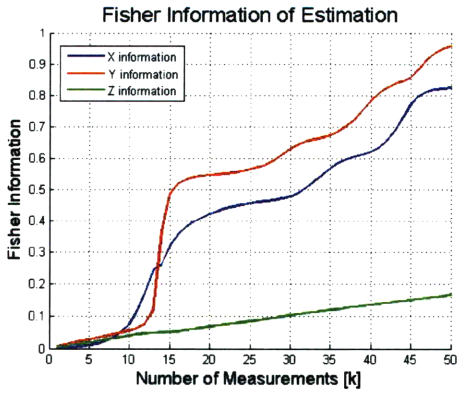

(c) Fisher Information

Figure 4-3: UAV trajectory optimization and EKF estimation results for a constant velocity target

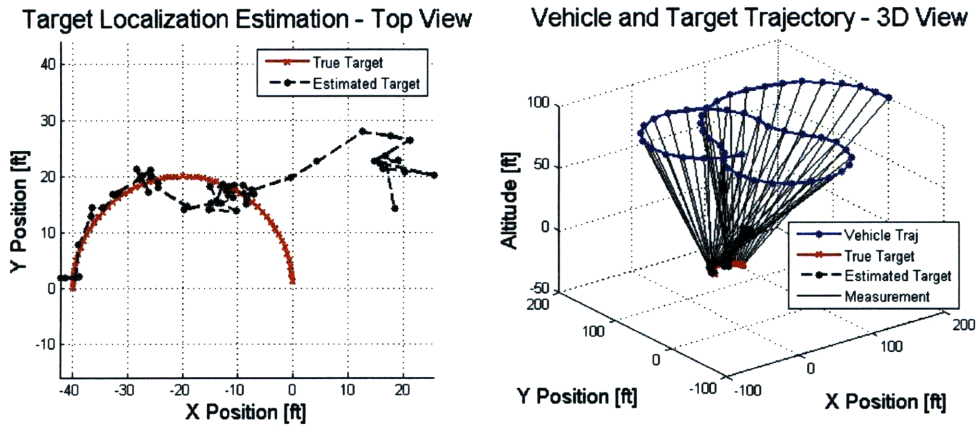

(a) Vehicle and Target Trajectories

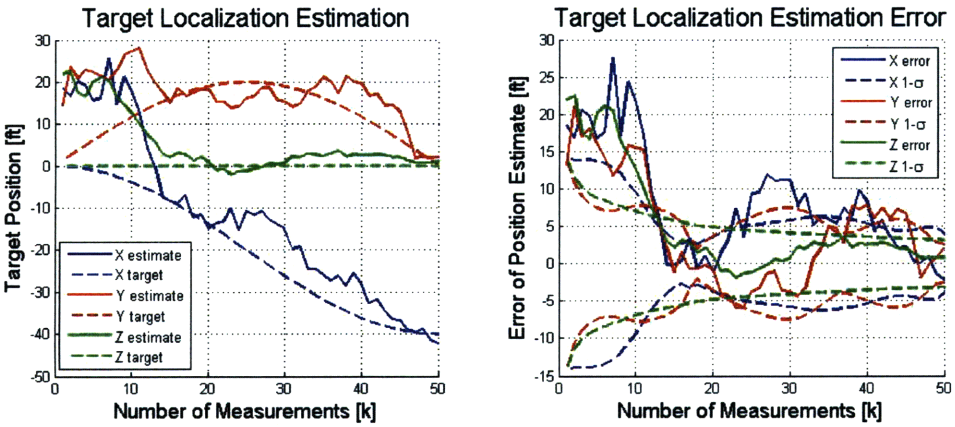

(b) Target Localization Estimation Results

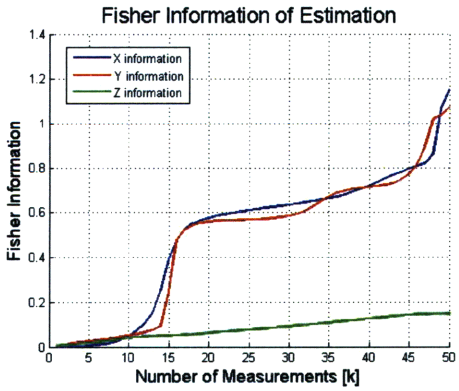

(c) Fisher Information

Figure 4-4: UAV trajectory optimization and EKF estimation results for a turning target

Table 4.1: Summary of results for 3-D EKF Estimation with Trajectory Optimization

Target Dynamics		Estimation Error	Estimation Variance	Fisher Information
Stationary	x	0.23	0.71	1.45
	y	0.28	0.68	1.52
	z	-0.81	7.92	0.12
	Total	0.89	9.30	3.09
Random Walk	x	-0.62	23.83	0.84
	y	2.74	29.68	0.88
	z	3.46	11.57	0.16
	Total	4.46	75.08	1.88
Constant Velocity	x	-2.82	23.58	0.82
	y	3.01	16.51	0.96
	z	2.82	8.34	0.17
	Total	5.00	48.43	1.95
Semi-circular	x	-2.21	4.35	1.15
	y	2.05	11.42	1.08
	z	0.86	9.86	0.15
	Total	3.14	25.62	2.38

of the UAV. The results for the simultaneous estimation and optimization are shown in Figure 4-5. Although the errors are quite large, the EKF manages to track the target and the filter remains stable, unlike the case presented in Chapter 2 using the ad-hoc trajectory. Furthermore, the information provided by the measurements using the optimized UAV trajectory is much higher than the results presented in Chapter 2 using the circular trajectory. This case clearly illustrates the benefit of optimizing and re-planning the UAV trajectory in real-time using an information-based approach.

The simultaneous trajectory optimization and target estimation using the Extended Kalman Filter shows that enhanced estimation performance can be obtained by optimizing the target trajectory using an information metric in real-time. For all the cases described above, the estimation converges rapidly, the EKF algorithm is considerably more stable than before, and the estimation achieves accurate results within only 50 measurements. In general, the estimation of the Z axis is worse than that of the other two dimensions. As mentioned before, this is because the information provided about the Z axis is much less than that of the X and Y axes since

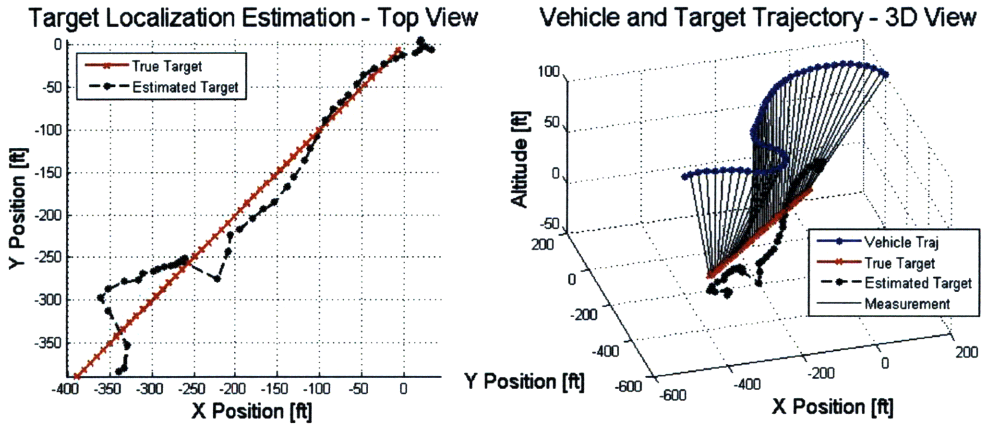

(a) Vehicle and Target Trajectories

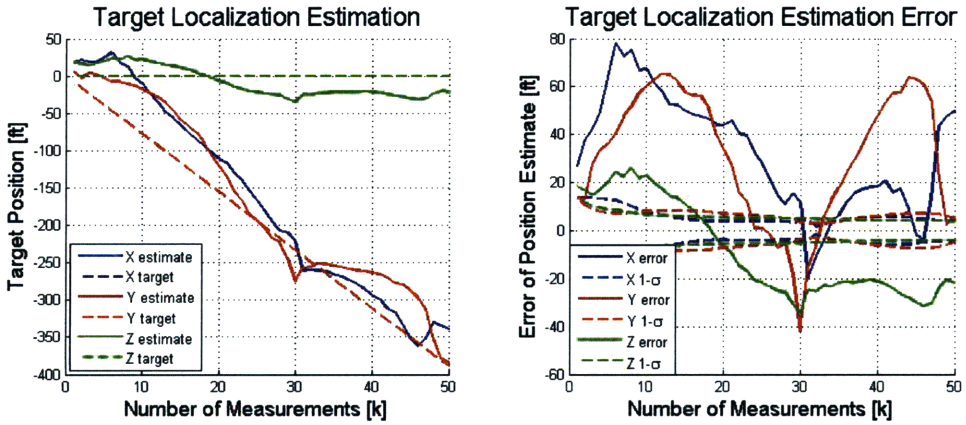

(b) Target Localization Estimation Results

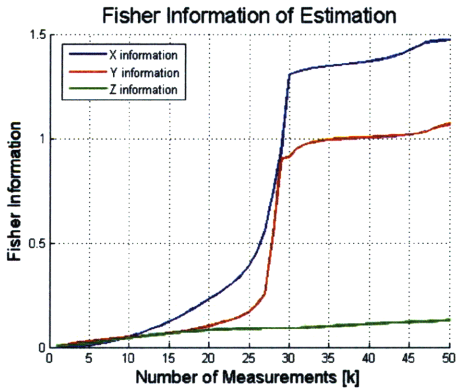

(c) Fisher Information

Figure 4-5: UAV trajectory optimization and EKF estimation results for a fast constant velocity target

measurements cannot be taken from below the target. Overall, the EKF combined with the trajectory optimizer performs very well, showing that it is more important to increase the information gain provided by each new measurement by designing a proper UAV trajectory than to waste bandwidth and computational resources by taking more sub-optimal measurements.

4.1.2 Trajectory Optimization with Particle Filter Estimation

This section describes the simultaneous UAV trajectory optimization and target estimation using a particle filtering algorithm. The particle filter described in Section 2.3.2 is combined with the trajectory optimization algorithm from Chapter 3. The sample mean of the particles at a given time step are used in the trajectory optimization algorithm instead of the true target value. The estimation and optimization algorithms are run in sequence, updating both in real-time. The performance of the combined trajectory optimizer and particle filter is tested using the same scenarios described above for the EKF and in Section 2.3.2 and the results for the stationary and slow moving cases are summarized in Table 4.2, which contains the same data as before. An additional case for a fast moving target is considered last and the particle filter shows good tracking performance even for this extreme target motion case.

The first case considered is for a stationary target. The UAV is initialized to $\mathbf{p}_0 = \begin{bmatrix} 200 & 0 & 100 \end{bmatrix}^T$ which is farther than the case considered in Section 2.3.2. The results for the stationary target case are shown in Figure 4-6. The trajectory shape is similar to the optimal trajectory shown in Figure 3-6 and displays the same spiralling and circling behavior as before. The target estimation performance is similar to the results obtained in Section 2.3.2 and the information content and variance for the X and Y dimensions for both cases are close. The mean of the estimation error is slightly worse using the optimal trajectory but the results are still under 5 ft (see Table 4.2). It is interesting to note the drastic increase in estimation performance when the information is sharply increased by the UAV passing close to the target. This can be

seen by looking at the estimation error and information plots in Figure 4-6. Overall the PF estimation using the optimal trajectory achieves similar performance to the case of an ad-hoc circular trajectory using only half the measurements.

The moving target case for a random walk target is explored next and the results are presented in Figure 4-7. The UAV trajectory is shown to spiral into the target and then circle around it to come in for a second pass. The information is shown to increase sharply when the UAV comes close to the target. Correspondingly, the X and Y estimation error and covariance decrease at these same times. Due to the random walk dynamics of the target, however, the estimation accuracy decreases as the relative range increases again. As explained in Section 2.3.2, the PF algorithm is quite sensitive to its tuning parameters and the propagation noise of the particles (σ_w) has to be adjusted to obtain adequate filter performance. If σ_w is too high the the estimation performance will be noisy, but is σ_w is too low the filter cannot track adequately and will diverge. If σ_w is properly tuned however, the particle filter is very stable and consistently achieves good convergence. The estimation accuracy is similar to the results obtained in Section 2.3.2, but using only half the measurements (see Table 4.2).

The constant velocity target case is considered next and the results are shown in Figure 4-8. The UAV trajectory closely resembles the optimal trajectory shown in Figure 3-15, where the UAV spirals towards the target and then circles around it. The information gain when the UAV passes close to the target can be seen in Figure 4-8, and the estimation error and variance are shown to decrease accordingly. As in the case of the EKF, the information obtained for the constant velocity tracking case is about half of that obtained using the ad-hoc trajectory from Chapter 2. The estimation performance is also shown to be worse (see Table 4.2). Since the optimal trajectory uses half the measurements than the ad-hoc trajectory the estimation performance is equitable. The optimal trajectory does, however, reduce the estimation bias successfully and although the results are noisier, they converge faster and remain closer to the true target value throughout the remainder of the estimation.

The final slow moving target case considered is for a target following a semi-

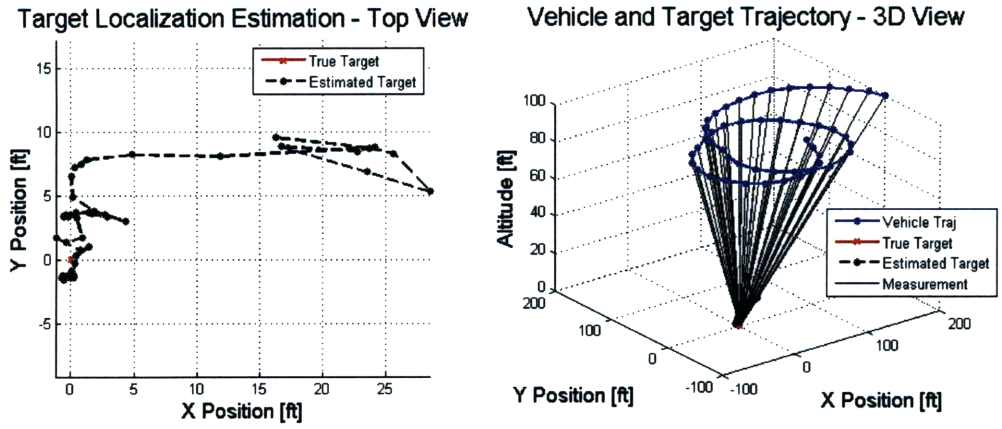

(a) Vehicle and Target Trajectories

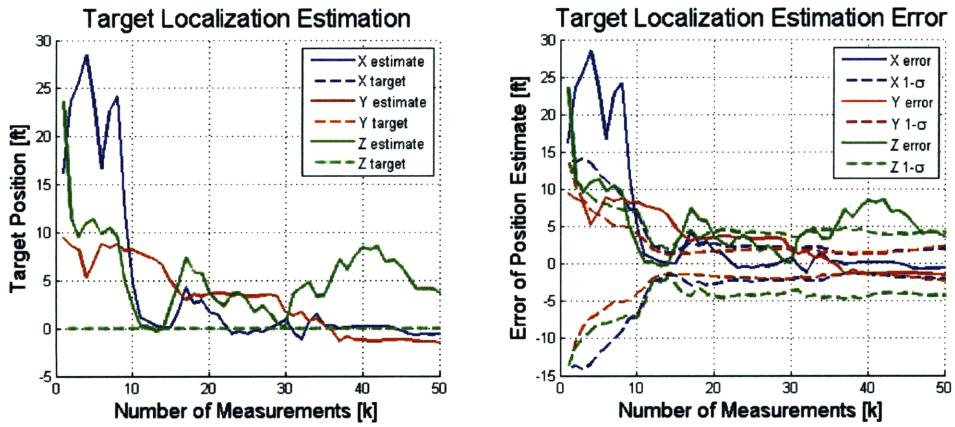

(b) Target Localization Estimation Results

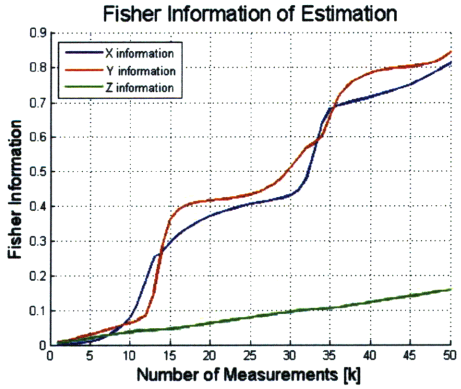

(c) Fisher Information

Figure 4-6: UAV trajectory optimization and particle filter estimation results for stationary target localization

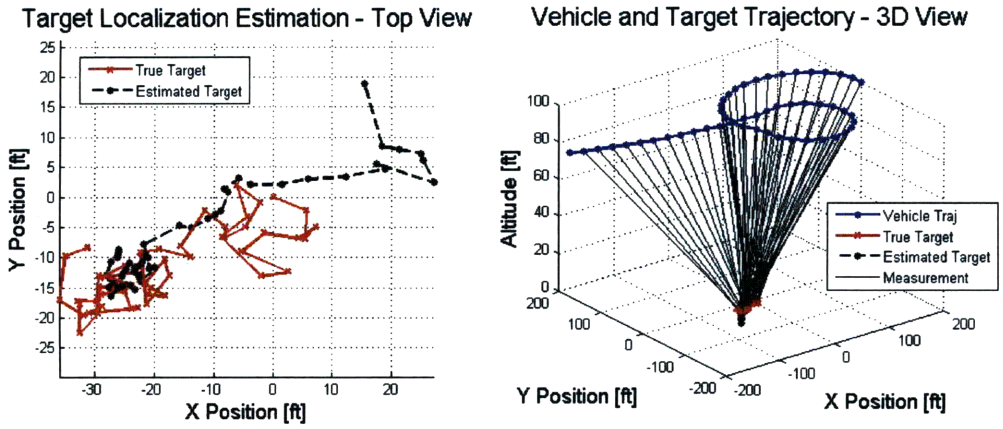

(a) Vehicle and Target Trajectories

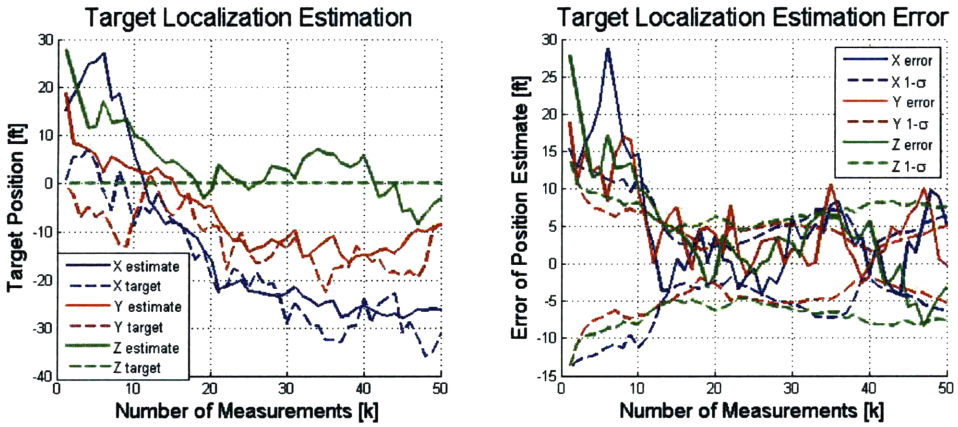

(b) Target Localization Estimation Results

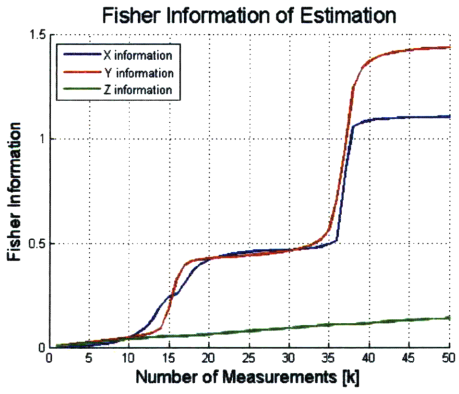

(c) Fisher Information

Figure 4-7: UAV trajectory optimization and particle filter estimation results for a target with random walk behavior

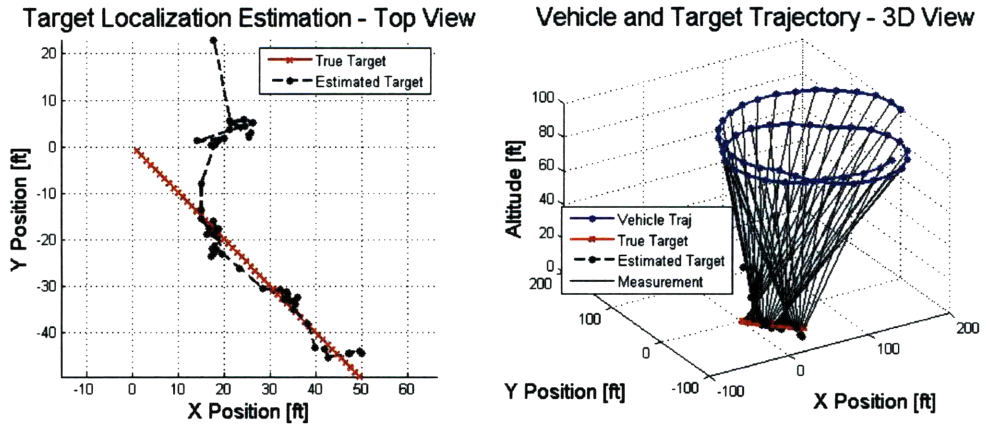

(a) Vehicle and Target Trajectories

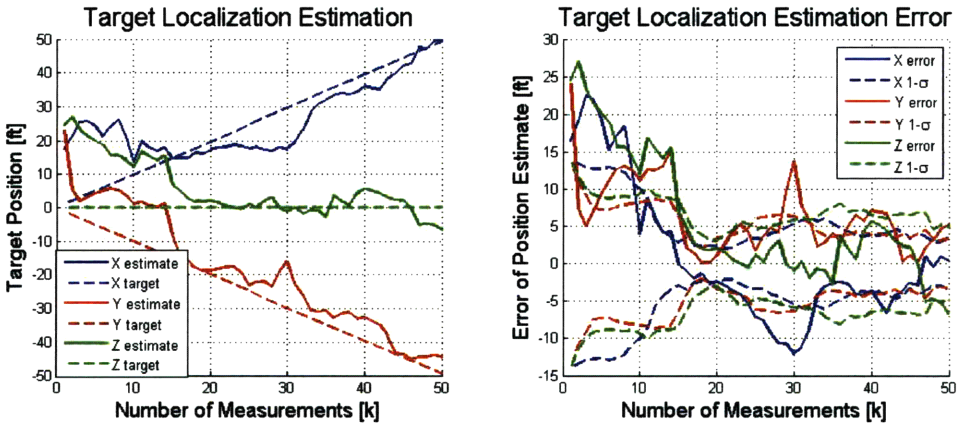

(b) Target Localization Estimation Results

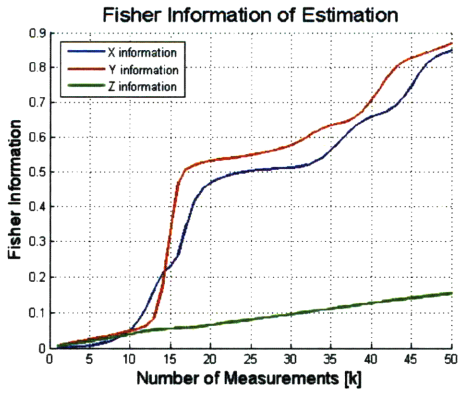

(c) Fisher Information

Figure 4-8: UAV trajectory optimization and particle filter estimation results for a constant velocity target

Table 4.2: Summary of results for 3-D Particle Filter Estimation with Trajectory Optimization

Target Dynamics		Estimation Error	Estimation Variance	Fisher Information
Stationary	x	-0.56	3.89	0.81
	y	-1.50	5.46	0.84
	z	3.60	17.97	0.16
	Total	3.94	27.33	1.81
Random Walk	x	5.17	44.76	1.11
	y	-0.26	28.56	1.44
	z	-3.14	57.45	0.14
	Total	6.05	130.77	2.68
Constant Velocity	x	0.42	15.67	0.85
	y	5.19	14.89	0.87
	z	-6.73	17.34	0.15
	Total	8.50	47.90	1.87
Semi-circular	x	0.04	65.37	1.45
	y	3.03	39.61	1.54
	z	-2.97	57.58	0.13
	Total	4.24	162.57	3.12

circular trajectory. As before the target behavior is considered stochastic and the particle propagation noise is increased to account for the uncertainty in the target's motion. The results for this scenario are presented in Figure 4-9 and in Table 4.2. The UAV trajectory spirals towards the target and then circles around it coming in for a second pass. Once again, the information plot shows sharp increases in X and Y information when the relative range to the target is the lowest. These information increases are shown to correspond with a reduction in uncertainty and an increase in estimation accuracy as seen in the estimation error plot of Figure 4-9. The resulting estimation error is lower than the results shown in Table 2.2 and the information for the X and Y axes is higher, even though only half the measurements are used.

An additional case involving a fast constant velocity target moving at half the speed of the UAV is considered. The results for this scenario are presented in Figure 4-10. The particle filter is able to track the target and even though the error is large compared to the slow moving target case, the filter remains stable and converges,

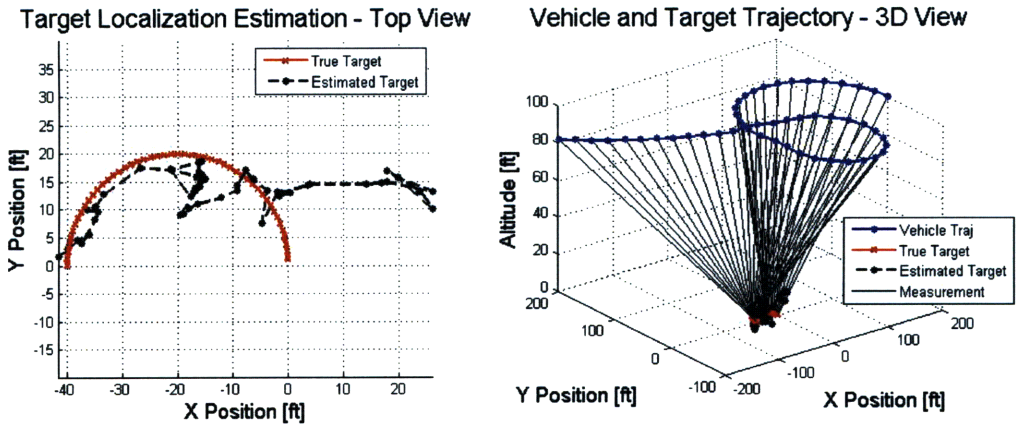

(a) Vehicle and Target Trajectories

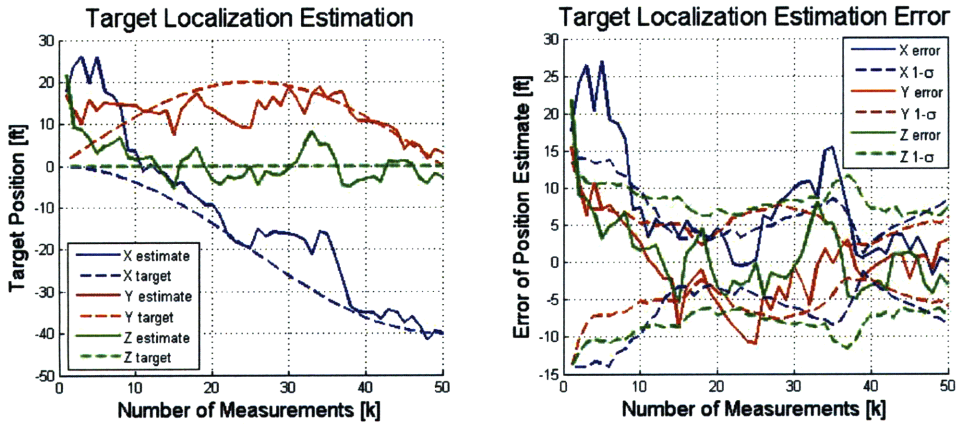

(b) Target Localization Estimation Results

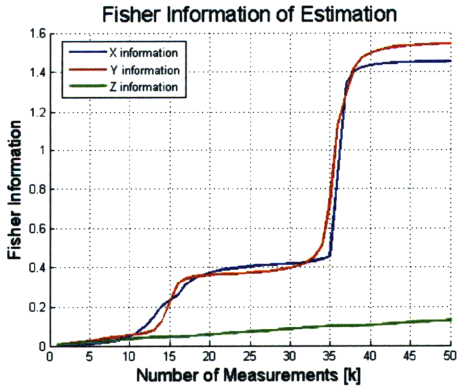

(c) Fisher Information

Figure 4-9: UAV trajectory optimization and particle filter estimation results for a turning target

unlike the case considered in Chapter 2 using the ad-hoc trajectory. This shows that using an optimized UAV trajectory results in enhanced estimation performance. Furthermore, the information content for this scenario is much higher than in the case considered in Chapter 2 with the ad-hoc circular trajectory, showing that increasing the information provided by the measurements improves the accuracy and convergence of the estimation.

Overall, the particle filtering algorithm combined with the UAV trajectory optimization works very well and achieves accurate estimation performance. The particle filter has very good convergence properties and is consistently more stable than the EKF for all the above scenarios. The Z axis estimation results are not as accurate as the X and Y estimation, due to the lack of information about the Z axis caused by the poor geometry of having all the measurements taken from above the target only. One issue with the PF is its sensitivity to its tuning parameters, especially to the particle propagation noise (σ_w). Higher values of σ_w increase the speed of convergence but make the estimation results noisier, whereas lower σ_w values make convergence slower but the estimation is a lot less noisy. Ideally, higher σ_w values should be used initially to increase the speed of filter convergence, however, as the estimation becomes more accurate, σ_w should be reduced to smooth out the estimation results. Future enhancements to the particle filter would involve adaptively recomputing σ_w leading to improved filter performance.

4.2 Trajectory Optimization for Targets with Stochastic Distribution

The approach taken in the previous sections uses the estimated target value instead of the true target location in the computations of the Fisher Information Matrix. In practice, this method is shown to work well, however no guarantees can be made about the stability or convergence of the combined algorithm. In fact, if the initial estimate of the target is too far away from the true value, the UAV trajectory would

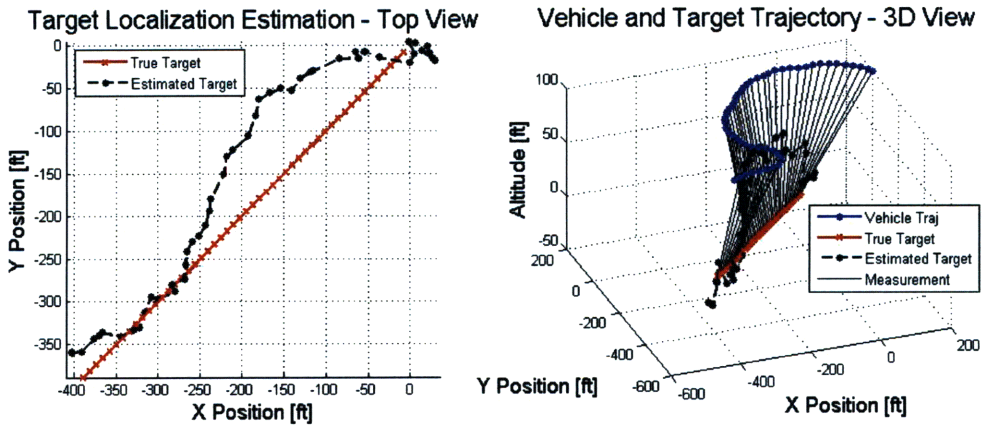

(a) Vehicle and Target Trajectories

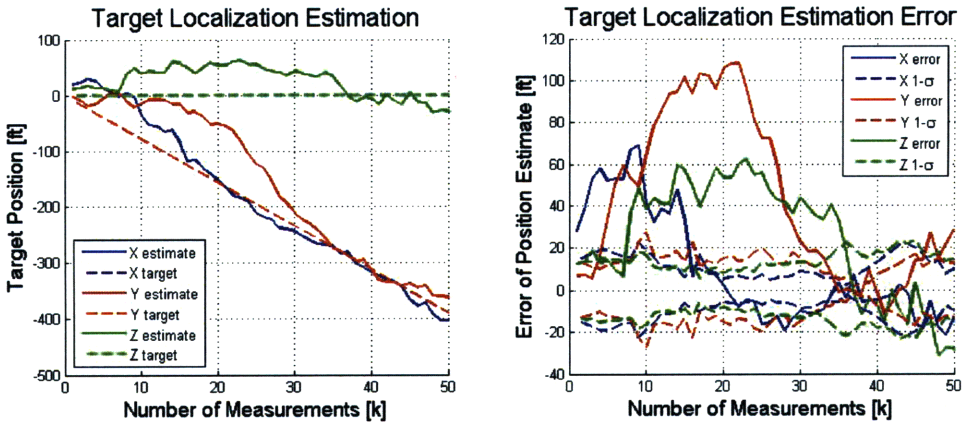

(b) Target Localization Estimation Results

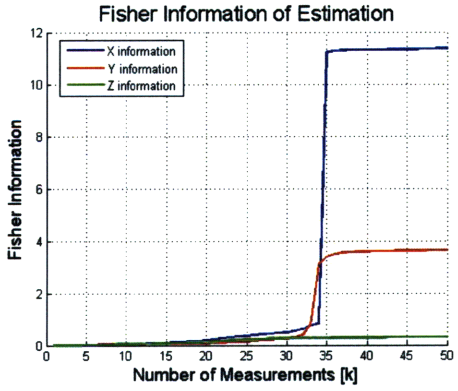

(c) Fisher Information

Figure 4-10: UAV trajectory optimization and particle filter estimation results for a fast constant velocity target

be considerably off from the desired optimal trajectory and the estimation algorithm would likely diverge. This dependency of the UAV trajectory on the single value of the target location estimate is undesirable and can be somewhat ameliorated by using a distributed target approach instead. Using an *a priori* distribution for the stochastic target, the expected value of the Fisher Information Matrix can be computed and used in the optimization in lieu of the FIM computed with the single target location estimate, leading to a more accurate consideration of the uncertainty in the target's position. This approach was first explored in [52] and is described in Section 4.2.1, where results for the trajectory optimization of a UAV around a uniformly distributed target are presented. The new optimization approach is then integrated with a particle filter estimation algorithm and the process is described in Section 4.2.2. The particle values and their respective weights are used to represent the stochastic distribution of the target at each time step and the FIM in the optimization is computed over the entire particle set. The resulting UAV trajectories and target location estimation are shown below.

4.2.1 Trajectory Optimization for Distributed Targets

This section describes the process of performing UAV trajectory optimization for tracking a stationary target using a probability density function of the stochastic target's distribution. The expected value of the Fisher Information Matrix is computed with respect to the target distribution instead of using the FIM at the estimated target location. The equation becomes,

$$\mathbb{E}_{\mathbf{x}}\{\mathbf{J}(\mathbf{x})\} = \int_D \mathbf{J}(\mathbf{x}) f_{\mathbf{x}}(\mathbf{x})\, d\mathbf{x} \tag{4.2}$$

where $f_{\mathbf{x}}(\mathbf{x})$ is the joint target distribution over its three dimensions and D is the domain of $f_{\mathbf{x}}(\mathbf{x})$. The objective function is then computed using the expected value of the FIM and is given by,

$$f(\mathbf{J}(\mathbf{x})) = \mathrm{Tr}\big\{\mathbb{E}_{\mathbf{x}}\{\mathbf{J}(\mathbf{x})\}^{-1}\big\} \tag{4.3}$$

The trajectory optimization for a fixed altitude UAV tracking a stationary target, presented in Section 3.2.2, is revisited using a distributed target. The target is assumed to be uniformly distributed over an area of 60 ft $\times$ 60 ft and the distribution is discretized using 81 points. The UAV trajectory results are shown in Figure 4-11. The shape of the trajectory does not change much due to the target distribution. The UAV still spirals towards the target and then circles around for a second pass. The total expected information is however higher than in Figure 3-6. To test the effects of a larger distribution area for the target, a uniform target distribution over an area of 120 $\times$ 120 is used instead. The results for this scenario are presented in 4-12 and this time the shape of the trajectory is affected by the target distribution. The UAV prefers to fly along the border of the distribution and circle around the entire area, instead of circling around the mean. The expected information is higher than that obtained in 3-6.

This trajectory optimization approach based on a probability distribution of the target provides UAV trajectories that are theoretically better than those computed using a single target estimate value, since they more accurately account for the uncertainty in the target estimate. For targets with very complex or widespread distributions the benefits of this approach are apparent. This method could also be used for UAV trajectory planning in the multiple-target scenario, by representing the target distribution using a multi-modal density. However, for the single UAV case with a uniform or normal *a priori* distribution with a relatively small uncertainty (one order of magnitude above the desired estimation accuracy), the optimized UAV trajectories are still very similar to the results obtained using the mean of the distribution, and the benefits of the distributed target method are marginal. Furthermore, optimization using the expected value of the FIM over the entire target distribution is a computationally intensive task which takes orders of magnitude longer to execute than the optimization using the mean of the target distribution. Since the results are not significantly different, the additional computational resource usage is not justified.

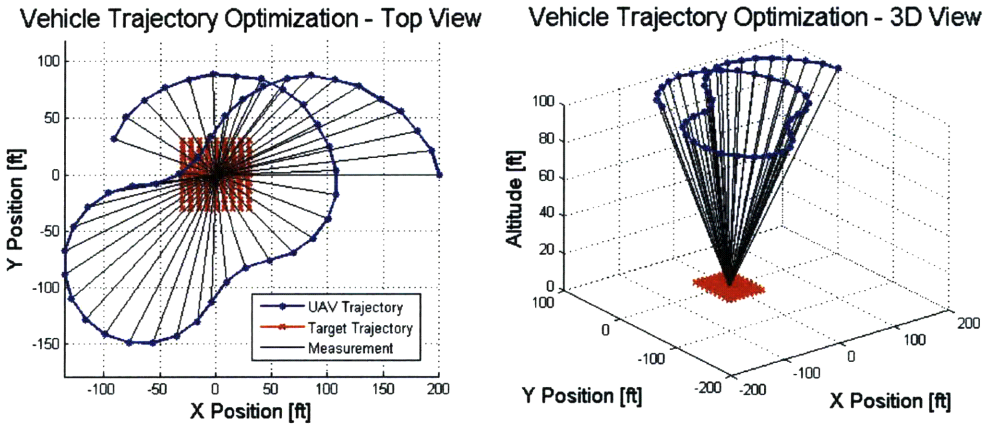

(a) Vehicle and Target Trajectories

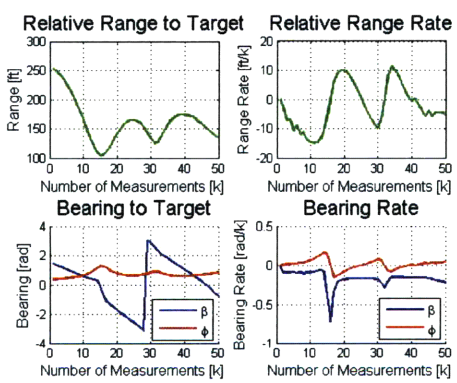

(b) Trajectory Parameters

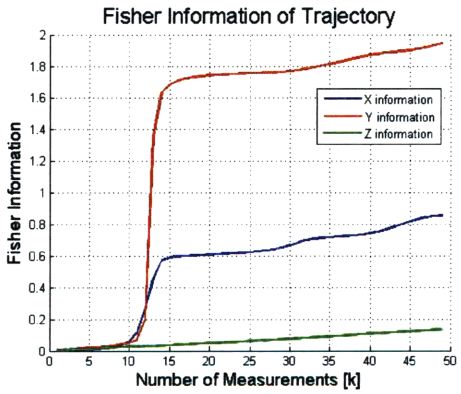

(c) Fisher Information

Figure 4-11: Optimal vehicle trajectory for a uniformly distributed target

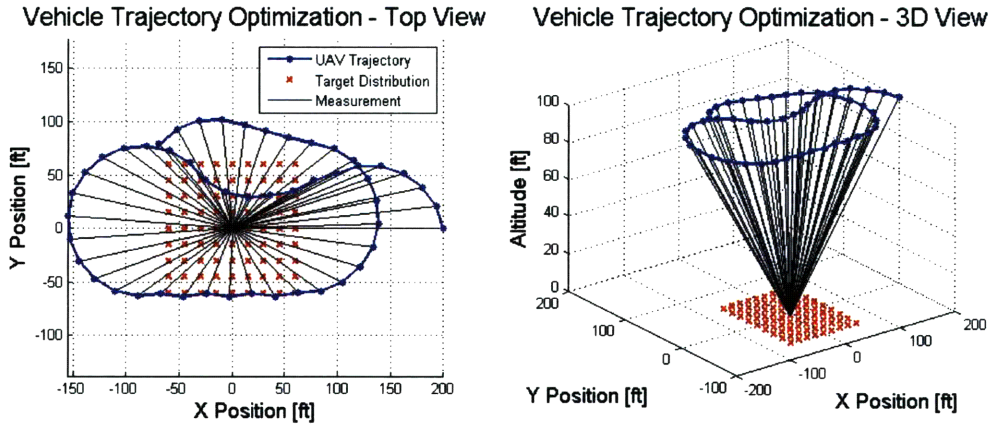

(a) Vehicle and Target Trajectories

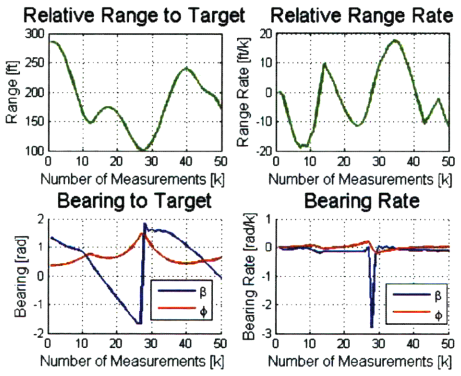

(b) Trajectory Parameters

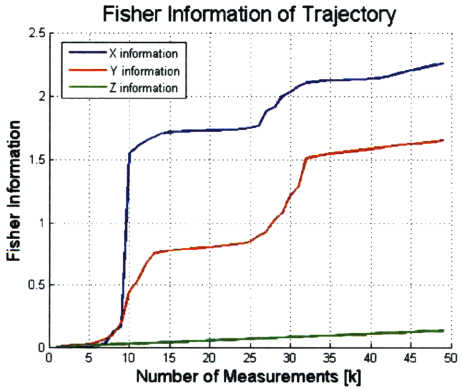

(c) Fisher Information

Figure 4-12: Optimal vehicle trajectory for a uniformly distributed target with large spread

4.2.2 Trajectory Optimization for Distributed Targets Using Particle Filter Estimation

One of the most interesting uses of the approach presented above is its easy integration with particle filter estimation. Since particle filters work by propagating a target distribution using weighted particles, the probability density function of the target is readily available at each time-step. The optimization can then use the particle values and their weights to compute the expected value of the Fisher Information Matrix over the particle set for every time step using,

$$\mathbb{E}_{\mathbf{x}}\{\mathbf{J}(\mathbf{x_k})\} = \sum_{i=1}^{N} \mathbf{J}(\mathbf{x_k^i}) m_k^i \tag{4.4}$$

where N is the number of particles and m^i is the associated weight of each particle used in the filter.

The results for the combined particle filter estimation and trajectory optimization over the stochastic target distribution are presented in Figure 4-13 and Table 4.3. The shape of the UAV trajectory is very similar to that obtained using the mean of the estimation for the trajectory optimization (see Figure 4-6). The total information provided by the measurements is also similar in both cases as is the final estimation error. The variance, however, using the distributed target approach is much lower (see Table 4.3). After 15 measurements the filter stabilizes and the estimation error and covariance remain fairly constant, showing that the distributed target optimization approach enhances the stability and robustness of the particle filter. Since the normal particle filter shown in Section 4.1.2 is already quite stable and converges rapidly, however, the uncertainty in the target location estimate is not large enough to produce a significant change in the trajectory shape.

Although this approach using the stochastic target distribution is more robust and theoretically more accurate, it suffers from a few practical drawbacks. The main issue is that the computation time required to perform optimization using a distributed target is orders of magnitude longer than the case using the sample mean of the target

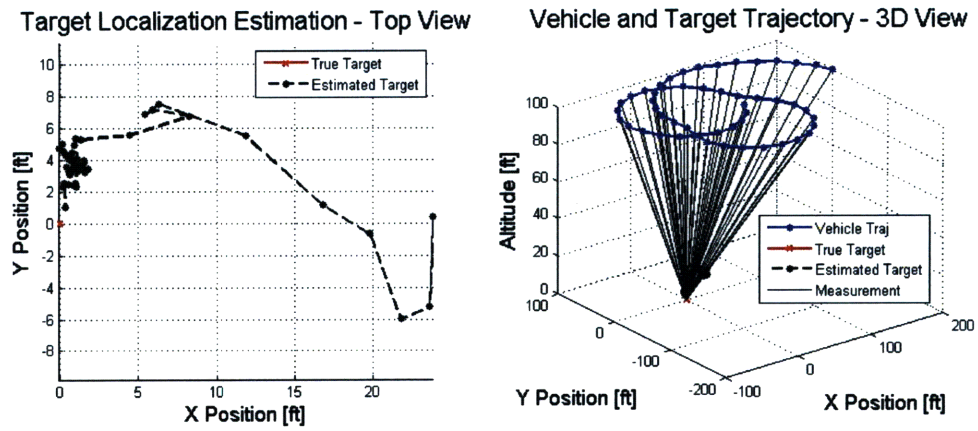

(a) Vehicle and Target Trajectories

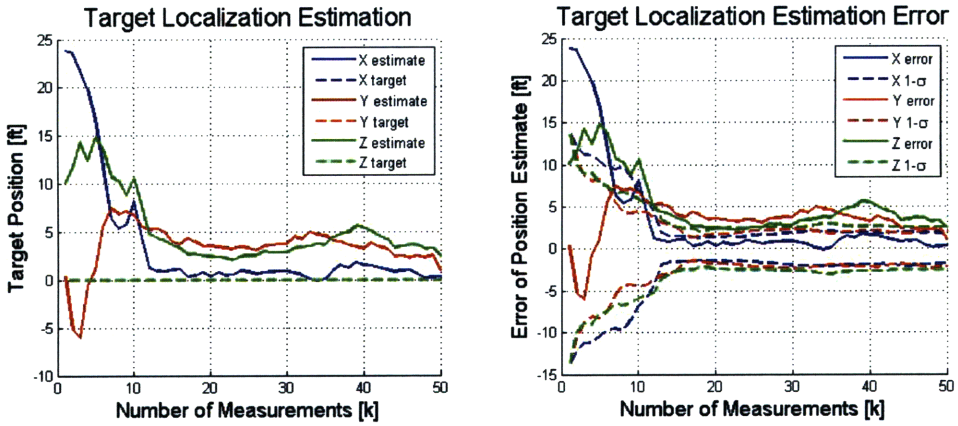

(b) Target Localization Estimation Results

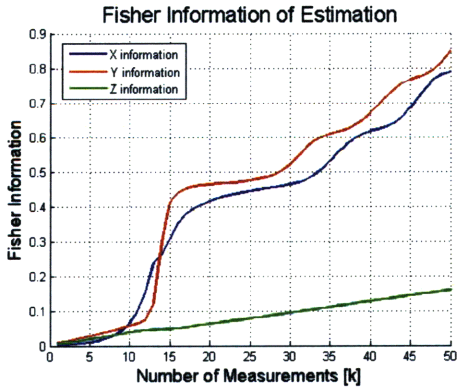

(c) Fisher Information

Figure 4-13: UAV trajectory optimization using particle filter weights

Table 4.3: Summary of results for 3-D Particle Filter Estimation with Trajectory Optimization Using Particle Distribution

Target Dynamics		Estimation Error	Estimation Variance	Fisher Information
Stationary	x	0.33	2.15	0.79
	y	1.03	2.80	0.85
	z	2.46	3.89	0.16
	Total	2.69	8.84	1.80

estimate. Reducing the number of particles in the PF could reduce the amount of computational resources required, but at the expense of lower PF estimation accuracy. In practice it is found that the PF algorithm requires at least 500 particles, making this distributed target optimization approach infeasible in real-time. Furthermore, the improvement in trajectory design for this new algorithm over the case using the mean of the target estimation is marginal. This is especially true when more measurements are available and the estimation accuracy increases, since the variance decreases, and as seen in Section 4.2.1, the trajectory for a distributed target with low variance is almost the same as that for a target centered at the origin.

For the 3-D bearings-only target tracking problem using small UAVs it is found that the best approach for target estimation is provided by executing simultaneous estimation and trajectory optimization. Optimizing the UAV flight path in real time leads to trajectories that maximize the amount of information provided by the measurements and reduce the uncertainty and error in the target location estimation. Although no guarantees of convergence can be made, both the EKF and the PF algorithms exhibit enhanced stability and convergence properties when an optimal trajectory is used. The EKF and particle filter with 500 particles show similar estimation performance and are equally well suited to dealing with stationary and stochastically moving targets. Both estimation algorithms, along with the optimization, take significantly less than 0.5 seconds to run and, although computational resources available onboard a UAV are very different from those of a traditional personal computer, the algorithm run-time suggests that there is a future for implementing methods like these

onboard small UAVs. The accuracy of the particle filter could be increased by using a larger number of particles, but this would come at the expense of increased computational resources. Additional improvements to the PF algorithm shown in Section 4.1.2 could be made by adequately tuning the filter parameters. With an adaptive tuning algorithm, the sensitivity of the PF performance on the tuning parameters could be exploited to improve the overall estimation results. The distributed target approach presented in this section is too expensive to implement in real-time, but could be used to initialize the optimization, especially if the uncertainty in the initial target estimate is very large.

Overall, the results presented in this chapter show that computing optimal information-based UAV trajectories in real-time is important and leads to increased accuracy and observability in the target estimation. The computational resources required to process the combined estimation and optimization described in Section 4.1 are moderate and these algorithms could be implemented on board a small UAV to improve target estimation and tracking performance.

Chapter 5

Conclusion

This work explores the challenges associated with localizing an unknown target in an unknown environment using a small UAV equipped with navigation and imaging capabilities. Estimation algorithms for the 3-D nonlinear bearings-only tracking problem are presented and trajectory optimization strategies based on information-theoretic techniques are considered. The problem of simultaneous target estimation and vehicle trajectory optimization is explored and the resulting algorithms produce vehicle trajectories that increase the information provided by the measurements, greatly enhancing the target estimation performance, removing biases, improving filter convergence, increasing estimation observability, and overall leading to improved target localization. The following sections summarize the content of this thesis, analyze and discuss the results obtained, and provide suggestions for future work and improvement.

5.1 Summary

Chapter 1 introduces and motivates the problem of target tracking and localization using small UAVs equipped with navigation and video capabilities. The main system models and dynamics are provided and the primary challenges associated with target localization and tracking using small UAVs are discussed. Chapter 1 also describes previous work in bearings-only target tracking and explores different issues associated with target estimation and vehicle trajectory optimization. Research in sensor place-

ment techniques and vision-based target localization is considered as well. The Fisher Information Matrix and the Cramér-Rao Lower Bound are introduced as measures for assessing estimation performance and provide a framework for the development of vehicle trajectories that increase the information provided by the measurements in order to improve the accuracy and observability of the estimation.

Chapter 2 provides a detailed analysis of the general target estimation problem. It begins by describing the Fisher Information Matrix and Cramér-Rao Lower Bound which are used to quantify the performance of different estimation algorithms. The challenges associated with different estimation algorithms such as the Least Squares estimator, the Extended Kalman Filter, and the Particle Filter are described. The close relationship of the EKF and the least-squares estimation algorithms to the Fisher Information Matrix is also described, showing the dependence of the estimation performance on the information content of the measurements. The chapter ends with applications of the Extended Kalman Filter (EKF) and the Particle Filter (PF) to the problem of 3-D target localization with bearings-only measurements. The known information includes the position of the UAV and the direction in which the camera is pointing, resulting in measurements composed of two angles (azimuth and elevation). The relative range from the UAV to the target is not measured, but can be determined through subsequent bearings measurements. Although the EKF and the PF are shown to be good tracking algorithms, this bearings-only estimation problem is nonlinear and several complications arise with these traditional filtering methods. For example, if proper estimation observability is not provided quickly the estimation algorithms diverge and the resulting instability leads to premature covariance collapse, as shown by Aidala [6]. Or, without proper estimation observability, the estimation results become biased and the uncertainty is increased. The cases shown in Chapter 2 use a predefined ad-hoc UAV trajectory which consists of a circular orbit above the target at a fixed altitude. For this trajectory, the estimation results and the information provided by the measurements are given for several different cases of target motion, and the close relationship between the information and the estimation performance is demonstrated. The examples in Chapter 2 show the sensitivity of the overall target

estimation problem to the trajectory taken by the UAV and illustrate the need for designing trajectories that maximize the information provided by the measurements and thus enhance estimation performance.

Chapter 3 describes the task of vehicle trajectory optimization with the goal of improving the target location estimate by increasing the information provided by the measurements. It starts by deriving the Fisher Information Matrix (FIM) for the 2-D and 3-D bearings-only target localization problems. A discussion and comparison of different cost functionals based on the FIM is provided next, focusing on the physical significance and mathematical qualities of each. For the 3-D bearings-only target localization problem the A-optimality criterion, involving the trace of the inverse of the FIM, is chosen as the objective function and optimal UAV trajectories are computed which maximize the amount of information available for different cases of target behavior and vehicle constraints. For the sensor placement (unconstrained vehicle motion) case the optimal trajectory is shown to be a circle above the target with a radius to altitude ratio of approximately 0.7. For the constrained vehicle motion scenario a fixed-wing UAV with a fixed velocity and maximum turn rate is considered as the platform vehicle and several cases of target motion are analyzed. The resulting trajectories for the stationary target case consist of spirals that increase the angular separation between subsequent measurements while reducing the relative range to the target. The UAV trajectories pass as close to the target as possible, within the vehicle constraints, and then circle around for the next pass. Sharper information increases are observed when the UAV passes close to the target. Restricting the maximum turn rate leads to limit cycles where the UAV orbits the target. An interesting result is that the optimal information-theoretic action in these cases involves following an orbit where the target is off-center. This leads to measurement points along the trajectory that pass as close to the target as possible, within the vehicle turn rate constraints, minimizing the relative range to the target. As the maximum allowable turn rate is increased, the trajectories become more spiral-like, passing closer to the target, and then circling back around for subsequent spiral passes. Slow moving target scenarios are considered next and the same spiral trends are observed for these cases, although

the trajectory is adjusted to account for the motion of the target. Fast moving targets are also considered and the resulting trajectories show that the UAV spirals are adjusted to minimize the relative range to the target while attempting to maintain as much angular separation between the measurements as possible. When the vehicle is close enough to the target it crosses overhead and the information is drastically increased. Multiple target scenarios are also considered and the UAV again spirals towards a target and then circles around and moves towards the next target, showing that minimizing the relative range to a farther target provides a sharper information increase than circling around a near target multiple times.

The information-theoretic optimization in Chapter 3 depends on the true target location, an unknown quantity, which is the conundrum faced in most joint estimation and trajectory planning problems. To address this issue and accommodate stochastic or unknown target behavior two approaches are explored in Chapter 4. The first invokes the Certainty Equivalence Principle by tying together the estimation from Chapter 2 and the optimization from Chapter 3, using the mean value of the estimation instead of the true target location in the optimization algorithm. Both, the estimation and the optimization, are run in sequence and updated simultaneously in real time. This approach is tested using both the EKF and the Particle Filter, and the algorithms are shown to converge leading to estimation results which are better than those obtained in Chapter 2. The results in Chapter 4 show that improved estimation accuracy and increased filter convergence are obtained by planning trajectories in real time to maximize the information, rather than using a predefined circular trajectory above the target which is currently the most common approach. The second method of dealing with stochastic targets consists of computing the expected value of the FIM with respect to a known target distribution in the optimization instead of using the deterministic FIM based on the estimated target value. This approach is combined with a particle filtering estimation algorithm, where the particles and weights of the filter are used to represent the probability distribution of the stochastic target. Although this method is theoretically more stable and increases filter convergence, the algorithm run-time is shown to be several orders of magnitude higher than that of

the simultaneous estimation and optimization approach described earlier, and could therefore only be used to initialize the UAV trajectory. The following section describes the results of this thesis in more detail and provides discussion on some of the noteworthy points.

5.2 Analysis and Discussion of Results

This thesis presents an information-theoretic approach for vehicle trajectory optimization in the 3-D bearings-only target localization problem. The optimal vehicle trajectories are shown to be spirals which increase the angular separation between the measurements while decreasing the relative range to the target. These trajectories maximize the amount of information provided by the measurements and are applicable to several types of target motion and vehicle dynamic constraints. The sensor placement case presented in Section 3.2.1 shows that, without considering vehicle motion constraints, the optimal trajectory is a circle orbiting the target, a result that is widely accepted in the current literature as the optimal UAV trajectory for target localization. However, this is only a particular case of the vehicle trajectory optimization problem with restricting assumptions on the vehicle dynamics. If vehicle constraints on velocity and turn rate are considered, spiral trajectories are shown to be better than circular trajectories centered on the target. Using the stationary target scenario as a baseline, different transient and limiting behavior is obtained by modifying the turn rate constraints. With a low maximum allowable turn rate, the initial spiral trajectory cannot get as close to the target as with a more relaxed constraint. This low turn rate constraint causes the UAV to converge onto a limit cycle, circling around the target. It is interesting to note that, for the information-theoretic optimal trajectory, the target is not in the center of the circle as most current literature suggests (see [62] and [10]). Rather, the UAV has phases of the trajectory where it is close to the target, showing that minimizing the relative range to the target while maintaining angular separation of the measurements results in a higher information content. As the turn rate constraint is relaxed, the UAV is free to make

sharper turns and the resulting trajectory is a spiral which passes as close to the target as possible within the vehicle turn rate constraint. Spiral trajectories using Hopf bifurcation techniques are presented by Quigley et al. [61] as ad-hoc solutions to the UAV trajectory planning problem for target localization. The spiral trajectories start by heading towards the target and subsequently converge onto a limit cycle that circles the target. This case can be compared to the scenario presented in Figure 3-7. The information-theoretic solution differs by making the initial trajectory pass as close to the target as possible and then come around, finally converging on a circular limit cycle around the target. The information gain as the UAV passes close to the target can be seen in the information plot of 3-7, illustrating the benefit of reducing the relative range to the target. Many results shown throughout the literature are obtained by making specific assumptions about the target motion or the vehicle dynamics, however, the algorithms presented in Chapter 3 provide a mathematical framework to handle several different types of vehicle constraints and dynamics, as well as many different target scenarios, including moving targets and multiple targets. This framework relies on maximizing the information provided by the measurements and results in trajectories that provide the best geometry for the measurement set, thus minimizing the target location estimation error for many different situations.

As mentioned in the previous section, an issue with information-based trajectory design is that the objective function relies on the value of the true target location. Chapter 4 addresses this issue by providing a suite of algorithms for performing target estimation and vehicle trajectory optimization in sequence, using the mean of the target estimate in the optimization objective function in lieu of the true target location. An important result of this thesis is that the performance of the simultaneous estimation and optimization algorithms explored in Chapter 4 is significantly better than the target estimation using a predefined trajectory seen in Chapter 2. It is well known that taking more measurements reduces estimation error, but the information provided by the vehicle trajectory also plays an important part in improving estimation accuracy. Some measurements provide more information than others and, by maximizing the amount of information provided by each new measurement, the estimation

performance can be enhanced. This is shown by comparing the estimation results, for both the EKF and the PF, using the circular trajectory from Chapter 2 to the later results using the optimal UAV trajectory. Even though 100 measurements are taken in the circular trajectory cases and only 50 are used for the optimal trajectory scenarios, the estimation error and uncertainty for both trajectory scenarios are very similar, and the information provided by the measurements is comparable, showing that equal estimation performance can be obtained using only half the measurements if the UAV trajectory is selected properly. The convergence properties of both the EKF and the PF estimation algorithms are also increased by optimizing the vehicle trajectories, as shown in the cases of tracking a fast moving target. The estimators using the ad-hoc circular trajectory are incapable of achieving tracking convergence, whereas optimizing the UAV trajectory in real time allows the estimators to track the target easily. Furthermore, for both the EKF and the PF, the estimation accuracy is shown to rapidly increase and the covariance decrease when a sharp information gain is obtained. All these results show that it is more important to increase the information provided by the measurements by designing a proper UAV trajectory, than to waste bandwidth and computational resources by taking more measurements that do not provide much new information. The measurements for the optimal trajectory scenario are taken every 0.5 seconds to ensure that enough time is provided for processing the estimation and optimization algorithms. This measurement rate is arbitrarily chosen and further analysis on the increase in information provided by the trajectory could be used to optimize the measurement rate, thus reducing processing requirements whilst still achieving the desired estimation accuracy. For example, since it is not necessary to waste bandwidth and computational resources if the new measurements do not provide a significant amount of new information, the algorithm could be tuned to take a measurement only when the change in information is above a certain threshold.

One of the primary conclusions of this thesis is that the Fisher Information Matrix provides a good framework for vehicle trajectory optimization. The FIM is independent of the estimation algorithm used and is based mainly on the physical and geomet-

rical properties of the system. Optimization based on the FIM therefore captures the essential geometric relationships associated with the estimation problem and focuses on increasing the information provided by the measurements, resulting in improved estimation performance. Another important property of the Fisher Information Matrix is that it is additive and can be updated recursively using a simple summation. This can be used for processing measurements from a single sensor over multiple time steps or for computing the FIM for multiple sensor measurements. A combination of these can also be used where multiple sensors take measurements over multiple time steps. It is interesting to note that the separate sensors are not required to have the same properties or measurement models and are not restricted to taking measurements at the same time steps. As long as the sensors are independent the Fisher Information Matrix is easily computed. This makes the information-theoretic approach particularly well suited to estimation problems involving heterogenous teams with several different sensing systems collaborating to provide a target location estimate. It is important to mention that the concepts of using the FIM to compute optimal trajectories for improved estimation performance and combining the optimization and estimation are not restricted to the bearings-only case. This approach can be used for any nonlinear system with any measurement model. Convergence properties may change based on the dynamics of the problem at hand but, since this approach relies on the underlying physical and geometric properties of the system, it is probable that this method will enhance the estimation performance for many types of nonlinear systems.

An interesting result is that the best suited objective function for trajectory optimization in the 3-D bearings-only target estimation problem is the A-optimality criterion, which closely resembles the geometric dilution of precision (GDOP) criteria often used in GPS navigation. This further illustrates that optimization using the FIM leads to trajectories that provide the best geometry for a given set of measurements. The trajectory optimization results presented in Chapter 3 show the tradeoff between simultaneously reducing the relative range to the target and increasing the angular separation between measurements, thus supporting the geometric intuition

about minimizing the estimation error presented in Chapter 1, and showing that information-based optimization captures these geometric and physical properties of the estimation problem.

The resulting trajectories shown in this thesis can be directly applied to small UAVs with gimballed camera systems. A gimballed camera can be pointed in any direction and made to look at the target, thus ensuring that the target always remains in the field of view of the camera. Since the trajectories that produce the most information usually maintain a flight path that is nearly orthogonal to the line-of-sight vector to the target, the desired placement for a fixed camera would probably be a side-looking mounting. This work could be extended to consider UAVs with fixed side-look cameras by including the field of view constraints in the trajectory optimization problem. For small fixed-wing UAVs, the main challenge associated with using a side-mounted camera is that these vehicles are particularly sensitive to wind and gusts, especially with respect to the bank angle. This often causes the target to move out of the field of view of the camera and thus proper measurements cannot be obtained. Using a gimballed camera system would mitigate this problem by allowing the camera to turn and point at the target even when the airplane is not at the desired bank angle, thus providing greater flexibility and increasing the usefulness of small UAVs in the target localization problem.

5.3 Future Work

There are several possible extensions of this work and a few ideas are described in this section. The first suggestion for future work involves the incorporation of behavior models for different target types. The results in this thesis consider stationary targets and moving targets with stochastic behavior models. The motion of the targets is assumed unknown and the best the filter can do is to use the process noise model to represent the uncertainty in the target motion. Incorporating actual behavior models of the target motion would improve the performance of the estimation by increasing accuracy and filter stability. This comes at the cost of reduced flexibility, since any

deviation by the target from the expected behavior model would cause serious problems with the estimation. Since this system is designed to be used in situations where no prior information is available a stochastic target model is considered appropriate for this thesis. As more information is collected and target types are classified, different behavior models of targets could be used to enhance estimation performance. For example, turn constraints or maximum vehicle speeds could be incorporated to limit the motion of the target. Additionally, information about the environment could be processed to produce probabilistic models of the target's behavior. For example, if a road is detected and a vehicle is on it, it is more likely that the vehicle will remain on the road than deviate off of it. Or if a lake or barrier is present, it is highly unlikely that a car or truck would turn into it, thus imposing a probabilistic constraint on the target's motion. Research of target estimation using hospitability and synthetic inclination maps is already in place and could be used in combination with the trajectory optimization strategies provided in this thesis. Terrain elevation data, such as DTED, could also be used to refine the estimation of the Z dimension and to restrict the motion of the target in this direction.

Another interesting target type that can be considered involves targets exhibiting evasive behavior. Evasive targets are those with knowledge of the pursuer's actions and intentions and which purposely attempt to increase the difficulty of the pursuer's task. These types of targets have been considered in a differential games framework, where the target acts to maximize his value and minimize that of the pursuer. In this case, the value function would involve the inverse of the FIM and the target would plan its trajectory by maximizing this function. Such targets could be considered by assuming that they will always execute maneuvers that reduce the observability of the estimation and decrease the information provided by the UAV's measurements, thus attempting to decrease the performance of the target location estimation.

This work could also be extended to include target localization for multiple targets. Chapter 3 shows results for UAV trajectory optimization in the multiple target scenario assuming that measurements of all the targets are obtained at every time step. In reality, one would image one target at every time step and further optimiza-

tion could be performed to determine which target to measure in order to obtain the highest overall information. Another problem, involving the estimation algorithm, in the multiple target scenario is that if multiple targets are imaged simultaneously the target localization task consists of a simultaneous data association and estimation problem. This type of estimation can be accomplished using particle filters but the task of determining which measurements are associated with each target is quite challenging, especially if the number of targets is unknown [9] [8].

Another interesting problem involves determining what the optimal camera mounting location is for the case of a UAV with a fixed-camera. This camera placement would depend on the type of target motion expected and would probably involve a side-look camera since the optimal information-theoretic trajectory maintains a nearly orthogonal heading to the line-of-sight vector to the target. As mentioned before however, side-look cameras are more difficult to use since wind and gusts affect the bank angle of the UAV the most, and this issue would need to be addressed before the system can be used in a realistic setting. Additionally, it would probably be advantageous to have a wider vertical field of view than horizontal field of view, since most of the change in viewing angle occurs in the vertical direction (due to the reducing relative range). It would also be interesting to determine what the optimal measurement rate is. Finding the slowest rate at which measurements can be taken whilst still providing the desired accuracy would free up computational resources and bandwidth which are fairly limited for small UAVs. This rate could also be made variable and measurements could be taken only when the expected additional information is above a certain threshold.

Other suggestions for improvement involve refining the UAV trajectory optimization and target estimation. For example, by using the future target location instead of the current target location estimate, the optimization would produce a better UAV trajectory and a more accurate estimation could be achieved. This would require the propagation of the target dynamics model and the time needed for planning and UAV maneuvering would have to be quantified. The resulting trajectory would improve the overall estimation performance by increasing accuracy and filter conver-

gence. Further improvements could be obtained by revisiting the assumptions on the sensor noise, such as the lack of sensor correlation, and applying that to both the estimation and optimization algorithms. Other optimization considerations could also include additional operational constraints involving obstacles in the environment such as mountains and buildings or vehicle no-fly zones.

Appendix A

Derivation of the Cramér-Rao Lower Bound and the Fisher Information Matrix

A.1 Theoretical Derivation

The derivation of the Fisher Information Matrix and the Information Inequality, also known as the Cramér-Rao Lower Bound, are shown below. The well known covariance inequality [46] is given by

$$\text{var}\{\delta\} \geq \frac{[\text{cov}\{\delta, \psi\}]^2}{\text{var}\{\psi\}} \tag{A.1}$$

where δ is any estimator of the function $g(x)$ whose argument x is an unknown parameter and $\psi(z, x)$ is any function, with a finite second moment, of the measurable quantity z and the unknown parameter x. Since $\text{cov}\{\delta, \psi\}$ depends on δ, the covariance inequality is of limited use in providing a bound for $\text{var}\{\delta\}$, however, if $\text{cov}\{\delta, \psi\}$ depends on δ only through $\mathbb{E}_{\mathbf{x}}\{\delta\} = g(x)$ and $\psi(z, x)$ is chosen as

$$\psi(z, x) = \frac{\frac{\partial}{\partial x} p(\mathbf{z}, x)}{p(\mathbf{z}, x)} = \frac{\partial}{\partial x} \log p(\mathbf{z}, x) \tag{A.2}$$

then the inequality above becomes[1]

$$\text{var}\{\delta\} \geq \frac{[g'(x)]^2}{\text{var}\left\{\frac{\partial}{\partial x}\log p(\mathbf{z}, x)\right\}} \tag{A.3}$$

Here $\mathbf{z}$ is the vector of measurements and is distributed with density given by $p(\mathbf{z}, x)$.

The function $\psi(z, x)$ represents the relative rate at which the density $p(\mathbf{z}, x)$ changes at z. The average of the square of this rate is given by

$$J(x) = \mathbb{E}_{\mathbf{x}}\left\{\left[\frac{\partial}{\partial x}\log p(\mathbf{z}, x)\right]^2\right\} = \int \left(\frac{p'(\mathbf{z}, x)}{p(\mathbf{z}, x)}\right)^2 p(\mathbf{z}, x)\, dx \tag{A.4}$$

$J(x)$ is the Fisher information that $\mathbf{z}$ contains about x. One interpretation of Fisher information is that the greater $J(x)$ is at $x = x_0$, the higher the relative rate of density change is and the easier it is to separate x_0 from the surrounding values of x. Therefore x can be estimated more accurately when the information is higher (this is true for large samples under certain assumptions, see [46]).

Under some not very limiting conditions (see [46]) the following can be written,

$$\mathbb{E}_{\mathbf{x}}\left\{\frac{\partial}{\partial x}\log p(\mathbf{z}, x)\right\} = 0 \tag{A.5}$$

which implies that

$$J(x) = \text{var}\left\{\frac{\partial}{\partial x}\log p(\mathbf{z}, x)\right\} \tag{A.6}$$

This gives the Information Inequality for any estimator δ of $g(x)$,

$$\text{var}\{\delta\} \geq \frac{[g'(x)]^2}{J(x)} \tag{A.7}$$

When estimating a real-valued parameter x, $g(x) = x$ and therefore $g'(x) = 1$, so the

[1]For a complete derivation see [46]

Information Inequality becomes

$$\text{var}\{\delta\} \geq \frac{1}{J(x)} \tag{A.8}$$

For estimators of x this implies that the lowest possible achievable variance of the estimator is bounded by the inverse of the Fisher information. This lower bound is also referred to in literature as the Cramér-Rao Lower Bound. An estimator that achieves this lower bound on the variance is said to be *efficient*.

For the multi-parameter case where we are trying to estimate n parameters $\mathbf{x} = \begin{bmatrix} x_1 \dots x_n \end{bmatrix}^T$, we have the $n \times n$ Fisher Information Matrix $\mathbf{J}(\mathbf{x})$ where

$$\mathbf{J_{ij}}(\mathbf{x}) = \mathbb{E}_{\mathbf{x}}\left\{ \frac{\partial}{\partial x_i} \log p(\mathbf{z}, \mathbf{x}) \frac{\partial}{\partial x_j} \log p(\mathbf{z}, \mathbf{x}) \right\} \tag{A.9}$$

As in the scalar case, the following can be written,

$$\mathbb{E}_{\mathbf{x}}\left\{ \frac{\partial}{\partial x_i} \log p(\mathbf{z}, \mathbf{x}) \right\} = 0 \tag{A.10}$$

implying

$$\mathbf{J_{ij}}(\mathbf{x}) = \text{cov}\left\{ \frac{\partial}{\partial x_i} \log p(\mathbf{z}, \mathbf{x}), \frac{\partial}{\partial x_j} \log p(\mathbf{z}, \mathbf{x}) \right\} \tag{A.11}$$

Since $\mathbf{J}(\mathbf{x})$ is the inverse of a covariance matrix it is usually positive definite. If the estimation is unobservable then the FIM will be positive semi-definite and the covariance will be infinite.

A.2 Recursive Form

For the target location estimation problem, the Cramér-Rao inequality is given by

$$\mathbb{E}\left\{ [\hat{\mathbf{X}}_{k|k} - \mathbf{X}_k][\hat{\mathbf{X}}_{k|k} - \mathbf{X}_k]^T \right\} \geq \mathbf{I}_k^{-1} \tag{A.12}$$

where

$$\mathbf{I}_k = \mathbb{E}\{[\nabla_{\mathbf{X}_k} \log p(\mathbf{X}_k, \mathbf{Z}_k)][\nabla_{\mathbf{X}_k} \log p(\mathbf{X}_k, \mathbf{Z}_k)]^T\} \tag{A.13}$$

$$\mathbf{I}_k = -\mathbb{E}\{\nabla_{\mathbf{X}_k}[\nabla_{\mathbf{X}_k} \log p(\mathbf{X}_k, \mathbf{Z}_k)]^T\} \tag{A.14}$$

$$\tag{A.15}$$

Here $\mathbf{X}_k$ is the target trajectory up to time k and is defined as $\mathbf{X}_k = \{\mathbf{x}_j, j = 0, ..., k\}$ and $\mathbf{Z}_k$ is the sequence of measurements up to time k such that $\mathbf{Z}_k = \{\mathbf{z}_j, j = 0, ..., k\}$. The above expression includes the fact that the target dynamics are stochastic (i.e. includes process noise). When the target state is deterministic $p(\mathbf{X}_k, \mathbf{Z}_k)$ is replaced with the likelihood function $p(\mathbf{Z}_k|\mathbf{X}_k)$ in the above equations. The expectations above are taken with respect to $\mathbf{X}_k$ and $\mathbf{Z}_k$. When the covariance of the unbiased estimator is equal to the CRLB, the estimator is considered statistically efficient.

The bound of interest is given by

$$\mathbf{P}_{k|k} = \mathbb{E}\{(\hat{\mathbf{x}}_{k|k} - \mathbf{x}_k)(\hat{\mathbf{x}}_{k|k} - \mathbf{x}_k)^T\} \geq \mathbf{J}_k^{-1} \tag{A.16}$$

where $\mathbf{x}_k$ is the state of the target at time k. Rewriting $\mathbf{X}_k = \begin{bmatrix} \mathbf{X}_{k-1}^T & \mathbf{x}_k^T \end{bmatrix}^T$, the information matrix for the entire target trajectory $\mathbf{I}_k$ can be written as

$$\mathbf{I}_k = \begin{bmatrix} \mathbf{A}_k & \mathbf{B}_k \\ \mathbf{B}_k^T & \mathbf{C}_k \end{bmatrix} \tag{A.17}$$

where

$$\mathbf{A}_k = -\mathbb{E}\left\{\nabla_{\mathbf{X}_{k-1}}\left[\nabla_{\mathbf{X}_{k-1}} \log p(\mathbf{X}_k, \mathbf{Z}_k)\right]^T\right\} \tag{A.18}$$

$$\mathbf{B}_k = -\mathbb{E}\left\{\nabla_{\mathbf{X}_{k-1}}\left[\nabla_{\mathbf{x}_k} \log p(\mathbf{X}_k, \mathbf{Z}_k)\right]^T\right\} \tag{A.19}$$

$$\mathbf{C}_k = -\mathbb{E}\left\{\nabla_{\mathbf{x}_k}\left[\nabla_{\mathbf{x}_k} \log p(\mathbf{X}_k, \mathbf{Z}_k)\right]^T\right\} \tag{A.20}$$

The lower bound for the covariance of the estimation error for $\mathbf{x}_k$ is given by the right

lower block of $\mathbf{I}_k^{-1}$ which can be written as

$$\mathbf{J}_k = \mathbf{C}_k - \mathbf{B}_k^T \mathbf{A}_k^{-1} \mathbf{B}_k \tag{A.21}$$

The dimensions of the matrices $\mathbf{A}_k$ and $\mathbf{B}_k$ grow as the time index k increases, which makes the expression for $\mathbf{J}_k$ given above computationally inefficient. A recursive method for computing the information matrix $\mathbf{J}_k$ was presented by Tichavsky et al. in [69]. The recursive form of $\mathbf{J}_k$ is given by

$$\mathbf{J}_{k+1} = \mathbf{D}_k^{22} - \mathbf{D}_k^{21} (\mathbf{J}_k + \mathbf{D}_k^{11})^{-1} \mathbf{D}_k^{12} \tag{A.22}$$

where

$$\mathbf{D}_k^{11} = -\mathbb{E}\left\{ \nabla_{\mathbf{x}_k} \left[\nabla_{\mathbf{x}_k} \log p(\mathbf{x}_{k+1}|\mathbf{x}_k) \right]^T \right\} \tag{A.23}$$

$$\mathbf{D}_k^{21} = -\mathbb{E}\left\{ \nabla_{\mathbf{x}_k} \left[\nabla_{\mathbf{x}_{k+1}} \log p(\mathbf{x}_{k+1}|\mathbf{x}_k) \right]^T \right\} \tag{A.24}$$

$$\mathbf{D}_k^{12} = -\mathbb{E}\left\{ \nabla_{\mathbf{x}_{k+1}} \left[\nabla_{\mathbf{x}_k} \log p(\mathbf{x}_{k+1}|\mathbf{x}_k) \right]^T \right\} = [\mathbf{D}_k^{21}]^T \tag{A.25}$$

$$\begin{aligned} \mathbf{D}_k^{22} = & -\mathbb{E}\left\{ \nabla_{\mathbf{x}_{k+1}} \left[\nabla_{\mathbf{x}_{k+1}} \log p(\mathbf{x}_{k+1}|\mathbf{x}_k) \right]^T \right\} \\ & -\mathbb{E}\left\{ \nabla_{\mathbf{x}_{k+1}} \left[\nabla_{\mathbf{x}_{k+1}} \log p(\mathbf{z}_{k+1}|\mathbf{x}_{k+1}) \right]^T \right\} \end{aligned} \tag{A.26}$$

For a complete derivation see [69] or [64]. To initialize the recursion, the matrix $\mathbf{J}_0$ is computed using

$$\mathbf{J}_0 = \mathbb{E}\left\{ \left[\nabla_{\mathbf{x}_0} \log p(\mathbf{x}_0) \right] \left[\nabla_{\mathbf{x}_0} \log p(\mathbf{x}_0) \right]^T \right\} \tag{A.27}$$

where $p(\mathbf{x}_0)$ is the initial density and the expectation is taken with respect to $\mathbf{x}_0$. If the initial distribution is Gaussian such that $p(\mathbf{x}_0) = \mathcal{N}(\mathbf{x}_0; \bar{\mathbf{x}}_0, \mathbf{P}_0)$ then the initial

information matrix is given by

$$\mathbf{J}_0 = \mathbb{E}\Big\{ \Big[\nabla_{\mathbf{x}_0} \log p(\mathbf{x}_0)\Big] \Big[\nabla_{\mathbf{x}_0} \log p(\mathbf{x}_0)\Big]^T \Big\} \tag{A.28}$$

$$= \mathbb{E}\Big\{ \Big[-\mathbf{P}_0^{-1}(\mathbf{x}_0 - \bar{\mathbf{x}}_0)\Big] \Big[-\mathbf{P}_0^{-1}(\mathbf{x}_0 - \bar{\mathbf{x}}_0)\Big]^T \Big\} \tag{A.29}$$

$$= \mathbf{P}_0^{-1}\mathbb{E}\big\{(\mathbf{x}_0 - \bar{\mathbf{x}}_0)(\mathbf{x}_0 - \bar{\mathbf{x}}_0)^T\big\}\mathbf{P}_0^{-1} \tag{A.30}$$

$$= \mathbf{P}_0^{-1}\mathbf{P}_0\mathbf{P}_0^{-1} = \mathbf{P}_0^{-1} \tag{A.31}$$

Appendix B

Particle Filtering Algorithm

GENERIC PARTICLE FILTER ALGORITHM IN MATLAB

```
% 3D Particle Filter

% Initial Parameters
Nthr = 5;
N = 2000;
sigmaW = 10;

% Initial estımation data
x0 = [20; 20; 20];
P0 = [200 0 0; 0 200 0; 0 0 200];

% Initialize particles
x(:,1,1) = sqrt(P0(1,1))*randn(N,1) + x0(1)*ones(N,1);
x(:,2,1) = sqrt(P0(2,2))*randn(N,1) + x0(2)*ones(N,1);
x(:,3,1) = sqrt(P0(3,3))*randn(N,1) + x0(3)*ones(N,1);
w(:,1) = (1/N)*ones(N,1);


% SIR algorithm
for k=1:length(Veh_z),
    % Propagate particles
    x(:,:,k+1) = x(:,:,k) + sigmaW*randn(N,3);

    % Compute weights based on a measurement (use likelihood function)
    for i=1:N,
        w(i,k+1) = w(i,k)*(1/sqrt(2*pi*sigma2))*exp(-(1/(2*sigma2))*...
            ((Veh_z(1,k)-atan2(Veh_pos(1,k)-x(i,1,k+1),Veh_pos(2,k)-x(i,2,k+1)))^2...
        +(Veh_z(2,k)-atan2(Veh_pos(3,k)-x(i,3,k+1), ...
            sqrt((Veh_pos(1,k)-x(i,1,k+1))^2+(Veh_pos(2,k)-x(i,2,k+1))^2)))^2));
```

```
    end
    sumW = sum(w(:,k+1));
    w(:,k+1) = w(:,k+1)/sumW;

    % See if resampling is needed
    Neff = 1/(w(:,k+1)'*w(:,k+1));

    if (Neff < Nthr),
        x(:,:,k+1) = SIR_resample(x(:,:,k+1),w(:,k+1));
        w(:,k+1) = (1/N)*ones(N,1);
    end

    % Compute new mean and covariance
    xhat_k(k,:) = w(:,k+1)'*x(:,:,k+1);
    cov_k = (x(:,:,k+1)-ones(N,1)*xhat_k(k,:))'*diag(w(:,k+1))*...
        (x(:,:,k+1)-ones(N,1)*xhat_k(k,:));

    var_k(1,k) = cov_k(1,1);
    var_k(2,k) = cov_k(2,2);
    var_k(3,k) = cov_k(3,3);
end
```

RESAMPLING FUNCTION

```
function xnew = SIR_resample(xold,w),

[Wsorted Wind] = sort(w,'descend');
Wsum = cumsum(Wsorted);

uni = sort(rand(length(xold),1),'ascend');

flag = 0;
i=1;
for k=1:length(uni),
    flag = 0;
    while(flag == 0),
        if (uni(k) < Wsum(i)),
            xnew(k,:) = xold(Wind(i),:);
            flag = 1;
        else,
            i = i+1;
        end
    end
end
```

Bibliography

[1] Air force doctrine document 2-5.2: Intelligence, surveillance, and reconnaissance operations. Technical report, United States Air Force, April 1999.

[2] Defense science board task force on precision targeting. Technical report, Office of the Under Secretary of Defense for Acquisition, Technology and Logistics, 2001.

[3] Unmanned aircraft systems roadmap, 2005-2030. Technical report, Office of the Secretary of Defense, August 2005.

[4] Unmanned systems roadmap, 2007-2032. Technical report, Office of the Secretary of Defense, December 2007.

[5] V. Aidala and S. Hammel. Utilization of modified polar coordinates for bearings-only tracking. *Automatic Control, IEEE Transactions on*, 28(3):283–294, Mar 1983.

[6] V. J. Aidala. Kalman filter behavior in bearings-only tracking applications. *Aerospace and Electronic Systems, IEEE Transactions on*, AES-15(1):29–39, Jan. 1979.

[7] V. J. Aidala and S. C. Nardone. Biased estimation properties of the pseudolinear tracking filter. *Aerospace and Electronic Systems, IEEE Transactions on*, AES-18(4):432–441, July 1982.

[8] Pablo O. Arambel, Jeff Silver, Jon Krant, Matthew Antone, and Thomas Strat. Multiple-hypothesis tracking of multiple ground targets from aerial video with

dynamic sensor control. In *Signal Processing, Sensor Fusion, and Target Recognition XIII, Proceedings of the SPIE*, August 2004.

[9] Yaakov Bar-Shalom, Thiagalingam Kirubarajan, and X.-Rong Li. *Estimation with Applications to Tracking and Navigation*. John Wiley & Sons, Inc., New York, NY, USA, 2002.

[10] D. B. Barber, J. Redding, T. Mclain, R. Beard, and C. Taylor. Vision-based target geo-location using a fixed-wing miniature air vehicle. *J. Intell. Robotics Syst.*, 47(4):361–382, 2006.

[11] K. Becker. Simple linear theory approach to tma observability. *Aerospace and Electronic Systems, IEEE Transactions on*, 29(2):575–578, Apr 1993.

[12] B. Bethke, M. Valenti, and J. How. Cooperative vision based estimation and tracking using multiple uavs. In *Conference of Cooperative Control and Optimization*, Gainesville, FL, January 2007.

[13] Anthony J. Calise, Eric N. Johnson, Ramachandra Sattigeri, Yoko Watanabe, and Venkatesh Madyastha. Estimation and guidance strategies for vision-based target tracking. In *American Control Conference*, Portland, OR, June 2005.

[14] Chi-Tsong Chen. *Linear System Theory and Design*. Oxford University Press, Inc, 1999.

[15] W. G. Cochran. Experiments for nonlinear functions. *Journal of the American Statistical Association*, December 1973.

[16] J. H. de Vlieger and R. H. J. G. Meyling. Maximum likelihood estimation for long-range target tracking using passive sonar measurements. *Signal Processing, IEEE Transactions on [see also Acoustics, Speech, and Signal Processing, IEEE Transactions on]*, 40(5):1216–1225, May 1992.

[17] J. A. Fawcett. Effect of course maneuvers on bearings-only range estimation. *Acoustics, Speech, and Signal Processing [see also IEEE Transactions on Signal Processing], IEEE Transactions on*, 36(8):1193–1199, Aug 1988.

[18] E. Fogel and M. Gavish. Nth-order dynamics target observability from angle measurements. *Aerospace and Electronic Systems, IEEE Transactions on*, 24(3):305–308, May 1988.

[19] E. Frew, C. Dixon, B. Argrow, and T. Brown. Radio source localization by a cooperating uav team. In *Infotech@Aerospace*, Arlington, Virginia, September 2005.

[20] Eric W. Frew. *Trajectory Design for Target Motion Estimation Using Monocular Vision.* PhD thesis, Stanford University, 2003.

[21] Eric W. Frew. Information-theoretic integration of sensing and communication for active robot networks. In *RoboComm '07: Proceedings of the 1st international conference on Robot communication and coordination*, pages 1–8, Piscataway, NJ, USA, 2007. IEEE Press.

[22] Arthur Gelb. *Applied Optimal Estimation.* The MIT Press, Cambridge, MA, 1974.

[23] D. Goshen-Meskin and I. Y. Bar-Itzhack. Observability analysis of piece-wise constant systems. i. theory. *Aerospace and Electronic Systems, IEEE Transactions on*, 28(4):1056–1067, Oct 1992.

[24] B. Grocholsky, A. Makarenko, and H. Durrant-Whyte. Information-theoretic control of multiple sensor platforms. In *Proceedings of the IEEE International Conference on Robotics and Automation*, Taipei, Taiwan, September 2003.

[25] S. E. Hammel and V. J. Aidala. Observability requirements for three-dimensional tracking via angle measurements. *Aerospace and Electronic Systems, IEEE Transactions on*, AES-21(2):200–207, March 1985.

[26] T. Hayashi, S. Enokida, and T. Ejima. A real-time target tracking method applicable to a robot's vision. *Robot and Human Interactive Communication, 2003. Proceedings. ROMAN 2003. The 12th IEEE International Workshop on*, pages 127–132, 31 Oct.-2 Nov. 2003.

[27] J. P. Helferty and D. R. Mudgett. Optimal observer trajectories for bearings only tracking by minimizing the trace of the cramer-rao lower bound. *Decision and Control, 1993., Proceedings of the 32nd IEEE Conference on*, pages 936–939 vol.1, 15-17 Dec 1993.

[28] J. P. Helferty, D. R. Mudgett, and J. E. Dzielski. Trajectory optimization for minimum range error in bearings-only source localization. *OCEANS '93. 'Engineering in Harmony with Ocean'. Proceedings*, pages II/229–II/234 vol.2, 18-21 Oct 1993.

[29] M. Hernandez. Optimal sensor trajectories in bearings-only tracking. In *Proceedings of the 7th International Conference on Information Fusion*, pages 893–900, Stockholm, Sweden, 2004.

[30] Alexander Hornberg. *Handbook of Machine Vision.* WILEY-VCH Verlag GmbH & Co. KGaA, 2006.

[31] C. Hue, J. P. Le Cadre, and P. Perez. Tracking multiple targets with particle filtering using multiple receivers. *Target Tracking: Algorithms and Applications (Ref. No. 2001/174), IEE*, 1:6/1–6/4 vol.1, 16-17 Oct. 2001.

[32] C. Hue, J. P. Le Cadre, and P. Perez. A particle filter to track multiple objects. *Multi-Object Tracking, 2001. Proceedings. 2001 IEEE Workshop on*, pages 61–68, 2001.

[33] C. Hue, J. P. Le Cadre, and P. Perez. Performance analysis of two sequential monte carlo methods and posterior cramer-rao bounds for multi-target tracking. *Information Fusion, 2002. Proceedings of the Fifth International Conference on*, 1:464–473 vol.1, 2002.

[34] C. Hue, J. P. Le Cadre, and P. Perez. Sequential monte carlo methods for multiple target tracking and data fusion. *Signal Processing, IEEE Transactions on [see also Acoustics, Speech, and Signal Processing, IEEE Transactions on]*, 50(2):309–325, Feb 2002.

[35] C. Hue, J. P. Le Cadre, and P. Perez. Tracking multiple objects with particle filtering. *Aerospace and Electronic Systems, IEEE Transactions on*, 38(3):791–812, Jul 2002.

[36] Gregory F. Ivey and Eric N. Johnson. Investigation of methods for target state estimation using vision sensors. In *AIAA Guidance, Navigation, and Control Conference and Exhibit*, San Francisco, CA, August 2005.

[37] Zhen Jia, A. Balasuriya, and S. Challa. Recent developments in vision based target tracking for autonomous vehicles navigation. *Intelligent Transportation Systems Conference, 2006. ITSC '06. IEEE*, pages 765–770, 2006.

[38] L. M. Kaplan and V. Cevher. Design considerations for a heterogeneous network of bearings-only sensors using sensor management. *Aerospace Conference, 2007 IEEE*, pages 1–14, March 2007.

[39] Jun Ming Kuang and Ming Liu. Stereo vision based moving target tracking for omni-directional mobile robots in 2d space. *Information Acquisition, 2007. ICIA '07. International Conference on*, pages 602–607, 8-11 July 2007.

[40] J. E. Le Cadre and C. Jauffret. Discrete-time observability and estimability analysis for bearings-only target motion analysis. *Aerospace and Electronic Systems, IEEE Transactions on*, 33(1):178–201, Jan. 1997.

[41] J. P. Le Cadre. Optimization of the observer motion for bearings-only target motion analysis. *Decision and Control, 1997., Proceedings of the 36th IEEE Conference on*, 4:3126–3131 vol.4, 10-12 Dec 1997.

[42] J. P. Le Cadre and H. Gauvrit. Optimization of the observer motion for bearings-only target motion analysis. *Data Fusion Symposium, 1996. ADFS '96., First Australian*, pages 190–195, 21-22 Nov 1996.

[43] J. P. Le Cadre, H. Gauvrit, and F. Trarieux. Approximations of the cramer-rao bound for multiple-target motion analysis. *Radar, Sonar and Navigation, IEE Proceedings* -, 147(3):105–113, Jun 2000.

[44] J. P. Le Cadre and O. Tremois. Properties and performance of extended target motion analysis. *Aerospace and Electronic Systems, IEEE Transactions on*, 32(1):66–83, Jan 1996.

[45] J. P. Le Cadre and O. Tremois. Bearings-only tracking for maneuvering sources. *Aerospace and Electronic Systems, IEEE Transactions on*, 34(1):179–193, Jan 1998.

[46] E. L. Lehmann and George Casella. *Theory of Point Estimation.* Springer Sciences+Business Media, LLC, New York, NY, 1998.

[47] J. Levine and R. Marino. Constant-speed target tracking via bearings-only measurements. *Aerospace and Electronic Systems, IEEE Transactions on*, 28(1):174–182, Jan 1992.

[48] A. G. Lindgren and Kai F. Gong. Position and velocity estimation via bearing observations. *Aerospace and Electronic Systems, IEEE Transactions on*, AES-14(4):564–577, July 1978.

[49] P. T. Liu. An optimum approach in target tracking with bearing measurements. *Journal of Optimization Theory and Applications*, 56(2):205–214, February 1988.

[50] A. Logothetis, A. Isaksson, and R. J. Evans. An information theoretic approach to observer path design for bearings-only tracking. *Decision and Control, 1997., Proceedings of the 36th IEEE Conference on*, 4:3132–3137 vol.4, Dec 1997.

[51] G. Gilbert C. Iler K. Glenn M. Satterly, K. Stubbs. Intelligence preparation of the battlespace - an airman's introduction. *Air and Space Power Journal - Chronicles Online Journal*, July 1999.

[52] M. Mandic and E. Frazzoli. Efficient sensor coverage for acoustic localization. *Decision and Control, 2007 46th IEEE Conference on*, pages 3597–3602, Dec. 2007.

[53] S. Martínez and F. Bullo. Optimal sensor placement and motion coordination for target tracking. *Automatica*, 42(4):661–668, April 2006.

[54] S. Nardone, A. Lindgren, and Kai Gong. Fundamental properties and performance of conventional bearings-only target motion analysis. *Automatic Control, IEEE Transactions on*, 29(9):775–787, Sep 1984.

[55] S. C. Nardone and V. J. Aidala. Observability criteria for bearings-only target motion analysis. *Aerospace and Electronic Systems, IEEE Transactions on*, AES-17(2):162–166, March 1981.

[56] S. C. Nardone and M. L. Graham. A closed-form solution to bearings-only target motion analysis. *Oceanic Engineering, IEEE Journal of*, 22(1):168–178, Jan 1997.

[57] Y. Oshman and P. Davidson. Optimization of observer trajectories for bearings-only target localization. *Aerospace and Electronic Systems, IEEE Transactions on*, 35(3):892–902, Jul 1999.

[58] Jarurat Ousingsawat and Mark E. Campbell. Optimal cooperative reconnaissance using multiple vehicles. *Journal Of Guidance, Control, and Dynamics*, 30(1), 2007.

[59] J. M. Passerieux and D. Van Cappel. Optimal observer maneuver for bearings-only tracking. *Aerospace and Electronic Systems, IEEE Transactions on*, 34(3):777–788, Jul 1998.

[60] R. A. Pomranky. *Human Robotics Interaction Army Technology Objective Raven Small Unmanned Aerial Vehicle Task Analysis and Modeling.* Army Research Laboratory, January 2006.

[61] M. Quigley, M. A. Goodrich, S. Griffiths, A. Eldredge, and R. W. Beard. Target acquisition, localization, and surveillance using a fixed-wing mini-uav and gimbaled camera. *Robotics and Automation, 2005. ICRA 2005. Proceedings of the 2005 IEEE International Conference on*, pages 2600–2605, April 2005.

[62] Fahd Rafi, Saad Khan, Khurram Shafiq, and Mubarak Shah. Autonomous target following by unmanned aerial vehicles. In *Proceedings of SPIE*, Orlando, FL, May 2006.

[63] Karl Johan Åström and Björn Wittenmark. *Adaptive Control.* Addison-Wesley Publishing Company, 1989.

[64] Branko Ristic, Sanjeev Arulampalam, and Neil Gordon. *Beyond the Kalman Filter: Particle Filters for Tracking Applications.* Artech House, 2004.

[65] S. Singh, Ba-Ngu Vo, A. Doucet, and R. Evans. Stochastic approximation for optimal observer trajectory planning. *Decision and Control, 2003. Proceedings. 42nd IEEE Conference on*, 6:6313–6318 Vol.6, 9-12 Dec. 2003.

[66] A. Sinha, T. Kirubarajan, and Y. Bar-Shalom. Optimal cooperative placement of gmti uavs for ground target tracking. *Aerospace Conference, 2004. Proceedings. 2004 IEEE*, 3:–1868 Vol.3, March 2004.

[67] Xiao-Jiao Tao, Cai-Rong Zou, and Zhen-Ya He. Passive target tracking using maximum likelihood estimation. *Aerospace and Electronic Systems, IEEE Transactions on*, 32(4):1348–1354, Oct 1996.

[68] James H. Taylor. The cramer-rao estimation error lower bound computation for deterministic nonlinear systems. *Decision and Control including the 17th Symposium on Adaptive Processes, 1978 IEEE Conference on*, 17:1178–1181, Jan. 1978.

[69] P. Tichavsky, C. H. Muravchik, and A. Nehorai. Posterior cramer-rao bounds for discrete-time nonlinear filtering. *Signal Processing, IEEE Transactions on [see also Acoustics, Speech, and Signal Processing, IEEE Transactions on]*, 46(5):1386–1396, May 1998.

[70] O. Tremois and J. P. Le Cadre. Optimal observer trajectory in bearings-only tracking for manoeuvring sources. *Radar, Sonar and Navigation, IEE Proceedings* -, 146(1):31–39, Feb 1999.

[71] O. Tremois and J. P. Le Cadre. Target motion analysis with multiple arrays: performance analysis. *Aerospace and Electronic Systems, IEEE Transactions on*, 32(3):1030–1046, Jul 1996.

[72] D. Uciński. *Optimal Measurement Methods for Distributed Parameter System Identification*. CRC Press, 2005.

[73] Yoko Watanabe, Eric N. Johnson, and Anthony J. Calise. Optimal 3-d guidance from a 2-d vision sensor. *AIAA Guidance, Navigation, and Control Conference*, August 2004.

[74] W. Whitacre and M. Campbell. Information-theoretic optimization of periodic orbits for cooperative geolocation. Technical report, Cornell University, Ithaca, NY, 2007.

[75] Richard A. Wise and Rolf T. Rysdyk. Uav coordination for autonomous target tracking. In *AIAA Guidance, Navigation, and Control Conference and Exhibit*, Keystone, CO, August 2006.